

MASTER OF SCIENCE THESIS

# Process Analysis & Simulation of Composite Pressure Vessels

Mohamed Khalifa

Faculty of Aerospace Engineering · Delft University of Technology



# Process Analysis & Simulation of Composite Pressure Vessels

by

**Mohamed Khalifa**

to obtain the degree of Master of Science  
at Delft University of Technology  
to be defended publicly on Thursday, September 29, 2022, at 09:00 AM

Student number	4646339	
Project duration	January 2022 - September 2022	
Thesis supervisors	Dr.ir. J.M.J.F. van Campen ir. Alejandro Soriano Sutil	TU Delft Plastic Omnium

*This report is confidential*

The work in this thesis was done in collaboration with Plastic Omnium. Their cooperation is gratefully acknowledged.



Copyright © Mohamed Khalifa  
All rights reserved.



DELFT UNIVERSITY OF TECHNOLOGY  
FACULTY OF AEROSPACE ENGINEERING  
DEPARTMENT OF AEROSPACE STRUCTURES AND MATERIALS

**GRADUATION COMMITTEE**

Dated: 29/09/2022

Chair holder:

---

Dr. S.R. Turteltaub

Committee members:

---

Dr.ir. J.M.J.F. van Campen

---

Dr.ir. O.K. Bergsma

---

ir. Alejandro Soriano Sutil



# Abstract

The automotive industry has been in an increasing drive toward finding more sustainable transportation alternatives to abandon the era of Internal Combustion Engines (ICE). This was manifested in the large market share of Battery Electric Vehicles (BEVs) that have been established in recent years. As BEVs are not an efficient option in long-haul transportation, Fuel-Cell Electric Vehicles (FCEVs) have presented themselves as a prominent choice. To maximize the attainable driving range, gaseous hydrogen is compressed to 70 MPa per recent regulations. As a result, hydrogen storage pressure vessels need to provide high structural integrity, whilst being as lightweight as possible. This has led to the introduction of Carbon Fiber Reinforced Polymer (CFRP), where type IV Composite Pressure Vessels (CPVs) with CFRP overwrap and plastic liner are gaining popularity.

The mass implementation of FCEVs is however directly dependent on the cost and reliability of CPVs. Increasing the reliability levels inherently leads to minimizing the materials used inducing cost reduction possibilities, and presenting FCEVs as a more feasible solution. To attain such high levels of reliability, a thorough understanding of the manufacturing process of CPVs is required. This research project aims at contributing to an increased level of understanding of CPVs by investigating the influence manufacturing parameters have on the final product quality. This study is done in collaboration with Plastic Omnium, which allowed for the possibility of obtaining experimental data for validation purposes.

The approach followed in this research project is by developing an analytical model that is capable of representing the manufacturing process of CPVs. The objective is to be able to link the manufacturing parameters to the vessel's quality for a given vessel configuration. The analytical model takes the vessel configuration as an input, alongside the definition of the considered manufactured parameters, winding tension force and internal liner pressure, and outputs quantitative predictions of changes in dimensions, compaction and burst performance. The model was found on the basis of adopting a common analysis method for composite materials, Classical Laminate Theory (CLT) and adapting it to be capable of representing the manufacturing process. A major challenge in developing such a model is dealing with uncured composite materials, where different assumptions were imposed for the model to be physically sound.

Hypotheses were generated using the analytical model for eight different vessel configurations, where either the vessel configuration was changed or the magnitude of manufacturing parameters. The proposed experimental campaign consists of microscope inspection and burst testing of 22 sub-scale vessels in total, where the obtained data were used to prove or disprove the hypotheses. The analytical model and experimental results showcased the significant influence varying tension force and internal pressure have on the end-product quality where at different parameter settings, differences up to 4 % in Fiber Volume Fraction (FVF), 4.5 % in porosity content and 8 % in burst performance were observed with respect to a baseline configuration. Changes in vessel configuration, by varying stacking sequence grouping or liner diameter, led to notable differences in compaction and burst performance.

The work presented in this report highlights the significance manufacturing parameters have on the scatter and reliability of CPVs and showcases the possibility of improving mechanical performance for a fixed design. Additionally, a framework is proposed in this work to help in defining the optimum process parameters for different vessel configurations. This work serves as a basis for future investigations into further optimizing the process parameters definition as it has been shown that there is still room for further improvements.





# Acknowledgments

This report marks the end of my five-year journey at TU Delft which did not lack any stress, sweat, and tears but also excitement, satisfaction and fun. As challenging as these years were, they have shaped me into the person I am today and I am eternally grateful for every second of it. Today I am proud to graduate as an Aerospace Engineer from Delft University of Technology, a title I have always dreamt of. Throughout this journey, there are several people that helped me, in some way or another, reach this point that I would like to extend my gratitude towards. However, a simple "thank you" would never suffice for these individuals.

The impact my supervisors have on me goes far beyond an academic level and this thesis work. I consider myself to be incredibly fortunate to be paired with both of my supervisors and mentors, Julien van Campen and Alejandro Soriano Sutil, with whom I will always be proud to be one of their students. To Julien, I would like to thank you and express my gratitude for your constant support throughout this journey, even before embarking on this thesis. Your continuous advice and constructive feedback coupled with doses of encouragement allowed this work to reach the state that it is today. To Alejandro, words can not express how grateful I am for all the support and advice you have provided throughout this thesis work. I will always cherish you being capable of squeezing time for quick calls whenever possible (even when you are in a whole different continent and timezone) and for the early and late hours spent manufacturing.

A thank you also goes to my internship supervisor, Dr. Martin Nebe, who without connecting me with Alejandro, this thesis would have not existed. Thank you is also due to everyone at Plastic Omnium and Delft Aerospace Structures & Materials Laboratory (DASML) that aided in completing the experimental work for this thesis project on such a tight schedule.

I am grateful to my friend group back in Egypt, who are as close as a family now, where we have stuck together since kindergarten and they have always made me feel like I never left. Thank you boys. Throughout my time in Delft, luckily, I was able to form a second family, who were never short of inspiring me and providing unconditional support. To all of them, you know yourself pretty well, thank you for everything.

One of the most valuable lessons I have learnt throughout this journey is the value of family. Thus, the most special thank you goes to my parents, Khaled and Rasha and to my brother Omar. Thank you for teaching me that being far from the eye, does not necessarily mean being far from the heart. Thank you for your continuous support and for always lifting me up whenever I am down. I hope this makes you proud.

There is a whole list of other individuals I would like to mention that have directly or indirectly contributed to this thesis in some way or another, but then this section would extend to more than a single page. To everyone, my deepest thank you and your contribution is deeply appreciated.

To the family we're born with, and the family we make along the way.

*Mohamed Khalifa  
Delft, September 2022*



# Contents

<b>Abstract</b>	<b>iii</b>
<b>Acknowledgments</b>	<b>iii</b>
<b>Nomenclature</b>	<b>vi</b>
<b>1 Introduction</b>	<b>1</b>
1.1 Composite Pressure Vessels in the Automotive Industry	2
1.2 Manufacturing of CPVs	3
1.2.1 Filament Winding Process	3
1.2.2 Filament Winding Trajectories and Patterns	4
1.2.3 Influence of Manufacturing Parameters	6
1.3 Analysis of CPVs	6
1.3.1 Analytical Models	6
1.3.2 Numerical Approaches	8
1.4 Experimental Characterization of CPVs	9
1.4.1 FVF & Porosity Testing	9
1.4.2 Material Coupon Testing for CPVs	10
1.4.3 Burst Pressure Testing	11
1.4.4 Fatigue Performance	12
1.4.5 Strain and Deformation Measurement During Pressurization	12
1.5 Research Focus and Reader's Guide	13
<b>2 Background into Quality Assessment of CPVs</b>	<b>14</b>
2.1 End-Product Quality Definition	14
2.2 Composite Microstructure in Filament Winding	15
2.2.1 Load Application in Composite Materials	15
2.2.2 Consolidation Process	15
2.2.3 Curing Process	16
2.3 Manufacturing Parameters & Vessel Configuration Effect on Quality	16
2.3.1 Relation Between Winding Tension Force and Internal Liner Pressure	16
2.3.2 Influence of Winding Tension on Quality	17
2.3.3 Influence of Stacking Sequence on Quality	19
2.3.4 Influence of Vessel Diameter on Quality	20
2.4 Methodology for Defining Manufacturing Parameters	20
2.4.1 Empirical Approach	20
2.4.2 Residual Stress Approach	21
2.5 Research Objectives and Questions	23
<b>3 Analytical Modelling</b>	<b>25</b>
3.1 Overview of Research Methodology	25
3.2 Analytical Model Description	26
3.2.1 Choice of Analytical Model	26
3.2.2 Model Assumptions	27
3.2.3 CLT Theory and Approach	27
3.2.4 Coordinate System and FBD	29
3.2.5 Material Properties	31
3.2.6 Model Approach and Methodology	31
3.3 Selection of Vessel Configurations & Model Results	33
3.3.1 Baseline Vessel Configuration	34
3.3.2 Summary of Testing Configurations	35
3.3.3 Influence of Varying Winding Tension Force	36
3.3.4 Influence of Varying Internal Pressure	38
3.3.5 Influence of Varying Stacking Sequence	40
3.3.6 Influence of Changing Vessel's Diameter	41
3.4 Analytical Model Hypothesis	43
<b>4 Manufacturing &amp; Experimental Testing</b>	<b>44</b>
4.1 Manufacturing and Burst Testing of CPVs	44
4.1.1 Liner Preparation and Assembly	44

4.1.2	Winding Process	44
4.1.3	Burst Testing	45
4.2	Microscope Sample Preparation and Testing	45
4.2.1	Microscope Sample Preparation	45
4.2.2	Microscope Testing	46
<b>5</b>	<b>Results &amp; Discussion</b>	<b>49</b>
5.1	Dimensions Results	49
5.1.1	Statistical Analysis	49
5.1.2	Observations	50
5.2	Burst Pressure Results	50
5.3	Microscope Testing Results	51
5.3.1	Comparing FVF Methods	53
5.3.2	Comparing Laminate Thickness	54
5.3.3	Statistical Analysis	55
5.3.4	Observations	55
5.4	Discussion	55
5.4.1	Influence of FVF	55
5.4.2	Influence of Winding Tension Force	58
5.4.3	Influence of Internal Liner Pressure	60
5.4.4	Influence of Diameter	63
5.4.5	Influence of Stacking Sequence	66
5.5	Framework for Determining Optimum Process Parameters	68
5.5.1	Limitations and Defects Induced by Tension and Internal Pressure	68
5.5.2	Relating Tension and Pressure with Compaction and Deformation	69
5.5.3	Steps to Derive the Optimum Process Parameters	69
5.5.4	Influence of Stacking Sequence and Diameter	70
<b>6</b>	<b>Conclusions &amp; Outlook</b>	<b>71</b>
6.1	Summary	71
6.1.1	Analytical Model	71
6.1.2	Experimental Campaign	71
6.2	Conclusions	72
6.3	Recommendations for Future Work	74
<b>A</b>	<b>Cylinder Stress Derivation</b>	<b>79</b>
<b>B</b>	<b>Analytical Model Verification</b>	<b>81</b>

# Nomenclature

## Abbreviations

<b>AE</b>	Acoustic Emissions
<b>BEVs</b>	Battery Electric Vehicles
<b>CDM</b>	Continuum Damage Mechanism
<b>CFRP</b>	Carbon Fibre Reinforced Polymer
<b>CLT</b>	Classical Lamination Theory
<b>CNG</b>	Compressed Natural Gas
<b>CPVs</b>	Composite Pressure Vessels
<b>DASML</b>	Delft Aerospace Structures & Materials Laboratory
<b>DOE</b>	Design of Experiment
<b>DIC</b>	Digital Image Correlation
<b>FBG</b>	Fibre Bragg Gratings
<b>FVF</b>	Fiber Volume Fraction
<b>FMF</b>	Fiber Mass Fraction
<b>FCEVs</b>	Fuel-Cell Electric Vehicles
<b>FEA</b>	Finite Element Analysis
<b>GTR</b>	Global Technical Regulation
<b>IA</b>	Image Analysis
<b>ISO</b>	International Standards Organization
<b>ICE</b>	Internal Combustion Engines

## Greek Symbols

$\alpha$	Thermal expansion	[°C <sup>-1</sup> ]
$\theta$	Winding angle	[°]
$\lambda$	Slippage coefficient	[-]
$\mu$	Friction coefficient	[-]
$\mu_d$	Dynamic viscosity	[Kg/ms]
$\delta$	Load transfer length	[m]
$\sigma^{ch}$	Chemical shrinkage stress	[Pa]
$\sigma^{th}$	Thermal stress	[Pa]
$\sigma^{wt}$	Stress by winding tension	[Pa]
$\sigma_c$	Average strength of fiber bundle	[Pa]
$\bar{\sigma}_f$	Average fiber strength	[Pa]
$\sigma_{fr}$	Fiber stress in radial direction	[Pa]
$\sigma_{Mr}$	Mandrel stress in radial direction	[Pa]
$\bar{\sigma}_m$	Average matrix strength	[Pa]
$\sigma_r$	Radial stress	[Pa]
$\sigma_x$	Axial stresses	[Pa]
$\sigma_y$	Hoop stresses	[Pa]
$\sigma_\theta$	Tangential stress	[Pa]
$\bar{\epsilon}_{bf}$	Average bundle strain	[-]
$\epsilon_r$	Radial strain	[-]
$\epsilon_s$	Meridional strain	[-]
$\epsilon_\theta$	Tangential strain	[-]
$\rho_{exp}$	Sample density	[Kg/m <sup>3</sup> ]
$\rho_f$	Fiber density	[Kg/m <sup>3</sup> ]
$\rho_m$	Matrix density	[Kg/m <sup>3</sup> ]
$\rho_{th}$	Theoretical density	[Kg/m <sup>3</sup> ]
$\rho_w$	Density of water	[Kg/m <sup>3</sup> ]
$\nu_m$	Mandrel's poisson's ratio	[-]

## Latin Symbols

A	Extensional stiffness matrix	[N/m]
B	Bending-extension coupling stiffness matrix	[N/m]
D	Bending stiffness matrix	[N/m]
$d_f$	Fiber diameter	[m]
E	Elastic Modulus	[Pa]
$E_f$	Fiber elastic modulus	[Pa]
$E_m$	Resin elastic modulus	[Pa]
$E_m^0$	Uncured resin elastic modulus	[Pa]
$E_m^\infty$	Fully cured resin elastic modulus	[Pa]
$E_1$	Longitudinal elastic modulus	[Pa]
$E_2$	Transverse elastic modulus	[Pa]
$f_b$	Transverse forces	[N]
$f_n$	Lateral forces	[N]
$f_w$	Friction forces	[N]
$G_{12}$	Shear stiffness modulus	[Pa]
$k$	permability	[ $m^2$ ]
L	Fiber bundle length	[m]
$M_a$	Initial mass of sample in air	[Kg]
$M_w$	Mass of sample in water	[Kg]
$N_p$	Number of tows	[-]
$N_s$	Meridional normal force	[N]
$N_\theta$	Tangential force	[N]
P	Consolidation pressure	[Pa]
$P_{ext}$	External pressure	[Pa]
$P_{int}$	Internal liner pressure	[Pa]
$P_r$	Resin pressure	[Pa]
Q	Reduced stiffness matrix	[Pa]
q	Flow rate	[ $m^3/s$ ]
R	Radius of the vessel	[m]
r	Arbitrary radial position	[m]
S	Residual hoop stress	[Pa]
T	Transformation matrix	[°]
$T_w$	Winding tension force	[N]
t	Ply thickness	[m]
u	Displacement	[m]
$u_m$	Mandrel displacement	[m]
$V_f$	Fiber volume fraction	[%]
v	Effective polar opening	[-]
$\nu_{12}$	Longitudinal Poisson's ratio	[-]
w	Bandwidth	[m]
x	Axial coordinate	[m]
Y	Dimensionless radius	[-]

# Introduction

Climate change is a pressing issue that is already impacting human health and putting lives at risk. As governments started growing more aware of the negative impact climate change has, and its direct connection with industrial activity, heavy regulations and incentives have been put into place to shift towards sustainable mobility. This awareness has also reached the public where several social movements emphasized the need for immediate action from the industrial parties. The automotive industry is the highest contributing sector to global emissions, as in the United States, it is responsible for 30% of the produced emissions [1]. As a result, the automotive industry knew no other alternative than to promptly react. This was manifested by the large-scale introduction of Battery Electric Vehicles (BEVs) into the market.

The transition to electric drive is more sustainable in comparison to the usage of Internal Combustion Engines (ICE), which are directly associated with fossil fuel use, emissions and noise [2]. BEVs do also provide performance improvements as they are capable of providing high torque via an efficient conversion from chemical to electric energy that is competitive with high-performance ICE. Nevertheless, the limitation of BEVs stems from the necessity to use batteries as a power source. The currently available batteries have low energy density, which does not exceed 0.15 kWh/kg, which translates into a heavy battery weight making batteries of high power rather unrealistic. Additionally, BEVs are attributed with long charging periods [3]. The forced short driving ranges and slow charging capabilities that are often associated with BEVs, make BEVs more appealing for city use. However, for long-haul applications, the automotive industry was forced to search for a different sustainable alternative.

The environmental impact of long-haul transportation should not be belittled, as according to the Environmental Protection Agency, the trucking industry represents only 1 % of the traffic. However, they still contribute to more than 23 % of the gas emissions of the transportation sector [4]. As BEVs are not applicable for long-haul applications, a pressing need for a different sustainable alternative is present. A prominent solution is offered by Fuel-Cell Electric Vehicles (FCEVs), due to their inherently high gravimetric energy density and rapid fueling times. FCEVs are electrically driven vehicles, where the electrical energy is supplied through a hydrogen-powered fuel cell. Fuel cells are considered the heart of FCEVs, where on a high level, hydrogen is supplied, and electrical energy is generated. The principle of working consists of supplying hydrogen to the anode side and atmospheric oxygen to the cathode side, then stripping hydrogen of its electrons where the electrons flow as electric current. The potential difference, between the anode and cathode, generates electrical voltage, which multiplies by stacking several fuel cells together and forming a fuel cell stack [5]. Consequently, as long as hydrogen and oxygen could be supplied, fuel cells are capable of producing electricity. Thus, refueling in FCEVs revolves around only refueling hydrogen tanks, which is the main reason why FCEVs have shorter refueling times in comparison with BEVs [6].

Hydrogen could be stored in liquid or gaseous form. Commonly hydrogen is stored in a compressed gaseous form. This stems from the low density of hydrogen of around 0.09 g/L, where comparable driving ranges to BEVs and ICE could only be attained by increasing hydrogen fuel density, which in specific is critical for long-haul applications. Typical fuel consumption values for passenger cars are 1 kg for 100 km, whereas for trucks it reaches 10 kg for 100 km, which is why pressurization of hydrogen is inevitable for FCEVs. Standard operating pressure values could reach 700 bars under a safety factor of 2.5 according to EU regulation No 134 [7].

Such a high pressurization level requires a reliable and robust tank capable of withstanding such a high load, whilst confining to the tight weight requirements. As a result, Carbon Fibre Reinforced Polymer (CFRP) directly found their application in pressure vessels due to their inherent high specific properties. An example of Composite Pressure Vessels (CPVs) could be seen in Figure 1.1. The purpose of this work is to boost the reliability levels of CPVs by aiding in the understanding of its manufacturing process in a more concrete manner. In this chapter, an overview of the development of pressure vessels and their regulations is presented in the following section. Afterwards, the state-of-the-art manufacturing method is described, with an introduction to how reliability is affected during manufacturing. This is followed by the applicable analysis methods for CPVs. Lastly, a brief summary of the research focus and the report structure is provided to ensure a smoother reading experience.

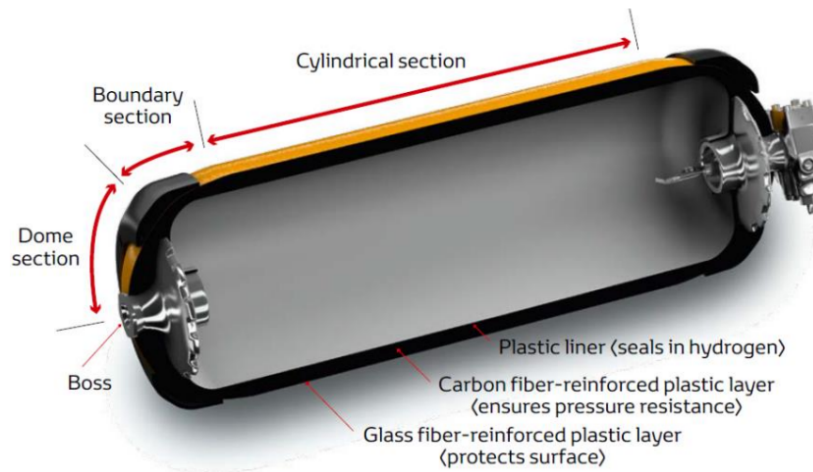


Figure 1.1: Schematic representation of type IV pressure vessels - adapted from [8]

## 1.1. Composite Pressure Vessels in the Automotive Industry

Pressure vessels are a very mature technology that has reached different applications in the aerospace and automotive industry. The most relevant application is in the automotive industry as storage tanks for Compressed Natural Gas (CNG), which is complimentary for the development of pressure vessels for FCEVs [9]. This is as the set of requirements and certification steps are fair similar and follow the same guidelines as EC79 [10] and Internal Standards Organization (ISO) 11439 [11]. Pressure vessels undergo various static and dynamic tests to certify their safety and operational stability by simulating the product use during its lifetime. Based on ISO 19881, pressure vessels that store compressed hydrogen should sustain nominal working pressure of 700 bars, whereas during testing, should reach a higher pressurization value [12].

The performance of a pressure vessel is often assessed via its burst pressure value or the value at which the vessel fails. The required burst pressure for certification should be a factor higher than the nominal working pressure of 700 bars. For example, in Global Technical Regulation (GTR) 13, the regulation limit for burst pressure is  $SF \cdot P_{nom}$ , where  $P_{nom}$  is the nominal working pressure and  $SF$  is a safety factor with values ranging from 2.25-3.5, based on the vessel type.

Pressure vessels used for hydrogen storage are required to be completely airtight as hydrogen is a flammable gas and any leakage could lead to endangering the safety of the passengers. The vessel should be able to safely withstand the designed internal pressure load by storing the compressed hydrogen during the entire lifecycle of the vessel. This should be done simultaneously while keeping the vessel weight as low as possible, to avoid increasing fuel consumption. To provide a larger driving range, pressure vessels should have the highest storage efficiency, while confining with the vehicle's storage requirements. Lastly, for the pressure vessel design and application to remain feasible and competitive, the vessel cost, during manufacturing and lifetime, should be as low as possible.

Spherical pressure vessels provide the highest ratio of volume for material among the different pressure vessel shapes. Also, spherical pressure vessels deliver almost twice the strength of a cylindrical pressure vessel, whilst having the same wall thickness as was concluded by Ibrahim et al. [13]. However, the limitation of spherical pressure vessels is difficulty in confining to the space restrictions imposed by customer requirements in vehicles and the difficulty in manufacturing [14]. Cylindrical pressure vessels with spherical dome ends, as seen in Figure 1.1, are a deviation of spherical pressure vessels designed for vehicle storage efficiency. An alternative prominent option is toroidal pressure vessels, which are an axisymmetric shell of revolution that is a product of revolving an arbitrary 2D shape through 360° [15]. Toroidal pressure vessels are a more volumetrically efficient vessel design, in comparison with cylindrical pressure vessels.

The cylindrical region allows for an increase in volumetric expansion. Ellipsoidal dome ends are chosen rather than flat or hemispherical dome ends as flat ends create high-stress concentrations in the cylindrical region whilst the hemispherical is more space efficient. Ellipsoidal dome ends are a compromise between both dome shapes that creates a smoother cylinder-dome transition region whilst being space efficient. The design of the dome part is critical as this is where the highest stress levels are experienced [16].

The required type and design of pressure vessels vary per application as different requirements are generated then. In Figure 1.2 the different types of pressure vessels could be visualized and are summarized in the list below [11]:



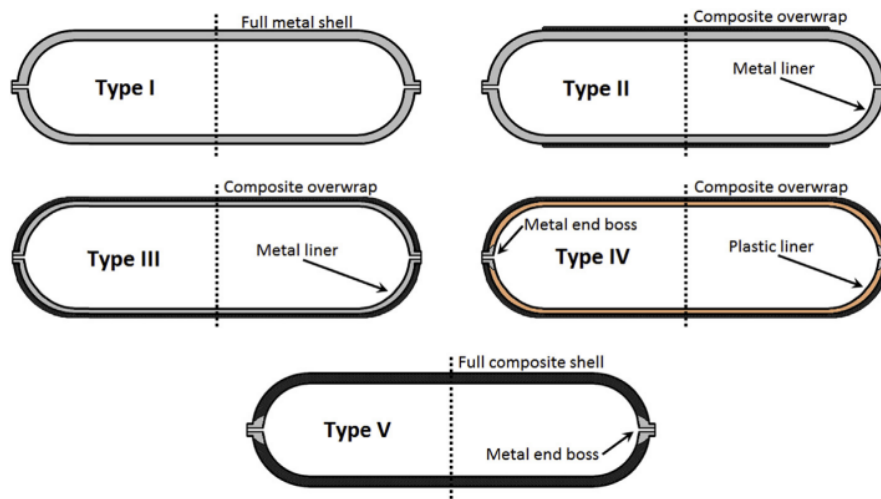


Figure 1.2: Types of pressure vessels - taken from [17]

- Type I: All-metal construction vessel
- Type II: Metal (mostly steel or aluminum) with a composite overwrap in the hoop direction
- Type III: Metal liner with a full composite overwrap
- Type IV: All-composite construction vessel overwrapping a plastic liner
- Type V: Liner-less composite vessel

With an increase in the development of pressure vessels, the usage of composite materials increases progressively. However, this in turn causes an increase in the costs of the pressure vessel but also a significant decrease in the pressure vessel weight due to high specific materials accompanied with CFRP materials. Type I is the cheapest pressure vessel as it is usually made up of steel, which is relatively cheaper in comparison with composite materials. Regarding bearing the structural loads, in type II vessels, the metal vessel and composite overwrap share the structural loads almost equally. While in types III and IV, the composite material bears all the structural loads, where it is assumed that the liner does not contribute to the structural integrity during the design process. Type I and II are most commonly used in CNG applications [18]. For hydrogen storage, type III and IV currently represent the most mature options available, where the difference is whether a metallic or polymer liner is used. Type V pressure vessel is still a relatively new technology and their development is stalled by certification. However, recently type V pressure vessels have found their way into aircraft applications [19].

## 1.2. Manufacturing of CPVs

In this section, the description of the filament winding process, which is the current state-of-the-art manufacturing method for type IV CPVs, and its attributes are described. In subsection 1.2.1, the filament winding technique is introduced along all the different types and a comparison between them. Afterwards, in subsection 1.2.2, the different filament trajectories and patterns possible in filament winding are introduced and profoundly described. Lastly, in subsection 1.2.3, an introduction into the influence manufacturing parameters could have on the end-product quality, and addressing the most influential one, the winding tension force.

### 1.2.1. Filament Winding Process

Originally introduced for use in the aerospace industry, filament winding is considered one of the oldest CFRP manufacturing techniques [20, 21]. Its use in CPVs stems from the fact that it is a well-established, fast and cost-efficient process for pipe- and tube-shaped structures [22]. The concept of filament winding relies on winding continuous filaments of fiber on a rotating mandrel under tension with a prescribed geometrical path [23].

Basic filament winding setups have two degrees of freedom, where the mandrel is allowed to rotate and the delivery eye is capable of moving along the mandrel's axial length. As the complexity of the product geometry increases, additional degrees of freedom are hence required which are attained with the introduction of robot-assisted filament winding technologies such as KUKA machines which can provide six degrees of freedom [24]. The six degrees of freedom are lateral and longitudinal displacement and rotation of the delivery eye and rotation of the mandrel around its longitudinal and vertical axis. These additional degrees of freedom allow for winding CPVs, especially the

complex geometry created by the dome regions.

Mandrels are used during winding to define the geometry of the final product. It could be an integral part of the final product as in type II to IV or could serve as a positive mould that is removed after curing as in type V vessels. Mandrel material should be stiff enough to withstand the applied tension and internal pressure during winding and resist deforming to avoid affecting the geometry of the final product. White and Zhang [25] concluded that the winding material has an influence on the induced residual stresses during manufacturing. Additionally, the thermal expansion of the mandrel during curing could lead to deformation and additional stresses applied to the laminate, which would affect the end-product quality of the vessel. Plastic mandrels are preferred over metal ones due to their lower structural weight. However, plastic has lower tolerance during the production of the mandrels and as it is less stiff, it is more likely to deform during winding and curing. The advantage is that plastic mandrels are associated with lower costs.

Three different filament winding types exist: wet, dry and prepreg winding [26]. Wet winding entails passing pre-tensioned dry fibers and dipping them into a resin bath, then feeding them into a delivery eye where it is wound over the liner. A schematic displaying the wet winding process could be seen in Figure 1.3. Dry winding involved winding dry fibers, and then impregnating the whole structure with resin. In prepreg winding, pre-impregnated fiber tows are wound on the mandrel. The most common and established methods are wet and prepreg winding.

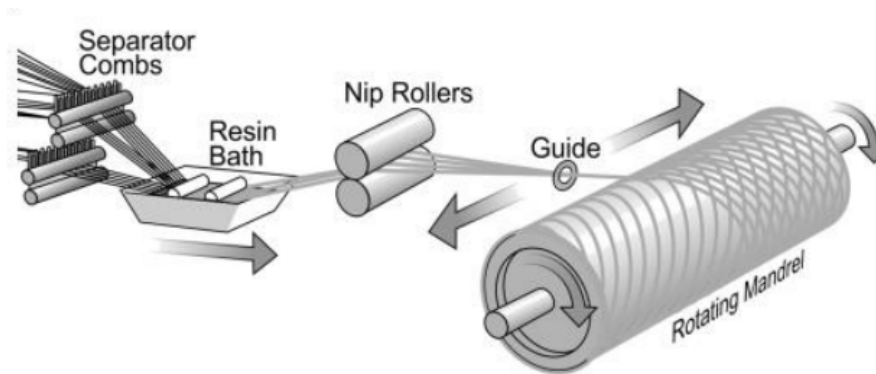


Figure 1.3: Schematic of the wet winding process - taken from [27]

Each winding process type has its advantage and disadvantage, which could be concluded following the process description. The favourable aspects of wet winding are the low costs of raw materials, as prepreg is relatively more expensive, low storage requirements needed and the availability of on-demand change in resin content. However, the resin content is difficult to control throughout the structure, which gives a rise to variability within the final product in terms of the volume content through the thickness. Additionally, wet winding often induces resin dripping and resin accumulation in certain areas which results in a poor external finish, which is not desirable. In the case of CPVs, resin tends to follow a potential gradient and accumulate at the dome regions, which happens in wet and prepreg winding. Moreover, the low resin viscosity required to cover the whole mandrel could lead to fiber slippage as there is no sufficient adhesion to the mandrel.

On the other hand, prepreg winding gives the advantage of controllability of resin content, as the tows are pre-impregnated, which then improves the final product's mechanical performance. Yet, prepreg winding is a more costly method as it requires more expensive material and storage conditions as prepreg needs to be cooled while stored.

Dry winding is similar to wet winding, where the difference is that resin is added after winding, thus, the advantages and disadvantages are similar. The difference is that dry winding grants higher resin content control and a disadvantage of being a two-step process, which requires more time (less time to wind but more time for the whole process), handling and costly as additional equipment would be needed to introduce the resin as vacuum bags, pumps, etc.

### 1.2.2. Filament Winding Trajectories and Patterns

Two different fiber trajectories are possible in filament winding, which are geodesic and non-geodesic trajectories [26]. Geodesic trajectories connect two arbitrary points by utilizing the shortest possible way by minimizing the arc length. Subsequently, this leads to geodesic trajectories being the most stable and economic technique for covering the surface of the mandrel during filament winding [28]. Geodesic trajectories for pressure vessels could be described using the following equation [28]:

$$\theta = \arcsin\left(\frac{\nu}{Y}\right) \quad (1.1)$$

where  $\theta$  is the winding angle,  $Y$  is dimensionless radius and  $\nu$  is dimensionless effective polar opening. Geodesic trajectories provide high tow stability but still limit the design space by limiting the available winding angle. By utilizing non-geodesic fiber trajectories, a larger design space is possible as it allows friction trajectories over the surface. The formulation and evaluation of non-geodesic trajectories are complicated where they are often determined with numerical solutions due to the inclusion of friction. Such numerical solutions have been earlier developed by Hoj-jati et al. [29] and Johansen et al. [30]. Further developments has been followed, where an example of a numerical solution for CPVs is presented by Zu et al. [31] in the following equation where  $r$  denotes an arbitrary position on the curved surface,  $x$  denotes the axial coordinate on the surface and  $\lambda$  denotes the slippage coefficient.

$$\frac{d\theta}{dx} = \lambda \left[ \frac{\sin\theta \tan\theta}{r} - \frac{r''}{1+r'^2} \cos\theta \right] - \frac{r' \tan\theta}{r} \quad (1.2)$$

Stability in non-geodesic winding is indicated by  $\lambda$  where it is represented by the ratio of transverse forces,  $f_b$ , to normal forces acting on the surface,  $f_n$ , represented in the following equation:

$$\lambda = \frac{f_b}{f_n} \quad (1.3)$$

As the transverse forces are counteracted by the friction force, the path is considered stable if the friction force is larger than the transverse forces, which could be written as follows, where  $f_w$  indicates the friction force and  $\mu$  indicates the friction coefficient.

$$|f_b| \leq |f_w| = |\mu f_n| \quad (1.4)$$

As a consequence, the non-geodesic path is considered stable if the friction coefficient,  $\mu$ , is larger than the slippage coefficient,  $\lambda$ . When  $\lambda$  is 0, the solution then results in a geodesic fiber path. When  $\lambda \neq 0$ , an iterative solution is used to obtain the non-geodesic winding trajectory as Runge-Kutta algorithm [32].

There are three different types of winding patterns, hoop, helical and polar, which could be visualized in Figure 1.4. Hoop (or circumferential) layer patterns are a product of winding at  $90^\circ$  alongside the tangential direction of the vessel. Helical layers are wound at a particular winding angle,  $\theta$ , turn at the end of the mandrel and return in the opposite direction with a winding angle of  $-\theta$ . The helical layers winding angles are between  $5-80^\circ$  [26]. In essence, hoop patterns are a specific case of helical patterns where the winding angle is  $90^\circ$ . Lastly, in a polar winding pattern, fibers are wound in a tangential direction to the polar opening of the mandrel, where the winding angles range between  $0-5^\circ$ . The trajectories and patterns are interlinked where trajectories could not allow certain patterns. Non-geodesic trajectory allows for all three different winding patterns but geodesic trajectory does not allow for polar winding due to its definition.

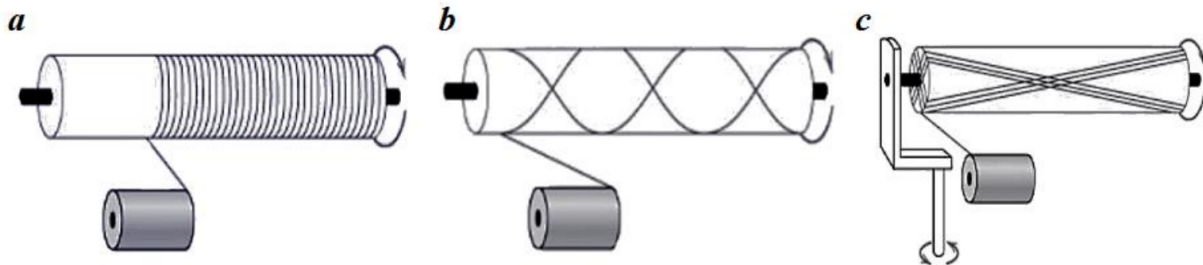


Figure 1.4: Schematic representation of three types of winding patterns; a) hoop winding; b) helical winding; c) polar winding - taken from [33]

Circumferential layers are used to wind the cylindrical part of the vessel, which provides an effective reinforcement to withstand tangential loads that are experienced. However, hoop patterns are not capable of covering the dome region of the vessel as fiber slippage would occur. As a result, helical layers are used to wind the dome region of the vessel. A distinction could be made between high and low-angle helical layers, where high-angle helical layers are used to reinforce the cylindrical region and tailor the tangential stiffness distribution in the transition area between

the dome and cylinder. Low-angle helical layers are used to withstand the meridional loads and provide structural integrity to domes [34]. Helical layers are also used to prevent a large stiffness gap between the cylindrical and dome section as that could lead to premature failure.

The number of tows,  $N_p$ , could be found using Equation 1.5, where  $R$  represents vessel radius and  $w$  is tow bandwidth [28]. An integer number of tows is preferred, otherwise, there would be overlap between tows. Depending on the magnitude of overlap, this could lead to an increase in the amount of material used, weight and cost, where the target is to always decrease these factors.

$$N_p = \frac{2\pi R}{w} \cos\theta \quad (1.5)$$

### 1.2.3. Influence of Manufacturing Parameters

During filament winding, the composite microstructure is formed. Manufacturing parameters could have a strong influence on the formation of the microstructure. Thus, understanding the influence each parameter could have and how to control it is essential on the road to improving CPVs reliability levels. In one of the earliest investigations, Cohen [35], investigated the influence of five different process parameters on the final product quality using a Design of Experiment (DOE) testing technique. These variables are:

- Winding tension force;
- Stacking sequence;
- Tension force gradient;
- Winding time;
- Cut vs uncut helical layers.

The final product quality was assessed based on the vessel's mechanical performance, Fiber Volume Fraction (FVF), resin and void content and residual stresses. The main conclusion of this investigation was that the winding tension force had the largest impact, in comparison with these other parameters. Increasing the winding tension force had a significant impact on the FVF, resin and void content distribution through the thickness and the burst pressure performance. To get a feel of the difference in increasing the tension force, by shifting the tension settings from low to high (almost 2 times higher), an observed 22.8 % increase in FVF gradient through the thickness, 9 % increase in FVF of the whole laminate and 23 % decrease in void content.

This conclusion of the significant influence of winding tension force was also observed by Mertiny and Ellyin [36], where a sole focus was implied on the effect of the winding tension force. A 60 % increase in tension force resulted in an increase in burst performance using ring tests and an absolute increase of almost 4 % in FVF. As a result, a strong correlation exists between varying the tension force and the vessel's mechanical performance. Other investigations were reviewed on the influence of different process parameters. However, the influence of winding tension force still surpasses these other process parameters.

The tension force is strongly linked with another manufacturing parameter, internal liner pressure, which is often overlooked as it is a more relevant parameter for type IV vessels. The interaction between these parameters is what defines the consolidation of the composite microstructure and defines the final geometry of the vessel. As a result, these parameters go by side by side and should be considered together, not independently.

## 1.3. Analysis of CPVs

Modelling of CPVs is a topic that has received much attention in literature where different analytical and numerical strategies have been proposed. Therefore, the background regarding the analysis of CPVs is rather extensive. Analytical models available vary greatly in complexity, where it begins with the relatively simple netting theory that the loads are carried exclusively by fibers [37], progressing towards Classical Lamination Theory (CLT) where the matrix is then taken into account [29, 38, 39, 40] and finally thick-walled theory where stress gradients through the thickness are accounted for [41]. As currently, a comprehensive analytical framework that is capable of detailing the stress state of CPVs accurately is not available, the focus is usually directed towards numerical and Finite Element Analysis (FEA) methods. In this section, these methods and approaches will be briefly discussed with emphasis put on their applicability and limitations.

### 1.3.1. Analytical Models

#### Netting Theory

The netting theory assumes that in the composite structure, the fibers are the only load-bearing structure carrying tensile loads, while the matrix contribution is disregarded. These tensile loads are introduced via the fiber tension while winding. Additionally, it is assumed that out-of-plane loads are not experienced by the composite structure, and all the experienced loads are membrane. Consequently, the optimum design of a vessel using the netting theory is an isotensoid solution, which is solely based on layering fiber orientations to carry tensile loads [42]. The relationship between the in-plane membrane loads and fiber tension in a bidirectional helical layer could be described using the following equation [43] where  $\sigma_f$  denotes fiber stress,  $t$  is ply thickness and  $\theta$  is the ply angle:

$$\begin{aligned} N_s &= \sigma_f t \cos^2 \theta \\ N_\theta &= \sigma_f t \sin^2 \theta \\ N_{s\theta} &= 0 \end{aligned} \quad (1.6)$$

### CLT

The contribution of the matrix strength is not negligible and has a critical role in withstanding internal forces. This contribution is included in CLT, which is considered a more detailed analysis method in comparison with the netting theory. The CLT analysis approach could be coupled to both winding trajectories, geodesic and non-geodesic, to allow for a detailed analysis of the dome shape and contour. However, due to the thin-wall assumption, which is not true for CPVs, the prediction of the thickness build-up is often inaccurate or with low confidence. There are several examples in literature for the use of CLT to predict the dome shape as by Hojjati et al. [29] where CLT is used to address the orthotropy of the composite material while a geodesic path is utilized by the filaments where it was displayed that the influence of matrix strength is significant on the dome shape solution. Additionally, in the work of Liang et al. [37], the optimum dome shape is compared to the one proposed by the netting theory methods by using geodesic filament winding paths, where the Tsai-Wu failure criterion is used. For helically wound layers, the force and moment resultants could be displayed using Equation 1.7 where A is the extensional stiffness matrix where subscripts  $_{s,\theta}$  denote global component axes and  $_{1-2}$  are local axes.

$$\begin{pmatrix} N_s \\ N_\theta \end{pmatrix} = \begin{bmatrix} A_{11} & A_{12} \\ A_{21} & A_{22} \end{bmatrix} \cdot \begin{pmatrix} \varepsilon_s \\ \varepsilon_\theta \end{pmatrix} \quad (1.7)$$

Both CLT and netting theory are distinguished by their low computational cost, whilst the CLT provides a higher level of complexity by being capable of capturing a larger range of effects in the analysis of CPVs. Apart from dome shape optimization, CLT has been used in other applications in literature. An example by Alcantar et al. [38] where a method to optimize the stacking sequence and thickness for CPVs utilizing CLT was proposed. However, this study does not solely rely on CPVs as the use of FEA is also involved. Additional work have also been proposed where the burst pressure was predicted using CPVs [39, 40]. The main limitation of CLT lies in its thin-walled assumption.

### 3D thick-walled theory

Due to the isostrain assumption followed by CLT which lowers its validity, there has been work into the use of thick wall analysis for CPVs. The approach provides a sufficient level of detail, but only for the cylindrical section of CPVs due to the complex geometries of the dome and cylinder-dome transition regions. In thick-walled theory, the displacement and radial stresses of the mandrel are expressed as follows:

$$\begin{bmatrix} u_{Mr} \\ \sigma_{Mr} \end{bmatrix} = \begin{bmatrix} r & \frac{1}{r} \\ \frac{E_M}{1-\nu_M} & \frac{E_M}{1+\nu_M} \frac{1}{r^2} \end{bmatrix} \begin{bmatrix} A \\ B \end{bmatrix} \quad (1.8)$$

where  $u_{Mr}$  and  $\sigma_{Mr}$  are the displacement and mandrel stress in radial direction respectively.  $E_m$  is the mandrel's stiffness,  $\nu_m$  is Poisson's ratio, A and B are constants and r is the mandrel radius. By setting boundary conditions on the cylinder, the strains in the cylinder could be determined alongside the stresses. By utilizing the following mechanical equilibrium expression, the stress distribution in the radial direction could be computed.

$$\frac{d\sigma_r}{dr} + \frac{\sigma_r - \sigma_\theta}{r} = 0 \quad (1.9)$$

The main limitation to the thick-walled theory is that it is limited to the cylindrical section of the vessel. The CPVs structural integrity is determined not entirely by the cylinder, but by the dome and cylinder-dome transition region. Additionally, information is missing by disregarding the domes as the dome constrains the cylinder via a rigid connection. This leads to bending loads at the cylinder-dome transition region as investigated by Balicevic et al. [41]. The meridional moment distribution could be displayed in Figure 1.5.

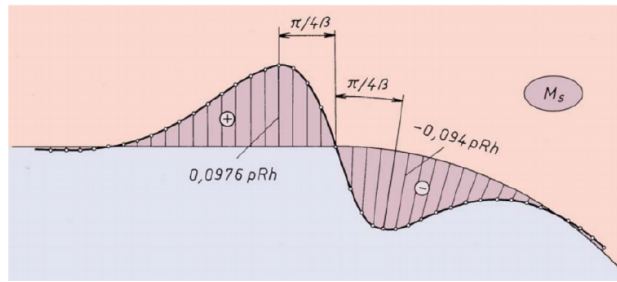


Figure 1.5: Variation of meridional moments in an isotropic vessel - taken from [41]

### 1.3.2. Numerical Approaches

As a consequence, to bridge this gap in the analysis methods and decrease the level of complexity, **FEA** is often used. This is motivated by the possibility to discretize complex geometries, accounting for material non-linearity at the material level, model large deformations and reproduce contacts between components [34]. As a result, this enables failure prediction of **CPVs**.

Different approaches exist for numerical modelling of **CPVs**. The most commonly used approach is the meoscale approach where the composite material and its constituents are viewed as a homogeneous orthotropic continuum. In the works of Leh et al. [44, 45, 46], a methodology for describing the geometry of **CPVs** was proposed based on using axis-symmetric shell elements where an example of the thickness build-up computations could be displayed in [Figure 1.6](#).

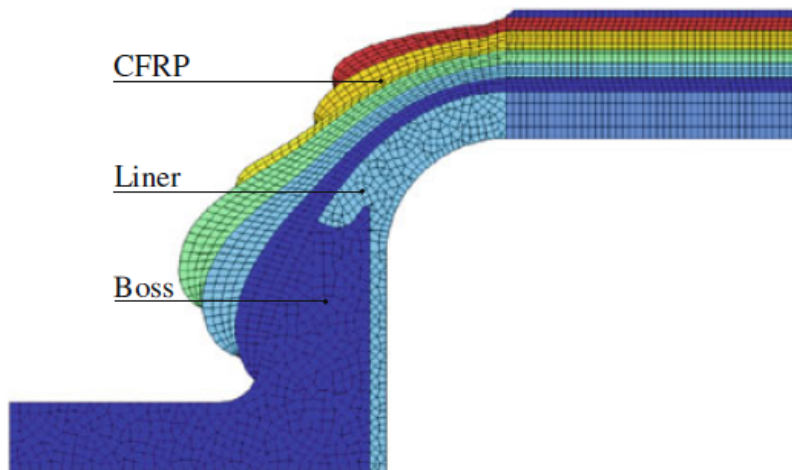


Figure 1.6: Finite Element model of **CPVs** composed of CFRP, liner and boss where distinct colors indicate different materials - taken from [45]

An advantage of such a modelling approach is that it allows for capturing damage progression trends and final burst pressure values. For damage progression, different failure criteria could be used as Hashin-Rottem [47], where an example was displayed by Wang et al. [48] based on Continuum Damage Mechanism (**CDM**). Ramirez et al. [49] also developed a model based on damage progression to predict the final burst pressure value of **CPVs**. An issue that was observed in all these previous models, was that the predicted burst pressure was underestimated in comparison with the one obtained from experimental results. Several reasons exist for such an inaccuracy, but one of the main points was not accounting for layer compaction leading to not accounting for material porosity variation in the vessel. Ellul and Camilleri [50] took into account such an effect and managed to find a good fit by using first ply failure criteria.

In more recent work, Nebe et al. [51] managed to find highly accurate predictions of the deformation behaviour, which was observed when compared with Digital Image Correlation (**DIC**) results. Additionally, by utilizing damage progression trends, the model was capable of predicting the burst pressure with a relatively high level of accuracy, which differs based on the vessel configuration. Such a high-fidelity model aids in providing answers for complex issues where the understanding may not be sufficient. However, this model was accompanied by high computational cost, which in an industrial context, is not practical for rapid iteration or optimization procedures. For seamless integration in the industry, a model would need to be computationally efficient, which would then require putting

less focus on being capable of capturing the full magnitude of damage mechanisms that may occur. But rather focus on the critical aspect that has the highest impact on the burst pressure prediction.

## 1.4. Experimental Characterization of CPVs

To assess the validity of the chosen analytical or numerical model, experimental work is often needed. In this section, an overview of the possible experimental setup in literature used for evaluating the end-product quality and mechanical response of the vessel is addressed and explained. Starting on a material level, the methods to determine the FVF and void content/porosity are explained in subsection 1.4.1. Following that, material coupon testing is addressed in subsection 1.4.2 to derive the mechanical properties of the plies to be used in analysis techniques. On a vessel level, one of the main assessment techniques is burst pressure testing, which is reviewed in subsection 1.4.3 and fatigue performance in subsection 1.4.4. Possible strain and deformation measurement methods during pressurization are addressed in subsection 1.4.5.

### 1.4.1. FVF & Porosity Testing

Measuring the FVF and porosity content of vessels could be used as a direct link between changes in configurations and the vessel's mechanical performance. There are four different methods to determine the fiber volume fraction; Archimedes test (ASTM D2734-16 [52], ASTM D792-13 [53]), resin burn-off, matrix digestion (ASTM D3171-15 [54]) and optical microscopy [55]. For these testing techniques, samples would need to be extracted by cutting the vessel. Therefore, vessels or rings would be manufactured for the sole purpose of FVF and porosity measurement.

#### Archimedes Test

Archimedes test is considered the simplest technique, where the void content could be estimated. The first step entails weighing the sample first in the air at around 23 °C. The next step is to immerse the sample in distilled water whilst maintaining the same temperature, then the mass is recorded again. To ensure a high level of reliability, this process could be repeated with different samples for the same vessel/ring. The specimen density could be computed using the following equation [55]:

$$\rho_{\text{exp}} = \frac{M_a}{(M_a - M_w)} \times \rho_w \quad (1.10)$$

where  $\rho_{\text{exp}}$  is the density of the sample,  $M_a$  is the initial mass in air,  $M_w$  is the mass in distilled water and  $\rho_w$  is the density of water. The theoretical density is computed using rule of mixture:

$$\rho_{th} = V_f \times \rho_f + (1 - V_f) \times \rho_m \quad (1.11)$$

where  $\rho_{th}$  is the theoretical density, subscript  $\rho_f$  indicates fiber and  $\rho_m$  indicates matrix. Afterwards, the void content could be found using the following equation:

$$\text{Void \%} = \frac{\rho_{th} - \rho_{\text{exp}}}{\rho_{th}} \times 100 \quad (1.12)$$

#### Resin Burn-off

The second method is resin burn-off, which is similar to the Archimedes test, where the sample is weighted and the expected composite density is determined using Equation 1.10. In this test, the sample is placed in an oven or a furnace at high temperatures to ensure complete burn-off of the resin in the sample. Afterwards, the sample is cooled and then weighted again. FVF, resin and void content could be found using the following three equations respectively [55]:

$$\begin{aligned} V_f &= \frac{M_2}{M_1} \times \frac{\rho_{\text{exp}}}{\rho_f} \\ V_m &= \frac{M_1 - M_2}{M_1} \times \frac{\rho_{\text{exp}}}{\rho_m} \\ \text{Void \%} &= (1 - V_f - V_m) \times 100 \end{aligned} \quad (1.13)$$

#### Acid Digestion

The following method is acid digestion, which essentially follows the same step as the resin burn-off. The difference is the approach in which the resin is removed. In this method, the resin is removed from the sample using nitric acid,

or any acid of a similar acidity based on ASTM D3171 [54]. The sample is then washed with both water and acetone and the remaining sample is dried in an oven. Once cooled down, the sample mass is measured and the previous set of equations could be used to find the FVF, resin and void content.

### Optical Microscopy

The last and most accurate method is optical microscopy. This method is based on Image Analysis (IA) estimation methods. Samples are placed in resin moulds to hold them in place and stabilize it under the microscope. It is then followed by grinding and polishing to have a clear vision of the cross-sectional surface to clearly distinguish the constituents of the composite microstructure. If the sample is cut in a way that the fiber direction of the cross-section is out-of-plane, the fiber diameter could be clearly visualized as seen in Figure 1.7. Voids could be identified as dark regions in such an image.

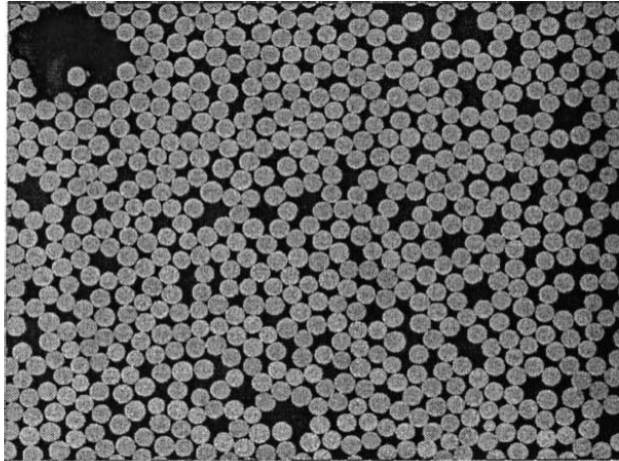


Figure 1.7: Image analysis results from optical microscope to determine FVF and void content - taken from [56]

Once an image is captured, additional post-processing steps are required, either using software or probabilistic function as Weibull distribution [57]. The approach followed is that for every pixel, an intensity value is assigned that is in the grey scale. Based on iterating and finding the intensity that selects the fibers, voids or resin, the volume content could be found by counting the number of pixels with such intensity with respect to the total number.

### Discussion

Comparing all these aforementioned techniques, the Archimedes test has the lowest accuracy and could only be used to estimate the void content. As additional information as FVF and resin content are often needed, such a method is not preferred. Moreover, resin-burn-off and acid digestion are of a similar level of accuracy as they are based on a similar approach. However, both methods come at a disadvantage in that there is a risk of burning off or dissolving the fibers or not having all the resin removed. An additional disadvantage is that information regarding the FVF, resin and void content distribution through the thickness is not possible to extract. Both methods are commonly used as various examples in literature are present for the use of resin burn-off [58, 59, 60] and acid digestion [34]. Optical microscopy is considered the most accurate method, however, it is very localized since the image taken at high magnification might not give a representation of the full sample. If multiple images or the entire sample is to be captured at high magnification, it would be very time-consuming. It also requires expensive equipment such as laser microscopes, which may not be accessible in every lab. Hence, for this research project, optical microscopy was preferred over the remaining approaches due to its high accuracy and the possibility of extracting additional data and images that would be helpful when comparing different configurations.

#### 1.4.2. Material Coupon Testing for CPVs

On a material level, strength and stiffness are important properties to be determined for composite materials. For CPVs, the coupon specimen should have been manufactured in a similar fashion as the actual vessel to give an accurate representation. To determine the properties of hoop layers, unidirectional flat plates are manufactured using filament winding while bi-directional are prepared for helical layers, where an example could be displayed in Figure 1.8. It should also be ensured that a similar curing level is achieved, which could lead that different curing being required as applying the same curing cycle to a flat plate and thick vessel would lead to burning the thin laminate or an insufficient cure level for the vessel.





Figure 1.8: Example of manufacturing of unidirectional flat test plates to determine material properties of hoop layers - taken from [61]

Ring samples are often manufactured for testing the transverse and shear properties of the vessel and inducing a ring expansion test. The difficulty in this approach is in applying uniform pressure without risking the possibility of inducing bending or stress concentrations. Additionally, ring samples create free-edge conditions, which are not representative of an actual vessel.

The simplest form of testing material properties is a flat material coupon, other options arise as rings, thin and thick-walled cylinders and an entire vessel. The accuracy of the obtained data increases progressively, but so does the complexity, cost and time. Thus, it is usually a trade-off between resources and reliability. To determine tensile properties of the flat test coupon, ASTM D3039/D3039M-07 [62] or ISO 527 [63] could be followed where the longitudinal and transverse elastic modulus could be obtained from testing the specimen at 0 and 90 °. For determining shear properties, ASTM D3518-94 [64] is used. Strain gauges are attached to measure the strain during these tests, and based on the force-displacement and stress-strain graphs, the properties could be directly determined.

### 1.4.3. Burst Pressure Testing

The testing standard followed in burst pressure testing is KHKS-0121 [65] where the vessel is clamped to keep in place whilst allowing axial and tangential expansion. Water is used as a pressurant during testing to reduce the energy released after a burst, making it safer than using any gas. Depending on the following regulation or standard, the loading rate and profile vary accordingly.

Different information could be extracted during burst testing vessels. The more the required information, the more complexity of the setup increases as additional equipment is now required. For example, if just the burst pressure value is required, then a chamber preventing debris from spreading and a pressure pump are required. If additional information is required, such as recording the vessel whilst testing, then a high-speed camera would need to be fitted with protection. An example of an advanced test setup was presented by Nebe [34], where information such as Acoustic Emissions (AE) and in-line strain measurement was recorded.

A common difficulty during testing is improper fitting and clamping to the boss parts of the vessel to the test chamber. This would lead to premature leaking and prevent the from reaching the required pressure values. Additionally, ensuring there is not any entrapped air between the sample and bearing to avoid water not evenly pressurizing the vessel is an aspect that could lead to unexpected failure modes. O-rings are designed to fit in boss parts to ensure proper fitting with the pressure pump to avoid water leakage.

Burst pressure values, as discussed in section 2.1, are one of the criteria that assess the end-product quality and could be used to give an indication of the mechanical performance of the vessel. As a result, during design iteration, it could be used as one of the assessment methods to investigate the influence of changing a design parameter. An example by Onder [58] where it was used as an assessment method by checking the influence of varying the stacking sequence. Additionally, Cohen [35] and Mertiny and Ellyin [66] used it to relate to changing the process parameters.

#### 1.4.4. Fatigue Performance

To assess the fatigue performance of pressure vessels, the vessels are loaded to the nominal working pressure for a defined amount of cycles in a so-called "cyclic loading" test. This type of testing is usually very expensive as it is energy demanding, thus, it is usually preceded by extensive numerical simulations to minimize the number of cyclic tests required. Cyclic tests are required by regulations as mentioned in EC79 [67], R134 [7] and GTR - 13 [68]. The vessel is required to pass as many cycles as required under ambient temperature (i.e. 22000), of which 11000 should be without any leaks. The composite material is commonly not the limiting factor during cyclic testing but the boss parts are.

#### 1.4.5. Strain and Deformation Measurement During Pressurization

Inline strain measurement during pressurization could provide valuable information. It could be used to validate failure mode and locations obtained from numerical simulations, where iteration could lead to a higher accuracy numerical model. Additionally, it could be used to explain the unexpected difference in burst pressure performance between expected and observed. Manufacturing-induced parameters, such as winding tension and internal pressure, could trigger the appearance of non-axisymmetric phenomenons [34]. An example would be tow slippage due to changes in these aforementioned parameters, which could lead to a local accumulation of wrinkled material in a certain area of the vessel. This defect could be a trigger for premature failure of the vessel, leading to an unexpected lower failure pressure. Thus, in-line monitoring of strain whilst pressurization could be used to identify such defects.

The most common option for in-line strain monitoring is strain gauges. During pressurization, the strain gauge deforms creating a change in resistance, which is recorded then strain could be obtained and correlated with the applied loads. Strain gauges are a very well-established and feasible option for strain measurements. The strain gauge should be aligned in the fiber direction, whether for helical or circumferential layers, to measure the change in length of these fiber tows. However, strain gauges only give information regarding surface strains, not through thickness deformation. Additionally, the focus should be applied while installing strain gauges as they are sensitive to inaccuracy if improper adhesion and care are given.

To obtain information on stress and strain distribution, Fibre Bragg Gratings (FBG) is used. FBG contains embedded optical glass fibers that are joined to the fibers whilst winding at the required layers. The strain deforms and breaks the fiber as the carbon fiber and FBG experience the same strain but different stresses due to the difference in stiffness between glass and carbon fiber. During pressurization, the light spectrum profile is altered, leading to a change in light wavelength, allowing for the determination of the magnitude and location of deformation. FBG is a more complicated method, in comparison with strain gauges, that requires experts for their application. In Figure 1.9, an example of a composite overlap vessel with FBG installed for structural health measurement.

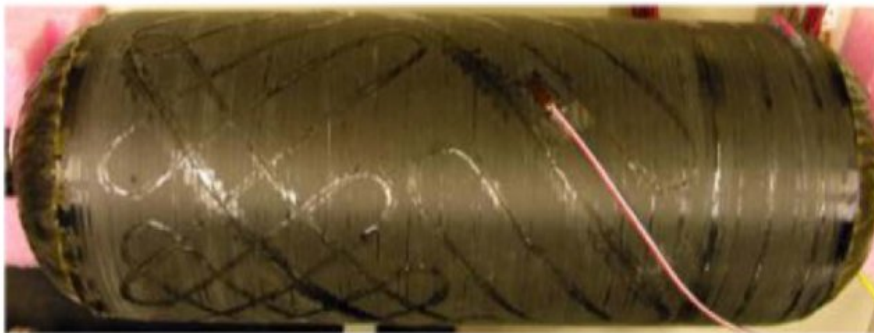


Figure 1.9: Composite pressure vessel with a surface-mounted FBG for inline strain measurement - taken from [69]

A third possible method for measuring surface strain during testing is DIC, which is a non-destructive 3D non-contact measurement technique. A random pattern of black and white dots is painted on the surface of the vessel to create a 50-50 contrast. A reference image before the deformation of the pattern is taken, then at again at different stages of pressurization. During pressurization, the pattern deforms and changes its location, thus, by comparing the images during pressurization with the reference image, information regarding deformation could be obtained. Multiple images could be taken from different locations and grouped together to extract information regarding the deformation of different sections of the vessel. An example of such an approach could be seen in Figure 1.10. However, DIC is heavily influenced by errors due to image noise levels, change in lens's focal length and quality of the applied pattern due to the use of protection glass [70]. Thus, DIC could be correlated with strain gauges to increase reliability levels of surface strain, but DIC would not obtain deformation measurement at locations where strain

gauges are attached. An option for full strain coverage is using **DIC** for surface strain and **FBG** for through the thickness strain measurement.

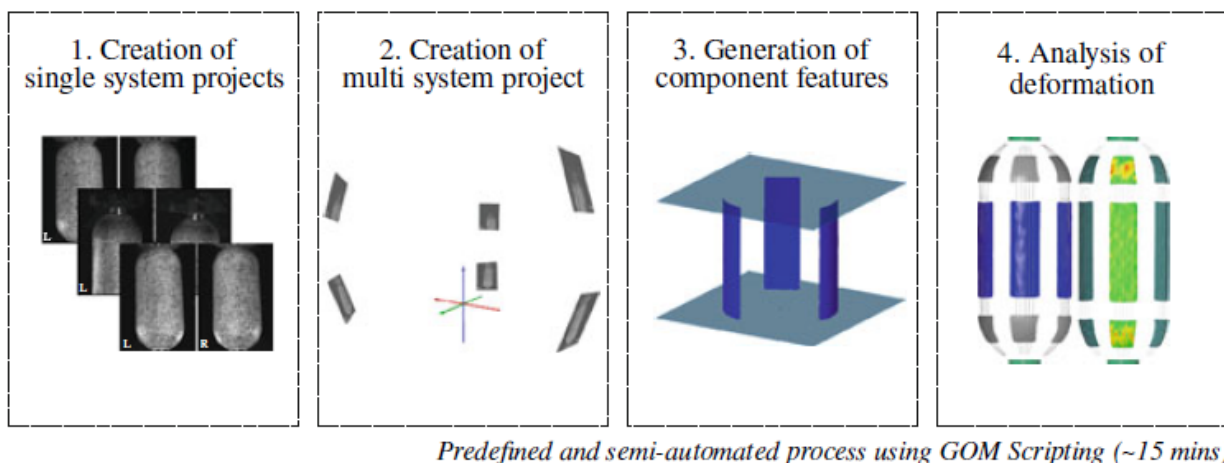


Figure 1.10: Overview of individual steps for the DIC postprocessing workflow - taken from [34]

**AE** signals emitted during pressurization could be detected by piezoelectric sensors, whether these signals are structure or airborne. In post-processing, the failure location and source could be identified. The produced **AE** vary based on the failed layers, where circumferential layers produce loud and clear emissions and helical layers produce low emissions, leading to difficulty in correlation as investigated by Torres [71]. Based on ASTM E1067/E1067M-18 standard [72], the vessel is loaded and unloaded progressively, then **AE** are monitored and compared to previous loading stages. Thus, **AE** is an option for full-scale strain monitoring but is a very complex technique.

## 1.5. Research Focus and Reader's Guide

The goal of this research project is to contribute to increasing the reliability levels of **CPVs**. Reliable **CPVs** are the ones that burst within the designed range and could handle the designed pressurized cycles, not necessarily the safest vessels. As discussed in subsection 1.2.3, manufacturing parameters play a significant role in the differences between burst pressure predictions and experimental results, especially the winding tension force. Therefore, to bridge this gap between analytical or numerical predictions and experimental results, a higher understanding of the influence these manufacturing parameters have on the final product quality is essential. This is also helpful in order to maximize the attainable mechanical performance for a fixed vessel configuration.

As a result, this thesis aims at investigating how two filament winding manufacturing parameters, winding tension force and internal liner pressure, affect the vessel's quality. Internal liner pressure was also included because these two parameters are heavily interlinked, and their interaction is what defines the consolidation process and the final vessel's dimensions. More in-depth investigation on the quality assessment, consolidation process, influence of manufacturing parameters on quality and methods of predicting them are addressed in chapter 2. Based on such an investigation, the research objectives and questions are then derived in the same chapter.

Analytical models commonly available for **CPVs** only consider the structure once cured, as seen in section 1.3 and thus, do not take into account the influence of the manufacturing parameters. To be able to do so, the analytical model needs to model the winding process and the loads that are experienced by uncured composite whilst winding. An analytical model capable of modelling such a scenario and relating the manufacturing parameters to the end-product quality via a quantitative analysis was developed and is described in chapter 3.

To compare and validate the predictions of the analytical model by varying manufacturing parameters and vessel configurations (stacking sequence and diameter), an experimental campaign was set, following the review in section 1.4, which is described in chapter 4. The results are then presented in chapter 5. In the same chapter, it is followed by a discussion and a comparison of the proposed hypothesis via the analytical model and the experimental results. The chapter is concluded with a proposed framework to derive the optimum process parameters for a given vessel configuration. Lastly, the report is finalized with a conclusion and recommendations for further work in chapter 6.

## Background into Quality Assessment of CPVs

This chapter is the main pillar of the literature review where the manufacturing process parameters involved in the filament winding process are related to the end-product quality. To start with, in [section 2.1](#), the term end-product quality is defined as it would be frequently used in this report. Afterwards, in [section 2.2](#), the changes in the composite microstructure and the consolidation process that occur during manufacturing are explained. The motivation behind choosing winding tension force and internal liner pressure, their relationship and influence on the product quality is profoundly discussed in [section 2.3](#). Furthermore, the current state-of-the-art methods commonly available in industry and literature to predict the required process parameters are summarized and discussed in [section 2.4](#). Concluding this literature review with stating the research objectives and questions in [section 2.5](#).

### 2.1. End-Product Quality Definition

Pressure vessels are commonly assessed based on their burst pressure performance, the pressure value at which the structure fails. However, there are several additional criteria on which the quality of the vessel is determined. Criteria either stem from customer requirements or imposed regulations. Below is a summary of the quality assessment criteria typically involved with pressure vessels:

- Burst pressure performance
- Fatigue performance
- Production cost
- Life-time cost
- Weight
- Volume
- Robustness and repeatability

Under [GTR-13](#) [67], the burst pressure value needs to be 225 % of the nominal working pressure, which is 700 bars for hydrogen storage. Not only attaining a burst pressure value is sufficient, but also a specific kind of failure is required, such as failure in the cylindrical region. Moreover, the vessel needs to withstand the nominal working pressure for a certain amount of cycles without leaks, which is what determines the vessel's fatigue performance. Additional performance parameters also exist as leaks and deformation nature [73].

The current trend in [FCEVs](#) is to tighten the customer requirements, thus, decreasing costs and weight and increasing the attainable volume. Decreasing the costs associated with pressure vessels would directly decrease the costs of [FCEVs](#), making it a more feasible alternative. In addition, decreasing the weight of the vessel would lead to less hydrogen needed, which could trigger a snowball effect leading to a more efficient design. To sustain the attainable driving ranges with [FCEVs](#), the volume needs to be maximized within the design of the geometry of pressure vessels. This is the main reason why cylindrical pressure vessels with spherical dome ends are opted for, as they provide the highest volumetric efficiency whilst confining with space requirements.

A developing issue with type IV [CPVs](#), when compared with metallic pressure vessels, have lower reliability in their performance. In this context, reliability is defined as the vessel's ability to consistently meet the designed performance. Due to the nature of composite materials and the complex manufacturing process, variability occurs in the final product. Therefore, an assessment criterion for pressure vessels is their robustness and repeatability during production.

In the context of this research project, the end-product quality would be assessed by the vessel's burst performance and its robustness. For the proposed vessel configurations, weight, cost and volume would be standardized as the amount of material and vessel dimensions would be fixed. However, this research project aims at increasing the reliability levels of [CPVs](#), which subsequently would lead to reducing the number of materials used.

## 2.2. Composite Microstructure in Filament Winding

### 2.2.1. Load Application in Composite Materials

Composite materials consist of two (or more) constituent materials with different properties that produce a final product with different properties than the individual materials. Several examples exist, but in the context of CPVs, the individual materials are carbon fibers and epoxy resin matrix, where the fibers are embedded in the resin. Fibers have higher strength and stiffness when compared to resin, thus, fibers define the strength and stiffness of the structure. The resin acts as a binder where the fibers are embedded and transfer loads between different fiber bundles. During layup design, fibers are aligned along the loading direction to increase the composite material's strength as in the transverse direction, the stiffness is defined by the resin's properties. The same scenario also applies during compression, where due to the low lateral fiber stability, the resin withstands the structural loads. Matrix-dominated loading scenarios are generally avoided by the layup design to improve the composite's strength.

Composite structures are designed to primarily withstand flexural loads. In CPVs, the vessel is under internal pressure loading, which is translated into the composite structure as tensile loading. Therefore, the fibers should be oriented towards that tensile load to optimize the load-bearing capability. As a result, the most efficient winding pattern would differ based on the geometry of the vessel. During stacking sequence design, emphasis is placed to avoid matrix-dominated loading scenarios and also a large difference in stiffness between the cylindrical and dome regions, which would induce premature failure in the cylinder-dome transition region.

### 2.2.2. Consolidation Process

At the start of winding, the liner is pressurized to minimize the experienced compression forces on the surface, which would reduce tangential and axial contraction. Ideally, the applied internal pressure should counteract the external pressure being applied by the winding tension force while winding. The interaction between both pressure components could be displayed in Figure 2.1 where the internal pressure is labelled as  $P_1$  and external as  $P$ . Misalignment between both pressure values would either cause contraction or expansion of the liner, which would affect the final product's dimensions. Thus, one value is usually derived from the other, depending on which is defined first.

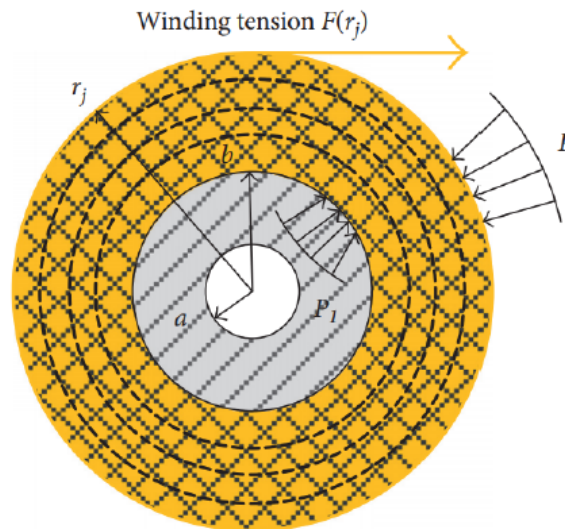


Figure 2.1: A schematic representing the internal and external pressure interaction in a cylinder cross-section  
- taken from Kang et al. [74]

While winding, resin tends to flow in the radial direction, due to the difference in pressure between the so-called *consolidation pressure*, which is the pressure experienced at the interface between the previously wound layer and the new layer, and the atmospheric pressure. The difference between consolidation pressure, which is finite, and atmospheric pressure, creates a pressure gradient that squeezes the resin to the outer surface. The flow of resin in the radial direction could be represented by Darcy's law, represented in Equation 2.1 where  $q$  is the flow rate,  $k$  is permeability,  $\mu_d$  is dynamic viscosity and  $\nabla P$  is the difference in pressure. The same applies while winding every new layer.

$$q = -\frac{k}{\mu_d} \nabla P \quad (2.1)$$

An increase in the internal or external pressure would directly increase this pressure difference, causing more resin

to flow outwards due to increasing the pressure gradient. The more resin flowing out, the lower the resin content in this layer, and thus, FVF increases. If the applied tension force or internal pressure is high, higher compaction is experienced would lead to excessive radial resin flow, causing an undesirably high FVF value. An example of the influence of compaction on the microstructure could be visualized in Figure 2.2. On the other hand, if lower compaction is experienced, the layers would not be properly confined, leading to low FVF and an increase in void content which could act as crack initiation sites and would decrease the structural performance of the composite structure. As a result, adequate control of the compaction levels by controlling manufacturing parameters is necessary to avoid manufacturing defects.

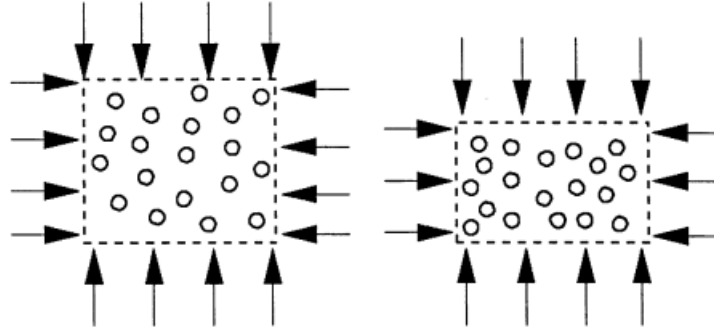


Figure 2.2: Stresses and response of the fiber bundle and resin during consolidation process - taken from [75]

Fibers are also affected during the consolidation process, where the fibers tend to move towards a new equilibrium position to relieve the experienced winding force. Therefore, the consolidation process affects both the fibers and resin, where this could be expressed using Equation 2.2 where  $p$  is the consolidation pressure,  $p_r$  is the resin pressure and  $\sigma_f$  is the fiber stresses in the radial direction [76]. If there is a high fiber content,  $p_r$  could be assumed to be zero and the fiber deformation dominates. The opposite occurs at low fiber content where  $p_r$  dominates.

$$P = P_r - \sigma_f \quad (2.2)$$

### 2.2.3. Curing Process

The following step is the curing stage after winding is done. Composites could be cured in ovens or autoclave, depending on the available equipment where the latter gives a higher quality due to higher confinement and more homogeneous curing level. Residual stresses generated during curing, especially for thick laminates, could have a significant impact on the end-product quality. These residual stresses are created due to chemical shrinkage and stress relaxation from the curing process. Residual stresses are present on a macro and micro level which could lead to shape distortion. Control of the residual stresses generated during curing could boost the vessel's quality. An example of controlling the curing residual stress proposed by Lee et al. [77] is by curing from the inside of the cylinder.

## 2.3. Manufacturing Parameters & Vessel Configuration Effect on Quality

In subsection 1.2.3, different manufacturing parameters involved in filament winding were investigated and reviewed and it was concluded that winding tension is one of the most influential manufacturing parameters. In this section, the direct relationship linking the tension force and internal liner pressure is explained, with emphasis on how this interaction affects the quality. Afterwards, a detailed overview of the influence of one main parameter, winding tension force, is investigated. Additional investigation is also done on the influence of varying the vessel configuration, which is defined by the stacking sequence and liner diameter, on the final quality.

### 2.3.1. Relation Between Winding Tension Force and Internal Liner Pressure

The winding tension force should not be considered independently, however, it is heavily interlinked with the internal liner pressure as they should counteract each other. The pressure exerted by the tension should be counteracted by internal pressure to prevent liner deformation which would influence the final dimensions of the vessel. The two parameters could be related together for one layer using the following equation [76]:

$$T_w \sin^2 \theta = P_{int} r \quad (2.3)$$

$T_w$  indicates the winding tension force,  $P_{int}$  is the internal radial pressure and  $r$  is the radial position vector. The winding angle,  $\theta$ , is defined from the axial direction of the vessel, thus, for a circumferential layer,  $\theta = 90^\circ$ . However, when considering the entire laminate, the internal pressure should be equal to the superposition of the pressure exerted by winding every layer to prevent plastic deformation.

Apart from preventing plastic deformation, the interaction between both parameters is what defines the consolidation process and defines the composite microstructure during winding. The magnitudes of the internal pressure and tension force define the compaction experienced by every layer, and thus, directly influence the FVF and residual stress distribution through the thickness. The difference between both pressure values is what derives the plastic deformation experienced. In other words, a layer experiencing high tension force and high internal pressure would experience high compaction and more resin would flow outwards as there are higher forces exerting force on the laminate as seen in Figure 2.2. However, if the pressure values are equal, then even at these high values, no plastic deformation occurs.

### 2.3.2. Influence of Winding Tension on Quality

#### Relating Winding Tension and FVF

In the investigation by Cohen [35], the FVF, resin and void content were measured for every sample with different process parameters. One of the interesting observations was that across all samples, it was found that FVF and void content are inversely proportional, where one increases, the other decreases. This is because when there is higher compaction, more resin is squeezed out and thus, FVF increases. This compaction also decreases the thickness and squeezes the layer more, decreasing the available space for voids.

An additional correlation that was observed is the direct relationship between winding tension force and FVF, where when one increases, the other follows. This in turn also leads to a decrease in porosity when FVF increases. The same was also observed from an investigation by Mertiny and Ellyin [36], where the correlation could be displayed in Figure 2.3. This reasoning for such correlation is that as the winding tension force is increased, the pressure exerted increases and the laminate is more compacted, squeezing more resin out of the fiber bed down a pressure gradient, creating an increase in FVF and decrease in void content.

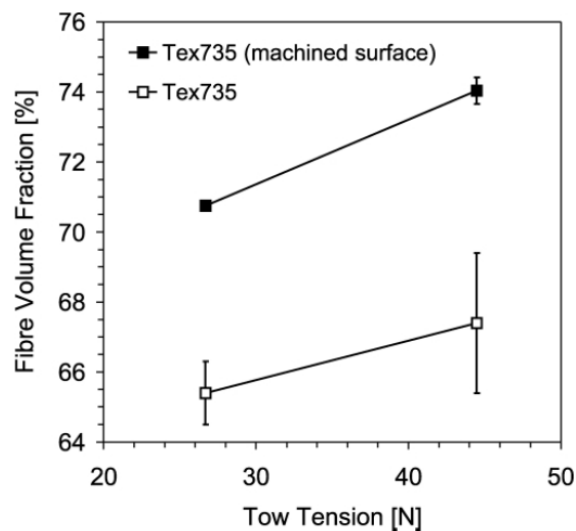


Figure 2.3: Dependency of FVF on the applied winding tension during filament winding - taken from [36]

#### Relating FVF and Quality

This could then be later related to quality as an increase in FVF, creates a direct in mechanical performance, in specific, the burst pressure. By ring testing in the investigation by Cohen [35], a directly proportional relationship was observed between increasing the FVF and an increase in burst pressure and fiber strain in the hoop direction, which is displayed in Figure 2.4.

In a later publication, Cohen [56] further investigated the relationship between FVF and vessel's strength, where similar trends as the ones found by Mertiny and Ellyin [36] were found. Such a relationship could be explained in a basic manner using the rule of mixture whereas the FVF, the composite strength would increase. Or as Tsai [78]

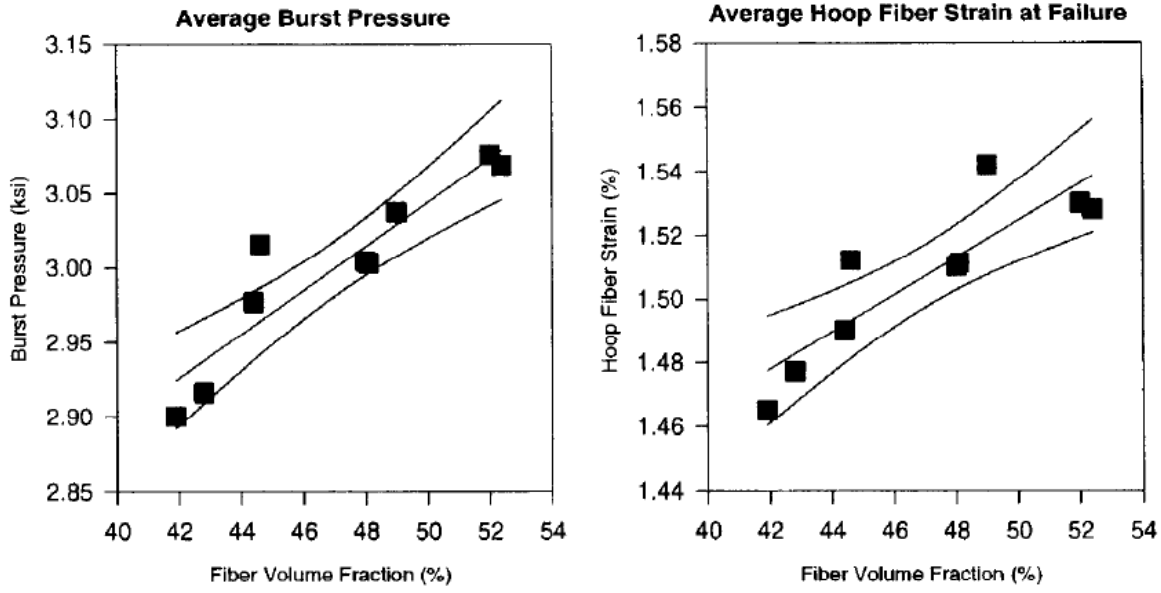


Figure 2.4: Fibre volume fraction against burst pressure (left) and against hoop fiber strain (right) - taken from [35]

proposed, by defining first the relation between load-transfer length,  $\delta$  and fiber modulus  $E_f$ , resin modulus  $E_m$ , fiber diameter  $d_f$  and FVF  $V_f$  as:

$$\delta = d_f \left[ \frac{3E_f}{2E_m} \frac{(1 - \sqrt{V_f})}{\sqrt{V_f}} \right]^{1/2} \quad (2.4)$$

Defining the average fiber bundle strain,  $\bar{\epsilon}_{bf}$ , in terms of fiber bundle length  $L$  and fiber probability failure as follows [78]:

$$\bar{\epsilon}_{bf} = \epsilon_0 L^{-1/\alpha} \Gamma \left( 1 + \frac{1}{\alpha} \right) \quad (2.5)$$

Combining the aforementioned equations, the average strength  $\sigma_c$  could be related to  $V_f$  using the following equation [78]:

$$\sigma_c = E_f \bar{\epsilon}_{bf} = \frac{1}{(\alpha e)^{1/\alpha} \Gamma(1 + 1/\alpha)} \left( \frac{L}{\delta} \right)^{1/\alpha} V_f \bar{\sigma}_f + (1 - V_f) \bar{\sigma}_m \quad (2.6)$$

where  $\bar{\sigma}_f$  and  $\bar{\sigma}_m$  indicate the average fiber and matrix strength respectively. In this derived equation, the strength could be related to the FVF, where a direct relationship exists and explains the observed trends.

Based on these investigations, the approach that would be followed in the experimental campaign is to prove a direct relationship exists between the tension force and FVF. As FVF then relates to the quality, FVF is used as an intermediate segue to link the tension and quality together.

### Influence of Tension on Thickness

Nebe [34] manufactured two identical vessels, but with different winding tension forces and found a decrease in thickness at a higher winding tension. The result could be displayed in Figure 2.5. This is due to higher compaction caused by the increase in tension force, causing a decrease in thickness. It could be noted that the cylinder-dome transition region experiences a smoother transition, which is noticed from the difference in slopes and in the detailed view. This change is due to ply readjustment towards the cylinder-dome transition region, which happens due to the smear-out of the plies when winding subsequent layers. The variation in slope and thickness leads to differences in stiffness distribution between the cylinder and dome region, which directly affects the vessel's mechanical performance. As a result, in the experimental campaign, an investigation would be done to link the changes in laminate thickness with changes in manufacturing parameters to validate such a result.



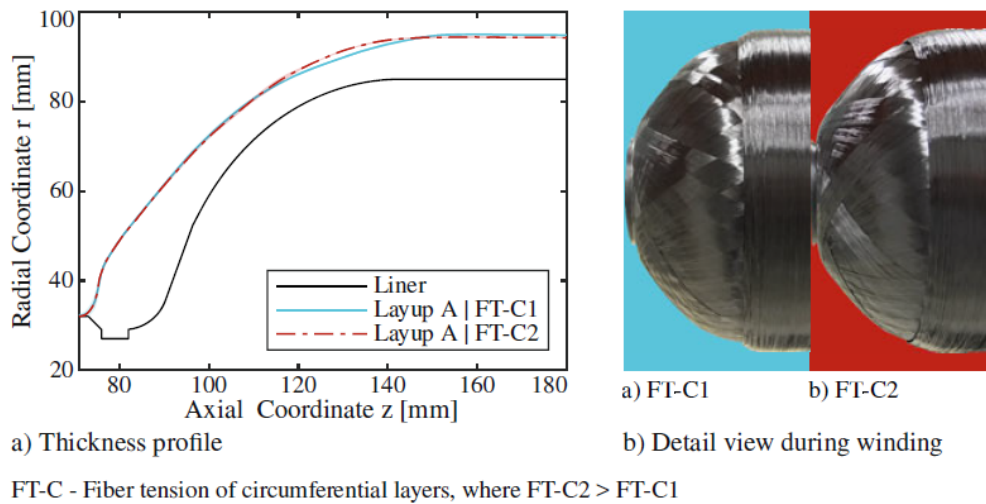


Figure 2.5: Influence of winding tension on wall thickness and circumferential layer readjustment at cylinder-dome transition region - taken from [34]

### Drawbacks of High Tension Force

Increasing the winding tension force does not always guarantee an increase in the vessel's strength as both do not follow a unidirectional trend. This is because, at a very high tension force, the FVF could be higher than desired, leaving the laminate very dry with little resin to ensure proper load transfer between fiber bundles. Additionally, in matrix-dominated loading scenarios, a lower FVF is actually desired to increase the composite's strength as more resin would be required. This is usually not the case in CPVs as if matrix-dominated loading occurs, this usually stems from poor stacking sequence design.

An additional drawback of a high tension force, without applying a corresponding change to the internal pressure, the vessel's length would be affected. This is because the liner would plastically deform due to a large compaction force being applied to the liner, especially from low-angle helical layers as these are the layers that create the highest axial forces while being wound around the dome region. To counteract this, the internal pressure should be correspondingly increased or the choice of the liner material should be changed to a stiffer liner material that is less responsive to deformations.

### 2.3.3. Influence of Stacking Sequence on Quality

In filament winding, besides the manufacturing parameters, the angle at which tow is wound on the surface determines the applied radial pressure and hence, the compaction experienced by every individual layer. As discussed earlier, compaction directly influences the FVF and porosity distribution through the thickness. Higher compaction would lead to higher FVF and lower porosity, which would boost the vessel's mechanical performance and strength. Therefore, varying the stacking sequence would affect the consolidation level through the thickness and the vessel's mechanical performance. Additionally, changing the stacking sequence would affect the stress and strain distribution through the thickness based on the stiffness contribution provided by every layer due to its winding angle. By varying the stiffness distribution through the thickness, different deformation behaviour and locations would be observed. Therefore, with a fixed number of layers and angles and varying the grouping and sequence of layers, significant differences in mechanical performance could be observed. An example by Nebe et al. [79], where a difference up to 67 % was observed in burst pressure by purely varying the stacking sequence for sub-scale vessels, where the differences arise from different failure modes and locations.

Circumferential layers provide the highest tangential compaction as the winding angle is aligned along the meridional direction of the vessel, leading to the highest compaction in the cylindrical section. On the contrary, low-angle helical layers provide minimal compaction in the cylindrical region, but the highest compaction in the dome region. Therefore, based on the grouping and positioning of every layer, different consolidation and compaction levels may be experienced, depending on if it is followed by a circumferential or helical layer for example. Nebe [34] provided an insight into such an influence by testing three different stacking sequences composed of circumferential and low-angle helical layers as seen in Figure 2.6.

Overall, there is not any noticeable change in FVF in the laminate as prepreg winding was used and thus, no resin loss should occur. Nevertheless, noticeable differences in FVF and porosity were observed when comparing hoop

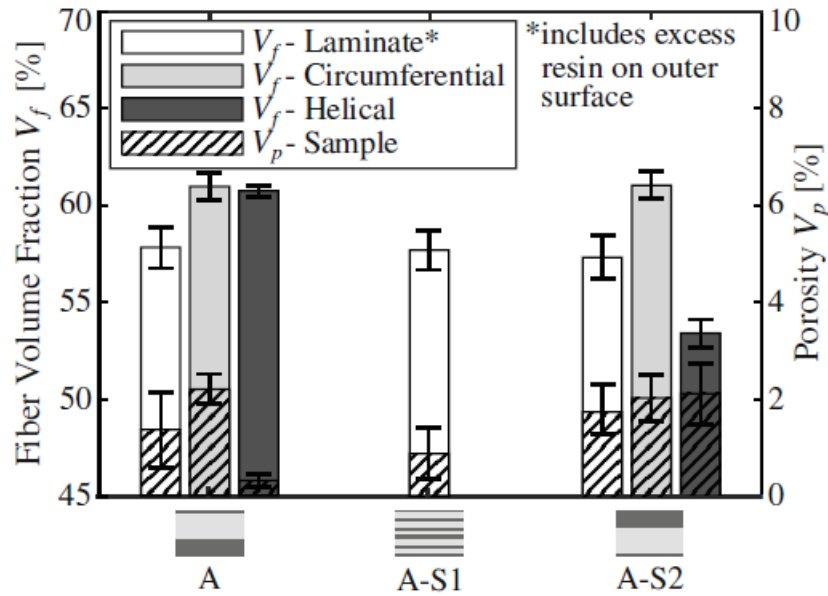


Figure 2.6: FVF and porosity obtained by means of acid digestion tests for 3 sequences composed of circumferential and low-angle helical layers but with different grouping and positioning - taken from [34]

and helical layers. In sequence A, the circumferential layers compact the helical layers underneath, leading to higher FVF and lower porosity in comparison with sequence A-S2. Additionally, the FVF of circumferential layers seems to be unchanged, as low-angle helical layers provide minimal compaction and thus, no change should be expected.

Having an alternating stacking sequence comes with the advantage of disrupting the crack propagation stream as the winding angle changes continuously. However, it comes with the disadvantage of taking longer winding time as companies tend to prefer grouping of similar winding angles to save time, and hence, resources. Additionally, in an alternating stacking sequence, more connector layers would be needed, which comes at an added weight value.

The investigation by Nebe [34] motivated the approach to testing different grouping of stacking sequences, similar to A and A-S2. This is to validate whether the same results would also be expected in wet winding. Additionally, to validate the analytical model applicability to account for different vessel configurations and to account for different confinement levels based on the preceding layers.

### 2.3.4. Influence of Vessel Diameter on Quality

Adjusting the vessel diameter, which could take place when switching from sub-scale to full-scale vessels would affect the required process parameters. The external pressure applied by the tension force decreases by increasing the vessel diameter. Thus, to compensate for such a decrease, an increase in winding tension force would be required to experience similar external pressure and compaction results. Changes to internal pressure could take place as well if the liner material changes while switching vessel diameter, which is common. Depending on the stiffness of the liner, an increase or decrease in internal pressure may be necessary to avoid liner expansion or contraction.

In a pressure vessel, stiffness is needed in the direction perpendicular to the pressure application. In the cylindrical section, the circumferential layer provides the highest stiffness in this area, high-angle helical layers in the upper dome regions and low-angle helical layers around the bosses. By increasing the vessel diameter, the required tangential reinforcement increases, thus, additional circumferential layers are required. However, to avoid a large stiffness difference between the cylindrical section of the vessel and other parts, helical layers need to be added as well to create a gradual stiffness change. This is necessary to prevent preliminary failure around the transition regions.

## 2.4. Methodology for Defining Manufacturing Parameters

### 2.4.1. Empirical Approach

There are different approaches for setting the winding tension force and internal liner pressure values in practice. Most commonly, a value for winding tension is set and then the internal pressure is derived to ensure equilibrium. The popular approach is based on trial and error, where different settings are tested and iterated until a suitable combination is found and fixed for later use. The tension force could be kept the same for circumferential and helical layers, or different values are used. An approach is to have two set values, a high and low, and apply the high

for helical and low for circumferential layers. This is as the circumferential layers exert the largest external pressure on the liner and a higher tension force is applied for helical layers to avoid tow slippage while winding. The connector layers, which are non-structural layers that are purely used to transition from one winding angle to the other, could also have a different tension setting to ensure tow stability.

The set values for tension force could differ depending on the type of winding, whether it is dry, wet or prepreg winding. Wet winding would generally require higher tension forces compared to the latter as there is no adhesion, as in prepreg winding. The value for internal pressure also varies depending on the vessel material, whereas in a less stiff liner, a high-pressure value could cause expansion of the liner affecting the final product's geometry. The internal pressure itself could be kept as a constant value throughout the winding, or have increments at different stages. This would be useful as the effect of the internal pressure on the top surface decreases by winding more layers.

### 2.4.2. Residual Stress Approach

A more analytical approach is based on understanding the residual stress generation during winding and based on a required residual stress magnitude, either compressive or tensile, a reverse derivation of the tension force could be performed. Whilst manufacturing, residual stresses are generated during winding and curing, where curing stresses could be split up into thermal stress and chemical shrinkage. The residual stress generated for thermoplastic prepreg winding is as follows [74]:

$$\sigma^{\text{total}} = \sigma^{\text{wt}} + \sigma^{\text{th}} + \sigma^{\text{ch}} \quad (2.7)$$

where  $\sigma^{\text{total}}$  is the total stress,  $\sigma^{\text{wt}}$  is stress caused by the winding tension,  $\sigma^{\text{th}}$  is thermal stress due to thermal gradient during curing and  $\sigma^{\text{ch}}$  is the chemical shrinkage induced during the curing process.  $\sigma^{\text{th}}$  are generated mainly in the cooling stage, where the difference between curing temperature and ambient temperature creates such stress. Additionally, as the resin is heavily dependent on the degree of cure and is an isotropic material, the volumetric shrinkage of resin exerts a strain on the vessel that contributes to this chemical shrinkage stress. Residual stresses in the final product could either cause microcracks and delamination and reduce the vessel's ability to resist load or boost the vessel's structural integrity. Thus, a sufficient understanding of residual stress formation is critical.

To relate the influence of winding tension force to residual stress formulation, Lu et al. [80] presented an interesting investigation by varying tension force patterns while winding circumferential and high-angle helical thermoplastic tapes. The hoop residual stress could be seen in [Figure 2.7](#) with the tension gradient on top. Zero tension force was applied in TTP5 to be used as a control for comparison. For TTP5, the inner layers are experiencing tensile residual stresses while the outer experiences compressive stresses. This shifts in TTP1, where there is a gradual increase in tension, and in TTP2 when there is a sudden jump. On the other hand, decreasing the tape tension as in TTP3 leads to significantly larger tensile and compressive stresses in the inner and outer surface respectively. Setting a large constant tension force as in TTP6 does not reduce nor affect the residual stresses that much, in comparison to TTP5. It could be concluded from this experiment, that with constant tension force, the residual stresses are tensile. With an increased slope, radial stresses become more compressive, whilst the opposite occurs with a decreasing tape tension force. Therefore, structural benefits could be attained with optimized residual stresses.

Compressive residual stresses aid in improving the vessel's structural performance as the first step in load application is to overcome such compressive residual stresses. However, during winding, if there are compressive stresses being experienced by the uncured composite, then manufacturing defects could take place as fiber misalignment or wrinkling. Additionally, when comparing metallic and plastic liners, to improve the vessel's fatigue life, compressive residual stresses in the liner would help when considering metallic liners, but not necessary for plastic counterparts.

In literature, work has been done on estimating the residual stresses during winding or during curing using numerical models separately. Kang et al. [74] considered the entire picture by taking into account all the different residual stresses experienced during manufacturing. The solving procedure followed by the model could be summarized in the flow chart in [Figure 2.8](#). The following assumptions were assumed in this model:

- Plane stress;
- Layers are visualized as discrete rings and stresses are superimposed;
- Composite modulus is obtained using the rule of mixture;
- Mandrel is isotropic and linear elastic.

The model combines all the experienced stresses as mentioned in [Equation 2.7](#). The winding stresses,  $\sigma^{\text{wt}}$  are determined by utilizing the thick-walled cylinder theory where the hoop and residual stresses along the cylinder length

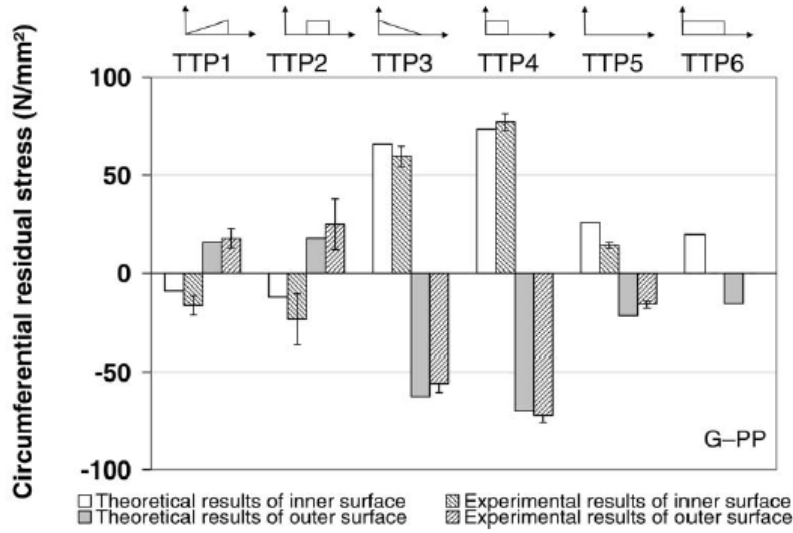


Figure 2.7: Simulation and experimental results of G-PP under different tape tensions - taken from [80]

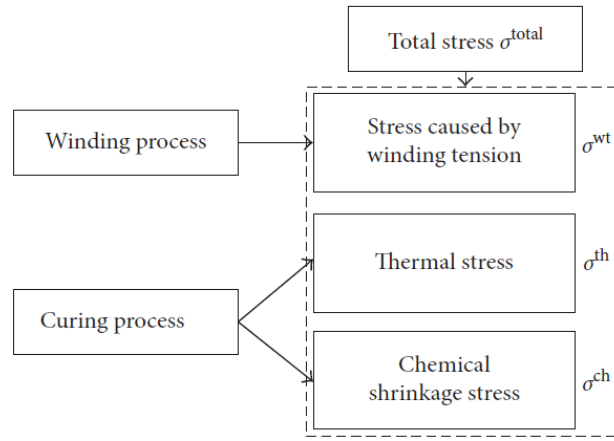


Figure 2.8: Overview of the residual stress calculation in the analytical model based on thick-walled theory - taken from Kang et al. [74]

are calculated based on the superposition principle. The hoop stresses along the cylinder's length,  $\sigma_{\theta}^{wt}$ , could be displayed using the following equation:

$$\sigma_{\theta}^{wt}(r_i, r_n) = \frac{F(r_i)}{h} + \sigma_{\theta}(i, i+1) + \dots + \sigma_{\theta}(i, n) = \frac{F(r_i)}{h} + \sum_{j=i+1}^n \sigma_{\theta}(i, j) \quad (2.8)$$

where  $F$  is the tension force,  $r_i$  is the radius of  $i$ th layer and  $h$  is the thickness. The limitation of this approach is that the entire uncured composite laminate is considered as a whole. This assumes that there is shear load transfer between each individual layer, but physically, this would not be the case as the resin is still in liquid form, and thus incapable of providing shear stiffness to the laminate to transfer loads between fiber bundles. The other limitation is by using the thick-walled theory, the analysis is hence limited to only the cylindrical section of the vessel and does not consider the dome and cylinder-dome transition region, which is a constraint of such an analysis method as previously discussed in [section 1.3](#).

Afterwards, the residual stresses due to thermal stress and chemical shrinkage are computed in the radial and hoop direction and then superimposed to stresses from winding to find the total residual stresses in the structure. By only considering the residual radial stresses, it would be in terms of the winding tension force. By assuming a desired residual stress value in the structure,  $S$ , the following equation could be set:

$$\sigma_r^{wh}(x) + \sigma_r^{th}(x) + \sigma_r^{ch}(x) = -\frac{1}{x} \int_x^m S dx = -\frac{m-x}{x} S \quad (2.9)$$

By making the tension force the subject of the formula and setting a value for  $S$ , the tension force could be estimated. By setting a value of 60 MPa, the results of this model could be displayed in Figure 2.9. It could be seen that to maintain constant radial stress while moving through the thickness, the tension force needs to be increased.

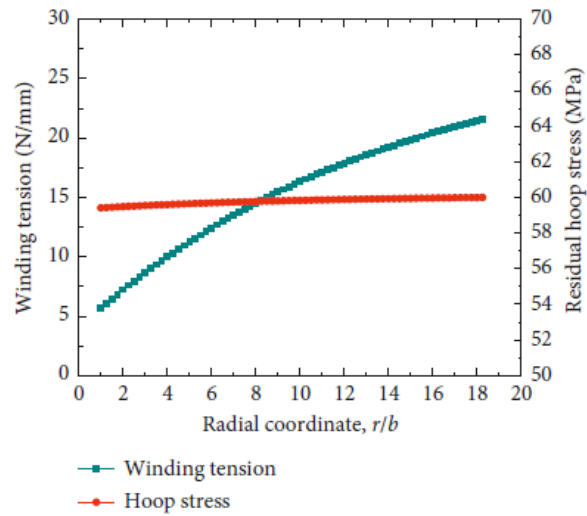


Figure 2.9: Designed winding tension following the inverse derivation method and the corresponding residual hoop stress - taken from [74]

## 2.5. Research Objectives and Questions

As discussed, a substantial amount of effort was placed on identifying the influential process parameters during filament winding and identifying their influence on the end-product quality. However, a research gap still exists in understanding and quantifying such an influence in a complete investigation, which is also validated via an experimental campaign. By a "complete" investigation, it is meant to consider the relation between winding tension force and internal pressure and their influence on the end-product in a full magnitude starting from the microstructure up to the vessel's burst performance. Additionally, investigate how these parameters would be affected by changes in the vessel configuration by changing the stacking sequence and vessel diameter. This would then lead to a framework to find the optimum process parameters for attaining the highest quality possible.

The aim is to grasp the full picture and increase the understanding levels of the manufacturing process of CPVs. This would then lead to an increase in reliability levels in the production of CPVs and the optimum use of the available material. This being a study supported by Plastic Omnium, emphasis was made to relate theoretical and analytical predictions to an experimental level to physically display such influence and relationships.

The research objective is:

**Investigating the effect of two manufacturing process variables, internal liner pressure and winding tension force, on the end product quality by applying a theoretical relationship between these variables and the end product quality and validating such a relation through experimental results.**

This research objective could then be split into multiple sub-goals which are necessary to make this happen. The sub-goals are:

- Explaining the effect of internal pressure and winding tension on the composite microstructure and end product quality
- Quantification of the effect of the internal pressure and winding tension on the end product quality using analytical models
- Quantification of the influence of the stacking sequence on the effect of internal pressure and winding tension on the end product quality analytically and experimentally
- Quantification of how the effect of internal pressure and winding tension on the end product quality varies by changing the CPV diameter analytically and experimentally
- Development of a method to determine the optimal internal pressure and winding tension values for a given vessel configuration

Consequently, the main research question is formulated as follows:

*Given a vessel configuration, how to estimate the required winding tension and internal liner pressure to optimize the end – product quality?*

This research question is further split up into more detailed sub-questions as follows, with an indication of where the questions are answered in the report:

1. *How do tension and pressure affect each other and affect the composite material microstructure during the filament winding process of CPVs?* - This was addressed theoretically in [chapter 2](#) but a final answer combining theory, analytical and experimental results in [chapter 5](#).
2. *How does changing the stacking sequence affect the required liner pressure and winding tension force during the filament winding process?* - Addressed in [chapter 2](#) and answer is concluded in [chapter 5](#), in specific [subsection 5.4.5](#).
3. *How does the required liner pressure and winding tension force vary by changing the liner's diameter?* - Again, a final answer is given in [chapter 5](#), in specific, [subsection 5.4.4](#).
4. *How could the obtained relations relating winding tension and internal pressure be validated using experimental results?* - Experimental campaign explained in [chapter 4](#), with the results and comparison presented in [chapter 5](#).
5. *How could the validated relations be generalized to form a method to determine the needed internal pressure and winding tension?* - Addressed in [section 5.5](#).

# Analytical Modelling

The development of a tool that is capable of relating the vessel's end-product quality to the change in process parameters is vital in understanding and quantifying such a relation. If validated, it would also serve as a tool to be used by engineers in the development phase to find the optimum process parameters to maximize the product quality for any vessel configuration. This chapter details the development of the proposed analytical model, with a validation plan.

First off, a brief overview of the followed research methodology to tackle the research questions is given in [section 3.1](#). Afterwards, in [section 3.2](#), the choice of the analytical model is motivated, along with a detailed description of the assumptions and methodology followed to develop the model. In an effort to validate the analytical model and the capability of predicting the vessel configurations, a few vessel configurations were proposed as described in [section 3.3](#). The hypothesis regarding experimental results is then summarized in [section 3.4](#).

## 3.1. Overview of Research Methodology

This section aims at introducing the proposed and followed methodology in this research project with aim of answering the research questions stated in [section 2.5](#). The methodology could be divided into three main stages; theoretical research, analytical modelling and experimental testing, which are briefly addressed in the following subsections.

### Theoretical Research Summary

Starting with the first stage, this work follows directly from the literature review and background research, previously presented in [chapter 1](#) and [chapter 2](#). A summary of the topics tackled in the literature review is listed below:

- Introduction to pressure vessels and their different geometries and types - [section 1.1](#)
- Manufacturing method of CPVs - [section 1.2](#)
- Analysis techniques for CPVs - [section 1.3](#)
- End-product quality definition - [section 2.1](#)
- Consolidation process - [section 2.2](#)
- Manufacturing parameters effect on quality, including the influence of stacking sequence and liner diameter - [section 2.3](#)
- Available methods for predicting optimum manufacturing parameters - [section 2.4](#)

### Rationale of Analytical Modelling

Before choosing the most practical analysis approach, the first step is setting the requirements for the proposed analytical model to fit. The requirements are as follows:

1. The model should allow the modelling of the uncured composite during winding;
2. The model should be capable of representing the influence different processes and manufacturing parameters, specifically the filament winding tension force and internal liner pressure, would have on the final product quality;
3. The model should allow for different vessel configurations, such as different stacking sequences and vessel diameters;
4. The model should allow for fast computational time, within seconds, to allow for rapid iteration and configuration testing;
5. The model should be used as a method for comparing different combinations of process parameters for a certain vessel configuration. Thus, the aim is to compare end-product quality aspects as burst pressure quantitatively for different vessel configurations.

The first requirement is a vital one as most of the current analysis methods for CPVs deal with the cured structure and then address the applied loads based on the loading scenarios applicable. However, models often do not take into

account loads and stresses experienced during the manufacturing process. Therefore, a challenge for this analytical model is to be capable of modelling the stresses experienced during the manufacturing process by every layer in a physically sound way that represents reality. Based on the obtained stress and strain predictions while winding, a quantitative analysis of the mechanical performance could be made based on the stress distribution after winding.

Vessel configuration, which is defined by a certain stacking sequence and liner diameter, is very likely to vary from one project to the other based on different customer requirements. The stacking sequence could change based on different operating pressure and the geometry would also change based on the available space within the vehicle. Therefore, the analytical model should adapt and allow for these different vessel configurations.

High-fidelity models that are capable of predicting the vessel's mechanical performance with a certain extent of accuracy are always accompanied by high computational costs. However, these models have limited compatibility in an industrial context, especially during development phases. In principle, models are required to put less emphasis on being able to capture all failure aspects but focus more on aspects that are more critical for failure prediction. In this thesis context, the focus was put on developing a time-efficient tool, capable of delivering quantitative analysis of failure predictions, within seconds, to allow for rapid iteration of process parameters in an industrial environment.

## Manufacturing and Experimental Testing

The next stage in this thesis project is to compare the outcome of the analytical model with different experimental data. Therefore, the approach is to manufacture and test different vessel configurations, with different combinations of process parameters. At a later stage compare and validate the analytical model results with experimental ones. For every proposed vessel configuration, a number of vessels were manufactured and then tested in different ways. The description of the manufacturing and testing campaign is explained in [chapter 4](#). The results and discussion, with comparison to the analytical model, would be addressed in [chapter 5](#) with aim of answering the proposed research questions.

## 3.2. Analytical Model Description

### 3.2.1. Choice of Analytical Model

In [section 1.3](#), analytical and numerical approaches applicable for the analysis of [CPVs](#) were discussed. For uncured composite analysis, there are different analytical and numerical modelling approaches available. Examples are modelling flow and stresses for saturated porous media as proposed by Lydzba and Shao [81] and numerical approaches using two-phase models.

Based on the aforementioned requirements, a [CPVs](#) analytical modelling approach was preferred over the numerical alternative. This mainly stems from the last two requirements, as an accurate analysis method for [CPVs](#) is not required and is not the aim of this model, but solely to be able to physically describe the winding process and stresses experienced. Based on this, a quantitative comparison between different vessel configurations and/or parameter settings to predict the mechanical performance of the vessel. Additionally, [CPVs](#) analytical approaches were preferred over saturated porous media analytical models, which could be applicable in the case of uncured composites, for their familiarity and lower level of complexity.

Of the three different analytical approaches, [CLT](#) was the one opted for. When comparing the netting theory and [CLT](#), both approaches are usually used for preliminary analysis of [CPVs](#). The difference lies that [CLT](#) is capable of accounting for the material orthotropy by taking into account matrix load-bearing capabilities, while the netting theory assumes all loads are solely carried by the fibers in tension. However, this difference itself is not relevant for this analysis, as the model deals with uncured composite material, thus, the resin is still in a liquid state and does not have any stiffness. The reasoning why [CLT](#) was preferred over netting theory was due to being able to calculate stresses through the thickness of every layer and that netting theory does not take compression into account as it assumes fibers are always in tension.

Kang et al. [74] proposed a method of modelling uncured composite materials in a similar fashion as intended but using 3D thick-walled analysis as discussed in [section 2.4](#). However, it is believed that thick-walled cylinder analysis is not relevant for this investigation. This is as considering the layers as thick composite laminate does not physically represent reality as these layers do not interact with each other, apart from introducing radial loads to others while winding every new layer. As a result, this makes the 3D stress theory inapplicable and not physically sound for this analysis.

Using [CLT](#), plane stress assumption is established for each layer of the composite, instead of the entire thick composite laminate. Thus, considering each individual layer separately, as a thin-walled layer, subject to internal and external pressure due to the internal liner pressure and filament winding tension respectively. The applied loads are out-of-plane but are translated into in-plane loads due to the geometrical nature of a cylinder.



### 3.2.2. Model Assumptions

Following the model selection, the imposed assumptions that would be used in this model would be addressed alongside their implications. As CLT was used as the analytical approach, it is accompanied by inherent assumptions. To start with, there are inherent assumptions accompanied by choosing the CLT analytical approach are:

1. Each layer of the laminate is assumed to be quasihomogeneous and orthotropic.
2. Thin-walled assumption is made such that its lateral dimensions are much larger than its thickness.
3. Plane stress assumption leading to no out-of-plane loads but the laminate is only loaded in-plane. This leads to considering all out-of-plane displacements are very small relative to in-plane displacements.

There are other assumptions that are not entirely relevant in this discussion as assuming the thermal cycle is the same throughout the surface and the model is time-independent so disregarding viscoelastic relaxation.

The model is limited to the cylindrical section of the vessel to avoid the complex geometry of the dome and transition region. The model assumes a cylinder of an arbitrary length, in which the influence of the tension and internal pressure are investigated by defining the tangential stresses in the laminate. As a result, this requires the following assumptions:

1. Vessel is modelled as a cylindrical region under plane stress assumption.
2. Forces in x-direction created by winding helical layers are not considered, only forces in the hoop direction.
3. Shear forces between layers do not exist.
4. Stresses for each layer could be obtained using the superposition principle.
5. The liner and connectors are non-structural components and do not contribute to the strength of the vessel but affect the composite microstructure during winding.

Modelling the vessel as a cylinder means that the additional sections of the vessel, such as the dome and cylinder-dome transition region, are ignored leading to a simpler geometry. The validity of such an assumption stems from the design methodology of CPVs where vessels are designed to burst in the cylindrical region by failure to the hoop region, thus, the analysis would primarily focus on investigating the variation of the tangential stresses in these critical layers. By imposing a plane stress assumption to the cylinder, a finite cylinder is considered which can extend and contract in the axial direction, thus, axial strain  $\epsilon_x$  is not zero. By imposing such an assumption, information regarding the layers wound on the dome region is missing, which decreases the validity and accuracy of the imposed model.

Additionally, the forces in the x-direction while winding helical layers are not considered. Following the same line of reasoning from the previous assumption, the limitation would be the same as before as well. If a full vessel were to be considered, then forces in the axial direction would be important as while winding helical layers on the dome region, axial forces are imposed by winding every layer, which would significantly increase the level of inaccuracy. Moreover, a limitation of disregarding the axial forces is that the strain estimation of the full vessel after winding would be highly inaccurate as the forces in the x-direction, especially while winding low-angle helical layers, are the main contributor. This also imposes an inaccuracy on the tangential stress distribution, as there is a coupling between axial loading and tangential stresses due to the unsymmetrical laminate.

As the model deals with uncured composite materials, the resin is still in a liquid state preventing any force transfer between layers, which is the main reason why the third assumption was imposed. The implications of this assumption lead to the invalidity of using the thick-walled cylinder theory, as discussed in the previous subsection. Therefore, every layer is to be considered as a separate laminate composed of one ply on its own. This assumption should increase the accuracy of the analytical model as the model becomes more physically sound.

Moreover, by utilising the superposition principle to predict the stresses experienced by every layer, it is then assumed that the stresses imposed while winding an individual layer, would be equally experienced by the previous layers as well. This is as layers are visualized as discrete rings that apply uniform pressure all around the cylindrical section.

Lastly, the liner and connector layers, which are used to switch between layers of different winding angles, are not considered structural components and do not contribute to the overall strength of the vessel. The liner however does deform whenever a mismatch between internal and external forces exists.

### 3.2.3. CLT Theory and Approach

The CLT is an elastic constitutive formulation that is used as a predictive tool to analyze the coupling effects that occur in composite structures, alongside predicting strain, displacement and stresses that are experienced by every

layer under mechanical loading. In essence, CLT is the same as the isotropic plate theory, however, the difference is that it allows for orthotropic materials, as composite structures. The applied forces, which are based on the defined loading case, could be related to the strains and curvatures around the mid-plane using Equation 1.7. The middle matrix, often described as the ABD matrix, is the matrix that defines the elastic properties of the laminate based on the fiber and matrix material properties used. The ABD matrix consists of three different matrices that are joined together.  $A$  matrix is referred to as the extensional stiffness matrix,  $B$  is the coupling stiffness matrix and  $D$  is the flexural stiffness matrix. Each individual matrix could be computed using the following relation:

$$\begin{aligned} A_{ij} &= \sum_{k=1}^n \{Q_{ij}\}_n (z_k - z_{k-1}) \\ B_{ij} &= \frac{1}{2} \sum_{k=1}^n \{Q_{ij}\}_n (z_k^2 - z_{k-1}^2) \\ D_{ij} &= \frac{1}{3} \sum_{k=1}^n \{Q_{ij}\}_n (z_k^3 - z_{k-1}^3) \end{aligned} \quad (3.1)$$

where  $z$  is the thickness and  $Q_{ij}$  is the reduced stiffness matrix, which directly depends on the material properties as the young's modulus along the fiber's longitudinal direction,  $E_1$ , young's modulus in the transverse direction,  $E_2$ , the Poisson's ratio in both directions,  $\nu_{12}$  and  $\nu_{21}$  and shear modulus,  $G_{12}$ . The  $Q$  matrix could be computed as follows:

$$\begin{aligned} Q_{xx} &= Q_{11}m^4 + 2(Q_{12} + 2Q_{66})m^2n^2 + Q_{22}n^4 \\ Q_{xy} &= (Q_{11} + Q_{22} - 4Q_{66})m^2n^2 + Q_{12}(m^4 + n^4) \\ Q_{yy} &= Q_{11}n^4 + 2(Q_{12} + 2Q_{66})m^2n^2 + Q_{22}m^4 \\ Q_{xs} &= (Q_{11} - Q_{12} - 2Q_{66})nm^3 + (Q_{12} - Q_{22} + 2Q_{66})n^3m \\ Q_{ys} &= (Q_{11} - Q_{12} - 2Q_{66})mn^3 + (Q_{12} - Q_{22} + 2Q_{66})m^3n \\ Q_{ss} &= (Q_{11} + Q_{22} - 2Q_{12} - 2Q_{66})n^2m^2 + Q_{66}(n^4 + m^4) \end{aligned} \quad (3.2)$$

where  $m$  is  $\cos\theta$  and  $n$  is  $\sin\theta$ , where  $\theta$  is the ply angle with respect to the global x-axis.  $Q_{11}$ ,  $Q_{12}$ ,  $Q_{22}$  and  $Q_{66}$  are determined using the following equation, utilizing the previously mentioned material properties;

$$\begin{aligned} Q &= 1 - \nu_{12}\nu_{21} \\ Q_{11} &= \frac{E_1}{Q} \\ Q_{22} &= \frac{E_2}{Q} \\ Q_{12} &= \frac{\nu_{12}E_2}{Q} \\ Q_{66} &= G_{12} \end{aligned} \quad (3.3)$$

Therefore, the ABD matrix is determined separately and then used, alongside the resultant force matrix to compute the strains and curvatures. Equation 1.7 could be expanded and flipped by inverting the ABD matrix as follows:

$$\begin{pmatrix} \varepsilon_x^0 \\ \varepsilon_y^0 \\ \varepsilon_s^0 \\ k_x \\ k_y \\ k_s \end{pmatrix} = \begin{bmatrix} A'_{xx} & A'_{xy} & A'_{xs} & B'_{xx} & B'_{xy} & B'_{xs} \\ A'_{xy} & A'_{yy} & A'_{ys} & B'_{yx} & B'_{yy} & B'_{ys} \\ A'_{xs} & A'_{ys} & A'_{ss} & B'_{sx} & B'_{sy} & B'_{ss} \\ C'_{xx} & C'_{xy} & C'_{xs} & D'_{xx} & D'_{xy} & D'_{xs} \\ C'_{yx} & C'_{yy} & C'_{ys} & D'_{xy} & D'_{yy} & D'_{ys} \\ C'_{sx} & C'_{sy} & C'_{ss} & D'_{xs} & D'_{ys} & D'_{ss} \end{bmatrix} \cdot \begin{pmatrix} N_x \\ N_y \\ N_s \\ M_x \\ M_y \\ M_s \end{pmatrix} \quad (3.4)$$

Afterwards, the strains around the mid-plane are translated to strains for each ply by using the thickness and curvature, as follows:

$$\begin{pmatrix} \varepsilon_x \\ \varepsilon_y \\ \varepsilon_s \end{pmatrix}^k = \begin{pmatrix} \varepsilon_x^0 \\ \varepsilon_y^0 \\ \varepsilon_s^0 \end{pmatrix} + z \begin{pmatrix} k_x \\ k_y \\ k_s \end{pmatrix} \quad (3.5)$$

Using the strains and stiffness matrix, the stresses in the global direction could be found using the following equation:

$$\begin{Bmatrix} \sigma_x \\ \sigma_y \\ \sigma_s \end{Bmatrix} = \begin{Bmatrix} Q_{xx} & Q_{xy} & Q_{xs} \\ Q_{yx} & Q_{yy} & Q_{ys} \\ Q_{sx} & Q_{sy} & Q_{ss} \end{Bmatrix} \begin{Bmatrix} \varepsilon_x \\ \varepsilon_y \\ \varepsilon_s \end{Bmatrix} \quad (3.6)$$

### 3.2.4. Coordinate System and FBD

From the previous set of equations, it could be identified that there were two different frames of reference used, the global coordinate system (x,y,z) and the principle coordinate system (1,2,3). Essentially, the difference between both systems is depending on the fiber direction, where 1 is always aligned along the fiber direction, 2 is transverse to 1 and 3 is perpendicular to both. The direction differs from one ply to the other depending on the angle. On the other hand, the global coordinate system is fixed irrespective of the ply angle. If the angle is 0°, both coordinate systems would coincide. A representation of these two coordinate systems as would be used on a section on a vessel could be seen in [Figure 3.1](#).

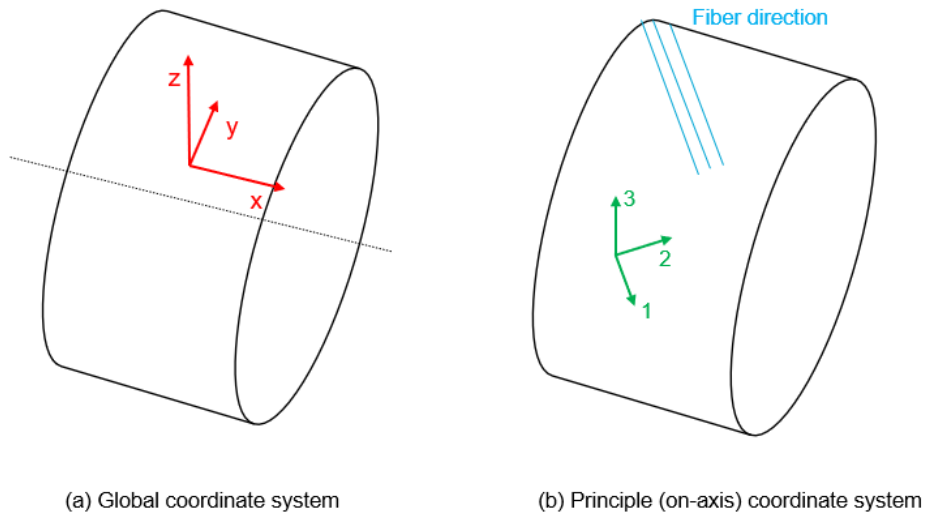


Figure 3.1: Schematic representation of the global and principle coordinate system used in the analytical model

A transformation between both coordinate systems could be made using the transformation matrix given in [Equation 3.7](#). This is often used to find the strains and stresses in the principle direction to be later on implemented in one of the failure criteria.

$$T = \begin{bmatrix} m^2 & n^2 & mn \\ n^2 & m^2 & -mn \\ -2mn & 2mn & m^2 - n^2 \end{bmatrix} \quad (3.7)$$

Regarding the forces being experienced while winding, as the model represents the uncured composite material during manufacturing, there are two pressure forces being experienced by the vessel. First off is the internal pressure inside the liner needed to maintain the liner during winding. Added to that, is a counteracting pressure force generated due to the winding tension force while winding each individual layer, creating an external pressure being applied on a liner. A schematic of the FBD displaying both these forces could be seen in [Figure 3.2](#).

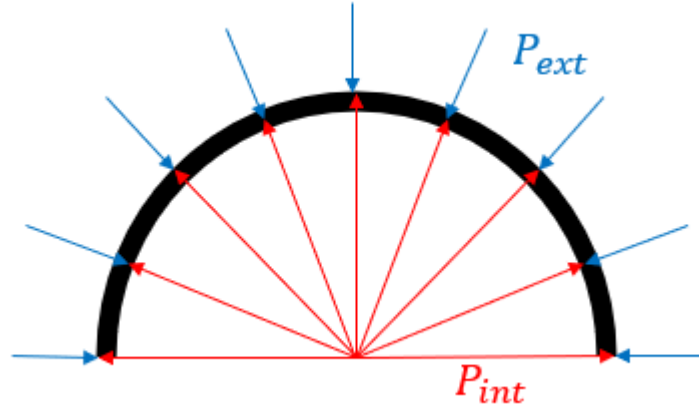


Figure 3.2: Schematic representation of FBD of forces experienced during winding on a cross-section of the vessel

Literature was used to find an expression for the external pressure being applied by winding a new layer. Lee and Springer [82] proposed a formulation that is based on the physics of filament winding, the pressure applied by the  $j + 1$  layer on the previously wound layer  $j$  could be expressed as:

$$P_{\text{ext}_y}^j = \frac{F^{j+1} \sin^2 \phi}{r_f^{j+1} b^{j+1}} \quad (3.8)$$

where  $F$  is the winding tension force,  $\phi$  is the winding angle specified based on the stacking sequence,  $r_f$  is fiber radial position and  $b$  is the tow bandwidth. This equation gives an expression of the external pressure generated in the hoop direction due to the winding of subsequent layers. Due to the  $\sin^2 \phi$  component, the hoop layers are then the layers which generate the highest external pressure in the hoop direction while being wound, leading to higher compaction. To find an expression for the axial external pressure caused by winding the helical layers, a similar expression as above is found:

$$P_{\text{ext}_x}^j = \frac{F^{j+1} \cos^2 \phi}{r_f^{j+1} b^{j+1}} \quad (3.9)$$

These two counteracting pressure forces and their interaction is what define the consolidation process. The resultant pressure, which is the difference between both pressure components, would cause two stress components, one in the axial direction (x-direction in the global coordinate system) and one in the hoop direction (y-direction in the global coordinate system). According to thin-walled cylinder theory, which is used in this case as CLT imposes thin-walled assumption as discussed earlier, the stresses in the axial and hoop direction could be given as follows, where the derivation is mentioned in [Appendix A](#):

$$\begin{aligned} \sigma_x &= \frac{Pd}{4t} = \frac{Pr}{2t} \\ \sigma_y &= \frac{Pd}{2t} = \frac{Pr}{t} \end{aligned} \quad (3.10)$$

where  $P$  in the previous equation indicates the pressure difference. These two stress components would then give rise to forces in the global  $x$  and  $y$  directions, which would be translated into the CLT model as  $N_x$  and  $N_y$ . Other components of the force matrix in [Equation 3.4](#) would then be zero.  $N_x$  and  $N_y$  are computed as follows:

$$\begin{aligned} N_x &= \sigma_x t = \frac{Pr}{2} \\ N_y &= \sigma_y t = Pr \end{aligned} \quad (3.11)$$

However, following the assumption that only the cylinder is considered and no axial forces exist,  $N_x$  is set to zero. If a full vessel is to be considered, this term would be readjusted then. Additionally, to visualize the radial stresses

through the thickness, force equilibrium of the forces along the radial direction of the vessel was taken and the following equation was formulated where the derivation could be found in [Appendix A](#):

$$\sigma_r = P_{int} - P_{ext} \quad (3.12)$$

where  $\sigma_r$  is the radial stress.

### 3.2.5. Material Properties

One of the challenges of predicting the stresses generated during the winding process is estimating the material properties to be used. Typically, analysis methods deal with cured composite structures and the material properties could then be directly obtained from coupon, substructure or structure testing and if not possible, then material data sheets are used. The approach followed is imposing assumptions on the already available material properties for the cured composite structure to estimate reasonable material properties for uncured material.

As have been displayed in [Equation 3.3](#), the required material properties are:  $E_1$ ,  $E_2$ ,  $\nu_{12}$  and  $G_{12}$ . The first assumption to be made is that  $E_1$  would be unchanged between cured and uncured stages, which is a conservative estimation. In a cured composite material,  $E_1$  could be reasonably obtained using the following rule of mixture expression:

$$E_1 = E_f \nu_f + E_m(1 - \nu_f) \quad (3.13)$$

where  $E_f$  is the fiber stiffness,  $E_m$  is resin stiffness and  $\nu_f$  is fiber volume. Due to the resin contribution, the stiffness of the cured composite material is actually less than the stiffness of the fiber alone. In the case of uncured composite, the resin is still in liquid form, and thus, does not contribute to the laminate stiffness. In other words,  $E_m$  is zero. This assumption is valid as the stiffness of the resin significantly varies by changing the degree of cure,  $\alpha$ . Bogetti and Gillespie Jr [83] derived the following expression of resin stiffness by relating to the degree of cure:

$$E_m = (1 - \alpha)E_m^0 + \alpha E_m^\infty \quad (3.14)$$

where  $E_m^0$  is the uncured resin modulus and  $E_m^\infty$  is the fully cured modulus. As  $E_m^0$  is approximated to be  $E_m^\infty/1000$ , it could be assumed that the uncured resin stiffness is indeed zero. Additionally, as the resin is still in an uncured state and in liquid form, the fiber volume is essentially the entire volume of the load-bearing material. Thus, in an uncured state, the stiffness should be equal to the fiber stiffness, which is why assuming the stiffness of the uncured composite in the longitudinal direction is equal to the cured state is a conservative estimate.

On the other hand, the stiffness in the fiber's lateral direction is expected to be significantly lower. This is because the stiffness in the lateral direction is matrix dominated, and as the resin in the uncured stage is still in liquid form, it does not contribute to the stiffness as discussed. Following the same line of logic, the Poisson's ratio would be expected to be lower and the shear stiffness,  $G_{12}$  is assumed to be zero as well. However, the values for the lateral and shear stiffness should not be inputted as zero to avoid singularity issues which would be experienced while computing the ABD matrix.

The carbon fiber material used is Toray's T700 and Huntsman's epoxy resin. In [Table 3.1](#) a comparison of the uncured and cured material properties is presented after making the previous assumptions.

Table 3.1: Material properties comparison between cured composite stage and the uncured stage

Material Property	Cured Stage	Uncured Stage
$E_1$	147 [GPa]	147 [GPa]
$E_2$	10 [GPa]	1 [MPa]
$\nu_{12}$	0.27 [-]	0.1 [-]
$G_{12}$	7 [GPa]	1 [MPa]

### 3.2.6. Model Approach and Methodology

The liner is pressurized during manufacturing generating a so-called *consolidation pressure*. This pressure contributes to the pressure gradient experienced while winding each layer, which in turn affects the resin flow. By winding several subsequent layers, the effect of the internal liner pressure decreases for the new layers. To counteract

this, the approach in practice is often to have a pressure schedule, where the internal liner pressure is increased in increments at several layers to maintain the effect the liner pressure has on the newly wound layers.

The flow chart summarizing the methodology and the logic behind how the model works could be displayed in [Figure 3.3](#). As just mentioned, for some layers there are increments in pressure increase. For these layers, there are additional followed steps as seen on the flow chart's right-hand side.

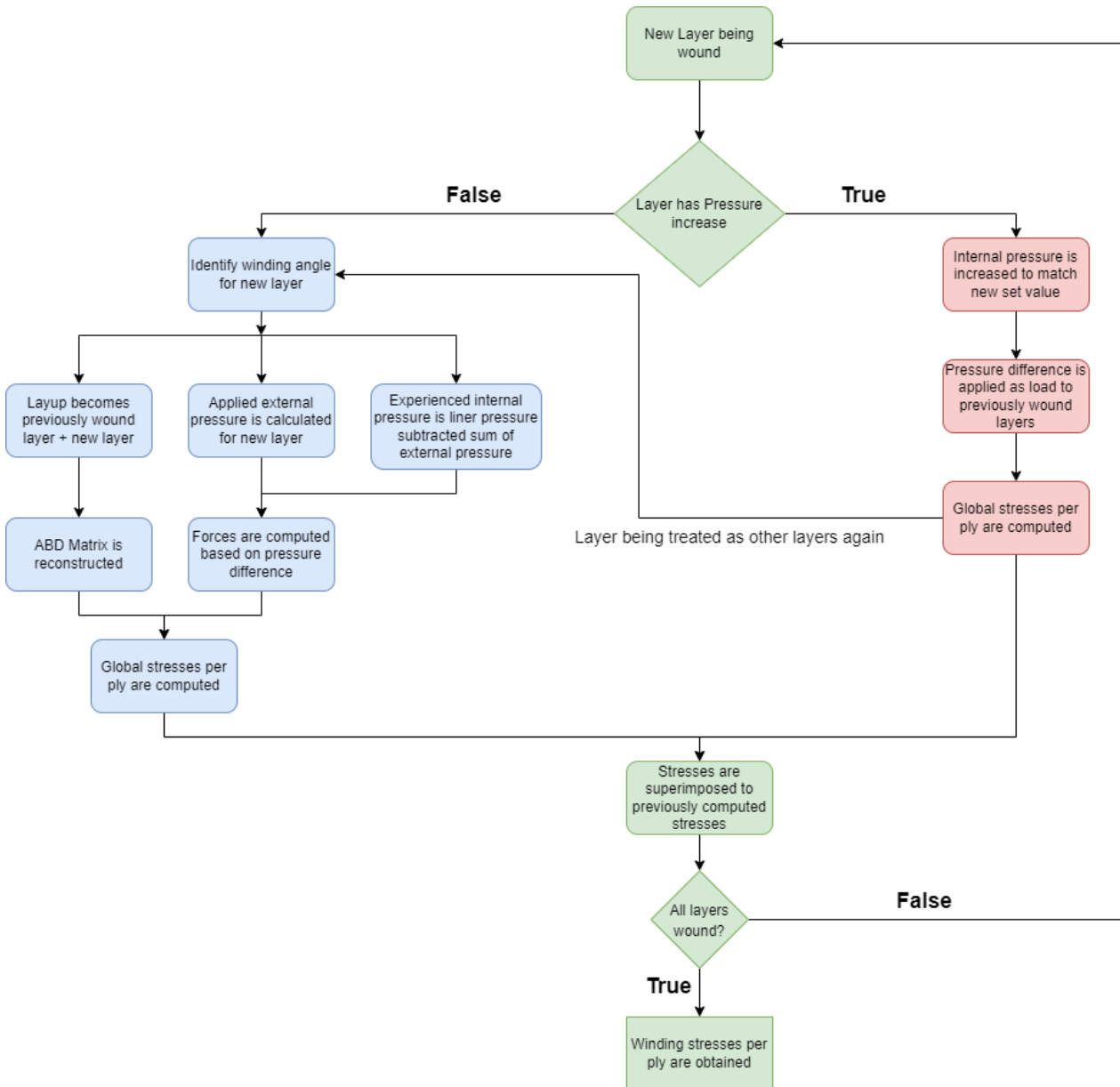


Figure 3.3: Flowchart describing the methodology behind the analytical model

Starting with the layers with no pressure increment, the first step is to redefine the layup by joining the new layer to the previously wound layers based on its winding angle. In other words, if two  $90^\circ$  layers were already wound and a new  $16^\circ$  layer is to be wound, then the layup is redefined from  $[90_2]$  into  $[90_2, 16]$ . In turn, this would mean that the ABD matrices needed to be recalculated to distribute the stresses per ply based on the winding angle as has been previously discussed in [subsection 3.2.3](#).

The applied external pressure in the hoop direction is calculated based on [Equation 3.8](#). For the first layer being wound directly on the liner, the experienced internal pressure would be equal to the initial starting internal liner pressure. However, by winding an additional layer, the experienced internal pressure decreases as there is a counter-acting external pressure exhausted by the first wound layer. To account for this decrease in the experienced internal pressure, the approach was to subtract the internal pressure from the external pressure from the previously wound layers. This could be visualized in [Figure 3.4](#), where it could be seen that while winding the second layer, the applied

external pressure is equal to the external pressure calculated using Equation 3.8 with the angle being that of the second layer. Additionally, the internal pressure is equal to the internal pressure experienced by the previous layer subtracted from it the external pressure applied by the previous layer. If the internal pressure becomes negative, a condition was added to keep it at zero as it is not possible to have negative internal pressure. Physically, this would represent the internal pressure pushing the layer and preventing it from being placed on the liner, which does not represent reality.

After redefining the layup and determining the internal and external pressure applicable for the new layer, the stresses in the global coordinate system are computed using the previously discussed CLT method in subsection 3.2.3. The applied stresses are distributed to the newly wound layer and the previously wound layers based on their winding angle. For the previously wound layers, the stresses are superimposed with the already existing residual stresses for winding previous layers. This could be visualized in Figure 3.4 when winding the first layer, the stress experienced by the first layer,  $\sigma_1$  is equal to the stresses experienced by winding the first layer,  $\sigma_{1,1}$ . While winding the second layer, a new stress component is added to  $\sigma_1$ , which is the stress experienced by the first layer due to winding the second layer,  $\sigma_{1,2}$ .

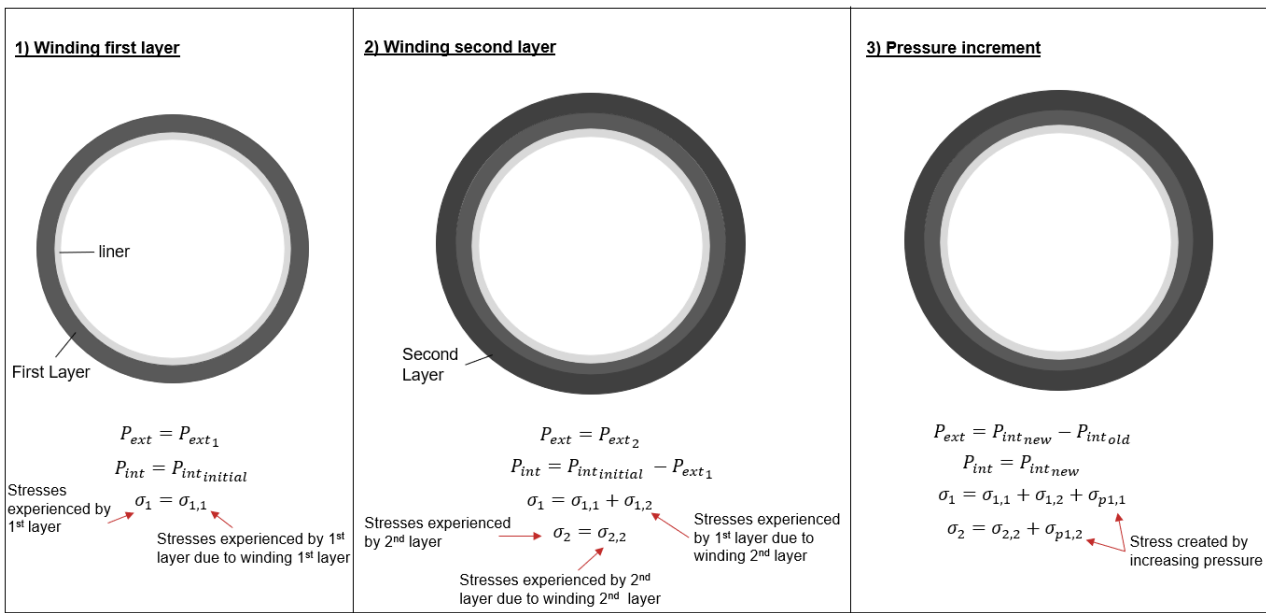


Figure 3.4: Schematic representation displaying the changes in the internal and external pressure and the stress increments while winding two successive layers, which could be visualized in steps 1 and 2. In step 3, the stress distribution and pressure changes during a pressure increment are displayed.

Whenever there is a pressure increment scheduled for a new layer, the difference in pressure created is applied as a load to the previous layers first. This could again be seen in Figure 3.4, wherein the third step,  $P_{ext}$  is equal to the increase in pressure created. The stresses are superimposed again as described by adding the stresses due to the first pressure increment,  $\sigma_{p1}$ . After applying the load due to the pressure increment, the new layer is treated as other layers again.

To summarize the stresses being experienced by each individual layer, Equation 3.15 could be used. In this equation,  $i$  indicates the layer number,  $n_L$  is the number of layers and  $n_p$  is the number of pressure increase steps. Due to this superposition of stresses, this would then lead to the stress distribution in the hoop direction being discontinuous as the normal force magnitude keeps on changing from layer to layer.

$$\sigma_i = \sum_{j=i}^{n_L} \sigma_{i,j} + \sum_{j>1}^{n_p} \sigma_{pj,i} \quad (3.15)$$

### 3.3. Selection of Vessel Configurations & Model Results

In this section, different proposals for vessel configurations are set and based on the results from the analytical model, qualitative and quantitative predictions are made on the end-product quality. These different vessel configurations would then be manufactured and tested, which would be discussed in more detail at a later stage in this report. A comparison would then be made between the results of the analytical model and experimental testing. Simultaneously, this section serves as a sensitivity analysis for the analytical model where the influence of changing

certain parameters on the results would be observed and compared with what is expected based on the literature or not. The proposed vessel configurations aim at investigating the following:

1. Influence of varying the winding tension force;
2. Influence of varying the internal pressure schedule;
3. Influence of changing the stacking sequence grouping;
4. Influence of changing the vessel diameter.

The approach followed is setting a baseline vessel configuration, which is a vessel that was previously designed and tested at Plastic Omnium. This baseline vessel configuration would serve as a default vessel where changes would be made with respect to that configuration to be able to isolate the influence of certain parameters. Comparison and evaluation of new configurations would also be made with respect to the baseline configuration.

### 3.3.1. Baseline Vessel Configuration

Originally, the baseline vessel configuration was designed for failure at an internal pressure of 1600 bars at the hoop layers in the cylindrical section. The baseline vessel stacking sequence and pressure schedule could be seen in [Figure 3.5](#). The baseline vessel would be later referred to as **Config 1**. The additional parameters to be known are:

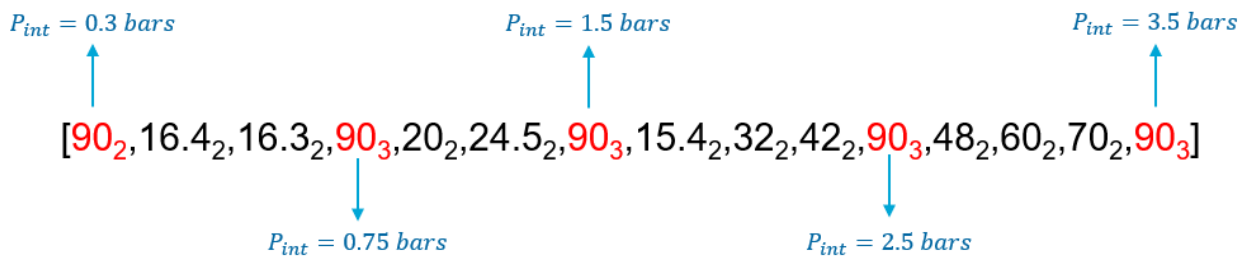


Figure 3.5: Pressure increase schedule for baseline vessel configuration. The layers highlighted in red are the layers where there is a pressure increment.

- Diameter = 140 [mm] (4L vessel);
- Winding tension = 17 [N] per tow;
- FVF = 60 %.

For every layer wound, there are two stress points computed, one for the top of the layer and the other for the bottom. Due to the asymmetry of the stacking sequence, it is expected that different strain and thus, stress values would be observed between both sides of the same layer. This is as the B matrix, will not be zero, leading to bending coupling and warping of the layers. The evolution of the hoop stress accumulation for each individual layer while winding the baseline vessel configuration could be displayed in [Figure 3.6](#).

The inner layers are the ones experiencing the highest stress. As for the first few layers, the layup is initially very small consisting of a few layers, so the load gets divided by a small number of layers. This could be seen where the stress value for these layers is mainly generated while winding the first 9 layers. While winding the subsequent layers, the stresses attributed to each individual layer is much smaller. Another main reason is that the first two layers are hoop layers, which are the stiffest in the hoop direction. They are followed by four layers of low-angle helical layers, which provide minimal tangential stiffness. Thus, when a load is applied, most of the stresses are redirected to the lower hoop layers, causing an increase in the residual hoop stresses for these layers.

Additionally, in the same figure, it could be seen that at the first pressure increase, the stresses in the lower hoop layers almost double and the top of the second hoop layer shifts to tension. The difference between these two values is the same reasoning why for the same layer there are differences in stress. From the [CLT](#) model description in [subsection 3.2.3](#), the strains were obtained around the mid-plane, then translated to every layer using the thickness and curvature as per [Equation 3.5](#). Before winding layer 7, the layup is asymmetric, causing the curvature to be high, thus warping the laminate causing the top to be under tension and the bottom of the laminate to be experiencing compression. This could be visualized when considering the global hoop strains during the first pressurization as displayed in [Figure 3.7](#). The strain increases while going up the laminate, and thus, the experienced loads become more tensile.



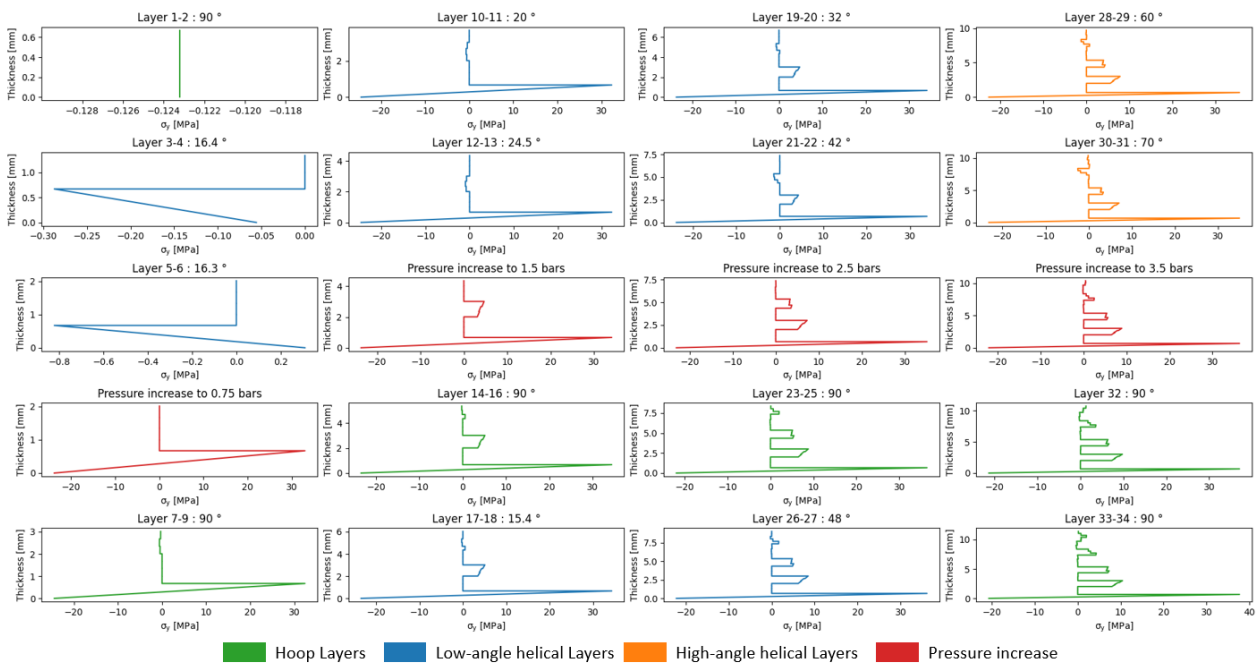


Figure 3.6: Evolution of hoop stress distribution through the thickness graph by winding every layer

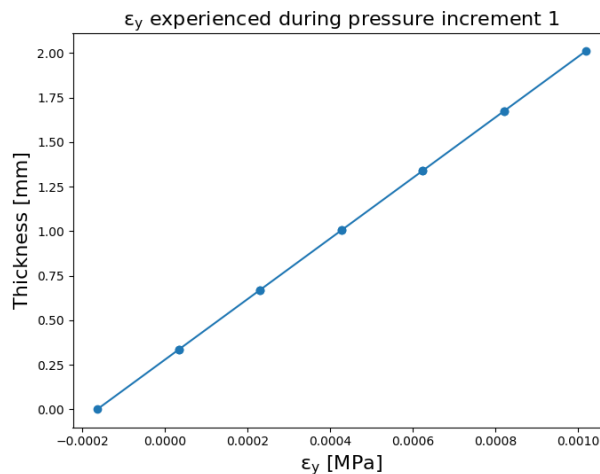










Figure 3.7: Global hoop strains induced during the first pressure increment from 0.3 to 0.75 bars for the baseline vessel configuration.

Another important thing to be noticed in Figure 3.6, is that the stresses added by each pressure increment decrease as the layup becomes thicker, so more layers to divide the stresses onto. Moreover, for the first pressure increase, most of the loads are again carried by the inner hoop layers as these are the stiffer plies in the hoop direction.

### 3.3.2. Summary of Testing Configurations

In the following subsections, additional configurations are proposed with the aim of investigating the influence of the previously stated parameters. There are two additional configurations that would not be discussed in this chapter but are to be used later on in chapter 5, which are Config 7 and Config 8, where the FVF was changed with respect to the baseline vessel to 50 % and 70 % respectively. These two configurations were previously manufactured and tested in an earlier investigation by Plastic Omnium. A summary of all the vessel configurations is presented in Table 3.2. For every configuration, there is a deviation in one parameter with respect to the baseline vessel, Config 1. This difference is highlighted in red for every row.

Table 3.2: Summary table of the proposed configurations where the entries highlighted in red are the changed parameter with respect to Config 1.

Vessel Configuration	Vessel Diameter [mm]	Winding Tension Force per tow [N]	Internal Pressure Range [bar]	FVF [%]	Stacking Sequence	
Config 1	140	17	0.3 to 3.6	60	[90 <sub>2</sub> ,16.4 <sub>2</sub> ,16.3 <sub>2</sub> ,90 <sub>3</sub> ,20 <sub>2</sub> ,24.5 <sub>2</sub> ,90 <sub>3</sub> ,15.4 <sub>2</sub> ,32 <sub>2</sub> ,42 <sub>2</sub> ,90 <sub>3</sub> ,48 <sub>2</sub> ,60 <sub>2</sub> ,70 <sub>2</sub> ,90 <sub>3</sub> ]	
Config 2	140	5	0.3 to 3.6	60	[90 <sub>2</sub> ,16.4 <sub>2</sub> ,16.3 <sub>2</sub> ,90 <sub>3</sub> ,20 <sub>2</sub> ,24.5 <sub>2</sub> ,90 <sub>3</sub> ,15.4 <sub>2</sub> ,32 <sub>2</sub> ,42 <sub>2</sub> ,90 <sub>3</sub> ,48 <sub>2</sub> ,60 <sub>2</sub> ,70 <sub>2</sub> ,90 <sub>3</sub> ]	
Config 3	140	17	0.48 to 5.6	60	[90 <sub>2</sub> ,16.4 <sub>2</sub> ,16.3 <sub>2</sub> ,90 <sub>3</sub> ,20 <sub>2</sub> ,24.5 <sub>2</sub> ,90 <sub>3</sub> ,15.4 <sub>2</sub> ,32 <sub>2</sub> ,42 <sub>2</sub> ,90 <sub>3</sub> ,48 <sub>2</sub> ,60 <sub>2</sub> ,70 <sub>2</sub> ,90 <sub>3</sub> ]	
Config 4	140	17	0.3 to 3.6	60	[90 <sub>3</sub> ,16.4 <sub>2</sub> ,16.3 <sub>2</sub> ,20 <sub>2</sub> ,24.5 <sub>2</sub> ,15.4 <sub>2</sub> ,32 <sub>2</sub> ,42 <sub>2</sub> ,48 <sub>2</sub> ,60 <sub>2</sub> ,70 <sub>2</sub> ,90 <sub>11</sub> ]	
Config 5	140	17	0.3 to 3.6	60	[90 <sub>14</sub> ,16.4 <sub>2</sub> ,16.3 <sub>2</sub> ,20 <sub>2</sub> ,24.5 <sub>2</sub> ,15.4 <sub>2</sub> ,32 <sub>2</sub> ,42 <sub>2</sub> ,48 <sub>2</sub> ,60 <sub>2</sub> ,70 <sub>2</sub> ]	
Config 6	250	17	0.3 to 3.6	60	[90 <sub>2</sub> ,16.4 <sub>2</sub> ,16.3 <sub>2</sub> ,90 <sub>3</sub> ,20 <sub>2</sub> ,24.5 <sub>2</sub> ,90 <sub>3</sub> ,15.4 <sub>2</sub> ,32 <sub>2</sub> ,42 <sub>2</sub> ,90 <sub>3</sub> ,48 <sub>2</sub> ,60 <sub>2</sub> ,70 <sub>2</sub> ,90 <sub>3</sub> ]	
Config 7	140	17	0.3 to 3.6	50	[90 <sub>2</sub> ,16.4 <sub>2</sub> ,16.3 <sub>2</sub> ,90 <sub>3</sub> ,20 <sub>2</sub> ,24.5 <sub>2</sub> ,90 <sub>3</sub> ,15.4 <sub>2</sub> ,32 <sub>2</sub> ,42 <sub>2</sub> ,90 <sub>3</sub> ,48 <sub>2</sub> ,60 <sub>2</sub> ,70 <sub>2</sub> ,90 <sub>3</sub> ]	
Config 8	140	17	0.3 to 3.6	70	[90 <sub>2</sub> ,16.4 <sub>2</sub> ,16.3 <sub>2</sub> ,90 <sub>3</sub> ,20 <sub>2</sub> ,24.5 <sub>2</sub> ,90 <sub>3</sub> ,15.4 <sub>2</sub> ,32 <sub>2</sub> ,42 <sub>2</sub> ,90 <sub>3</sub> ,48 <sub>2</sub> ,60 <sub>2</sub> ,70 <sub>2</sub> ,90 <sub>3</sub> ]	

### 3.3.3. Influence of Varying Winding Tension Force

To isolate the influence of the winding tension force on the end-product quality, a new vessel configuration is proposed with a different winding tension force relative to the baseline vessel configuration. In the baseline vessel, a winding tension of 17 N was used for winding the defined layers and 10 N for the connectors. In the proposed configuration, which would be referred to as **Config 2**, a lower winding tension of 5 N per spool was designed, which is around 70 % lower. Such a significant change was made to clearly observe the influence of tension force in experimental results and step out of the bounds of scatter. For the connectors, a tension force of 10 N was maintained to avoid slippage of connectors.

It was discussed in [chapter 2](#) that a lower winding tension force would lead to a lower external pressure being applied while winding. This in turn leads to a less compaction force being applied, which lowers the pressure gradient for resin flow. As less resin is squeezed out down a potential gradient, the **FVF** through-the-thickness would be lower than having a higher tension force. Having a lower **FVF** is expected to directly lead to a lower burst performance as fibers are the main load-bearing component in **CPVs**. Therefore, it is expected based on background information from the literature that having a lower winding tension force, would lead to lower final product quality.

From the analytical model perspective, the same should be expected as following from [Equation 3.8](#), a lower winding tension force would directly lead to a lower external pressure being applied, which would also lead to lower compaction as per the previous discussion. The differences in pressure,  $P_{int} - P_{ext}$ , while winding every layer for Config 1 and 2 could be visualized in [Figure 3.8](#). The red solid line indicates the zero line, where if the graph is under, then it indicates that the external pressure is higher and vice versa. This graph does not display the compaction but is beneficial to visualize the pressure difference while winding every layer, and thus, anticipate the deformation each configuration would have on the final product quality. In other words, whenever  $P_{ext}$  is higher than  $P_{int}$  then there is a compaction force being applied to the liner. If this is the trend for all the low-angle helical layers, which are the ones which compact the liner axially the most, then a decrease in length is expected. If it is the other way around, then an increase in length is expected. The same could be done for the diameter and circumferential layers, but during experimental testing, it would be harder to measure and correlate.

Whilst comparing these two configurations, it could be seen that for the helical layers, especially the low-angle ones, the difference in pressure is positive for Config 2 and negative for Config 1. As a result, it is expected that Config 2 would have an increase in length, while Config 1 would have a decrease in the final vessel's length after winding.

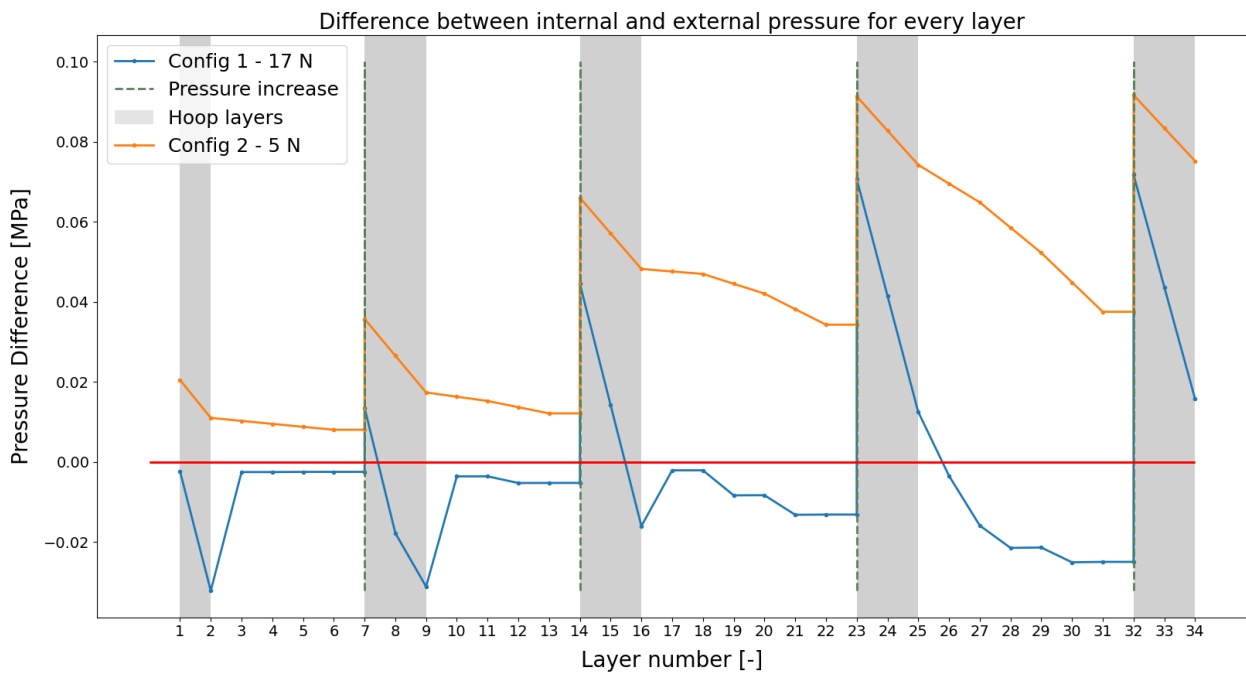


Figure 3.8: Difference in pressure,  $P_{int} - P_{ext}$ , for every layer for the baseline configuration and Config 2, which is at a lower winding tension force.

To visualize the compaction, the overall radial stress distribution for every layer could be utilized, which is shown for Config 1 and 2 in Figure 3.9. While winding every layer, radial compaction is exerted using Equation 3.12 based on the experienced internal and external pressure. This applied radial compaction is experienced by the layer itself, and the layers underneath. The radial stresses for every layer are then found by superimposing the radial stresses exerted on it by the following layers. As a result, this explains the decreasing shape of the radial stress and the zero value for the last layer. A difference in pressure would exist in the final product between the residual radial stress and internal pressure, which would be experienced by the liner and hence deform it.

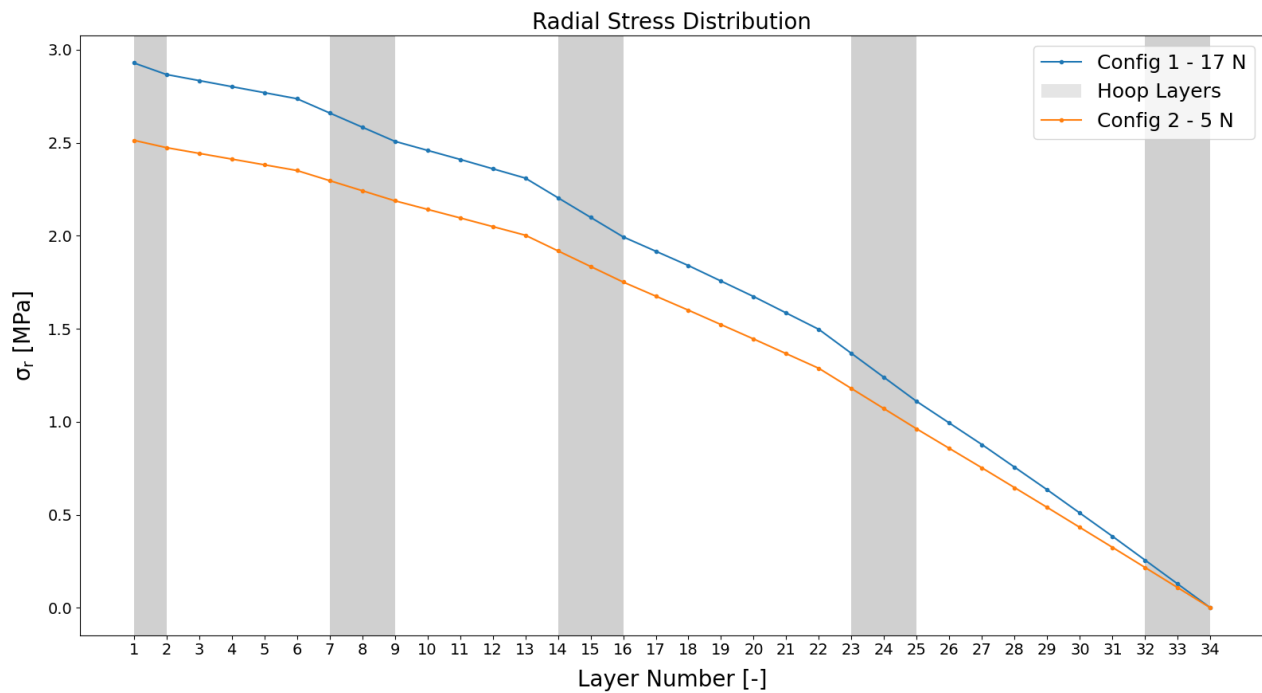


Figure 3.9: Radial stresses generated during winding two different configurations with different winding tension forces, Config 1 and Config 2.

Based on Figure 3.9, as the stacking sequence remains unchanged, it could be seen that for every individual layer,

the radial stresses experienced by every layer are higher in Config 1. Thus, increasing the winding tension force increases the radial compaction due to an increase in the applied external pressure. As a result of an increase in radial compaction, more resin will hence be squeezed out of the fiber bed, which would consequently lead to an expected increase in FVF and a decrease in porosity content by increasing tension force. Following this line of reasoning, based on the analytical model results, it is expected that a lower FVF and larger porosity content would be present in Config 2 when compared with Config 1.

The hoop stress distribution through the thickness could be later displayed in Figure 3.10. First off, it could be seen that hoop layers are the layers that carry the most stress as they are the layers with the highest tangential stiffness. Helical layers carry almost zero stresses, especially at the first layers as these helical layers are low-angle ones. Tensile loads are better than compressive loads for winding stresses. This is as the uncured composite is incapable of bearing any compressive loads, as the resin is still in liquid form. This then entails that the fibers would have to bend or wrinkle to bear compressive loads, which would significantly impact the vessel's mechanical performance. However, the preference would be to have the residual hoop stress distribution around zero to prevent any tensile residual stresses in the end product.

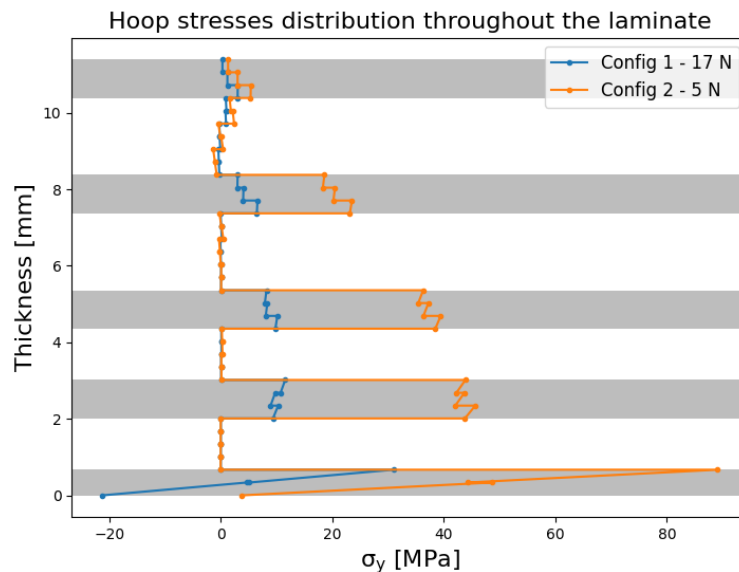


Figure 3.10: Hoop stress distribution between baseline vessel, Config 1, and Config 2 which has a lower winding tension force of 5N.

Based on the hoop and radial stress distribution, and the expected lower FVF and higher porosity content in Config 2. As FVF and burst performance are directly related, it is hence expected that the burst performance of Config 2 would be lower than Config 1, due to a decrease in the winding tension force.

### 3.3.4. Influence of Varying Internal Pressure

The next proposed configuration aims at relating the influence of internal pressure on the final product quality. The effect caused by internal pressure is similar to the one caused by winding tension and would follow the same line of thought, however, what is different is the triggering factor. The proposed configuration would have a 60 % higher internal pressure schedule compared to the baseline. A 60 % higher pressure schedule was proposed to be high enough to be able to clearly visualize the difference such a change causes to FVF, void volume and burst performance during testing. Thus, internal pressure values range from 0.48 to 5.6 bars. This configuration would be referred to as **Config 3**.

Increasing the internal liner pressure means that the pressure at the interface between the liner and the innermost layer increases. As a result, this leads to a direct increase in compaction as there is a higher pressure force being exerted on the laminate. Additionally, an increase in pressure gradient increases as the difference between internal pressure and atmospheric pressure increases, thus, more resin would be drawn out of the fiber bed towards the top surface causing an increase in FVF and a decrease in porosity gradient through the thickness.

By investigating the pressure difference graph in Figure 3.11, for most of the layers, the pressure difference in Config 3 is higher than in Config 1. This could be attributed to the increase in internal pressure. After a few layers after a pressure increase, the two graphs tend to coincide. This is as the internal pressure is counteracted by more layers and at some point reaches zero, and as the external pressure is the same, both layers coincide. Having a higher internal

pressure and a positive pressure difference would then mean that the external pressure exerted by the helical layers is being fully counteracted and additional internal pressure is available to expand the liner even. Thus, a positive increase in length is expected for Config 3, or at least the vessel length would be higher than Config 1.

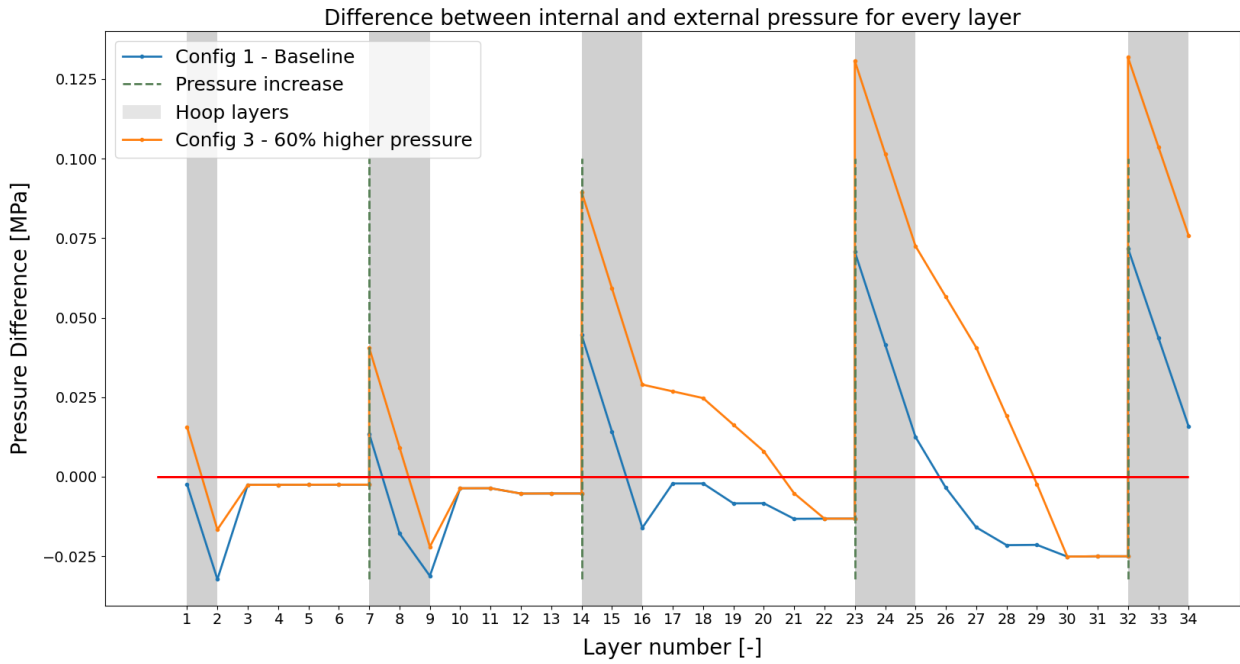


Figure 3.11: Difference in pressure,  $P_{int} - P_{ext}$ , for every layer for the baseline configuration and Config 3, which is at a higher internal pressure schedule.

The difference in compaction could be visualized when considering the difference in radial stresses between Config 1 and Config 3 as displayed in Figure 3.12. The radial stresses in Config 3 are higher than in Config 1, which indicates that higher radial compaction is thus experienced in Config 3. As a result, a higher pressure gradient would then be available, which would tempt resin to squeeze out of the fiber bed, creating a higher FVF and lower porosity content in Config 3, when compared to the baseline vessel.

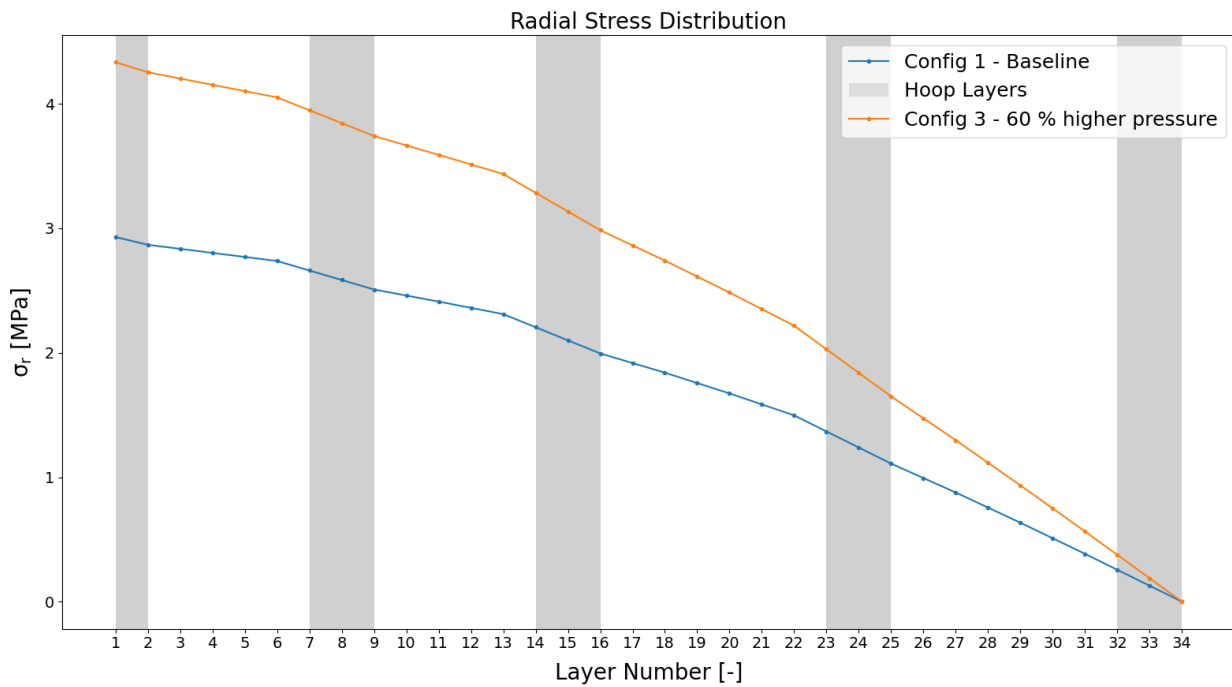


Figure 3.12: Radial stresses generated during winding two different configurations with different internal pressure, Config 1 and Config 3.

The hoop stress distribution comparison between both configurations is presented in [Figure 3.13](#). At higher internal pressure, there are higher tensile stresses being experienced as the liner is exerting more tensile loads on the laminate wishing to expand more in the tangential direction. When selecting an internal pressure value, the magnitude of tensile stresses should be observed first, as if it is too high, might cause the liner to already burst during winding, in case the liner is not stiff or strong enough to withstand such pressure loading with limited support from uncured composite materials.

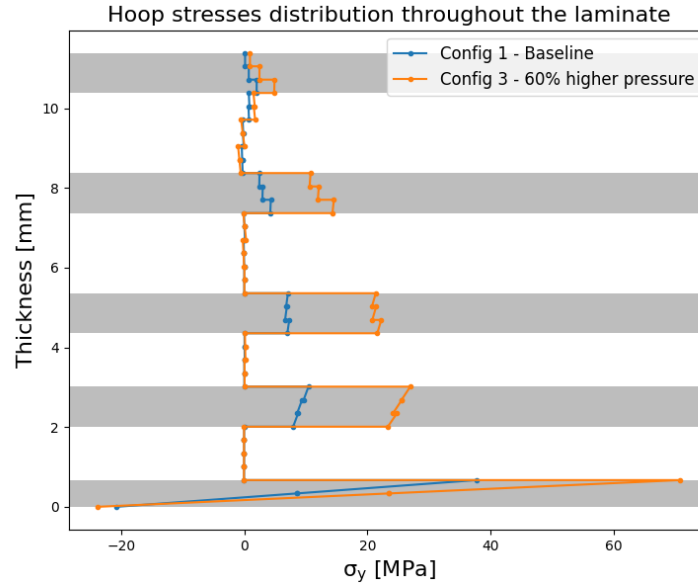


Figure 3.13: Hoop stress distribution between baseline vessel, Config 1, and Config 3 which has 60 % higher internal pressure.

Based on the expected higher compaction, which leads to higher [FVF](#) and lower porosity content distribution through the thickness, and reasonable tangential stress distribution, it is hence expected that Config 3 would have a higher burst pressure performance than Config 1.

### 3.3.5. Influence of Varying Stacking Sequence

Following the discussion in [subsection 2.3.3](#), especially the investigation by Nebe [34] on the influence of the stacking sequence grouping displayed in [Figure 2.6](#), two different vessel configurations are proposed to test whether the same effect would be expected in wet winding, as the study was based on prepreg winding. In essence, using the same layers but with different grouping and positioning and under the same process parameters, would lead to different end-product quality.

The first proposed configuration, **Config 4** groups the helical layers first then followed by the hoop layers. While the second proposed configuration, **Config 5**, does the opposite by winding the hoop layers first then the helical layers. The winding tension, vessel diameter and [FVF](#) remained unchanged with respect to the baseline. The pressure schedule increments are unchanged as well, but the layers at which pressure is added have changed, where the approach followed was to add a pressure increment after every 3 hoop layers, as they create the highest external pressure.

To visualize the difference in compaction, the radial stress distribution for these two configurations could be seen in [Figure 3.14](#). By looking at the hoop layers, which are represented by grey and are in layer numbers 24-34 in Config 4 and 1-14 in Config 5, it is apparent that higher radial stresses are experienced by the hoop layers in Config 5. This is as the high-angle helical layers, exert high radial compaction on the hoop layers, leading to an increase in compaction experienced by these layers and hence, a higher [FVF](#) and lower porosity content in hoop layers in Config 5.

Considering the helical layers in both configurations, layers 3-24 in Config 4 and 14-34 in Config 5, there is a difference in compaction in both layers as well. The difference is more clearly seen in the last layers, where in Config 4, the helical layers experience higher radial compaction. This is as they are followed by hoop layers, which provide high radial compaction in the cylindrical region. This would then trigger the resin flow out of the surface, causing a higher [FVF](#) and lower porosity content in the helical layers in Config 4.

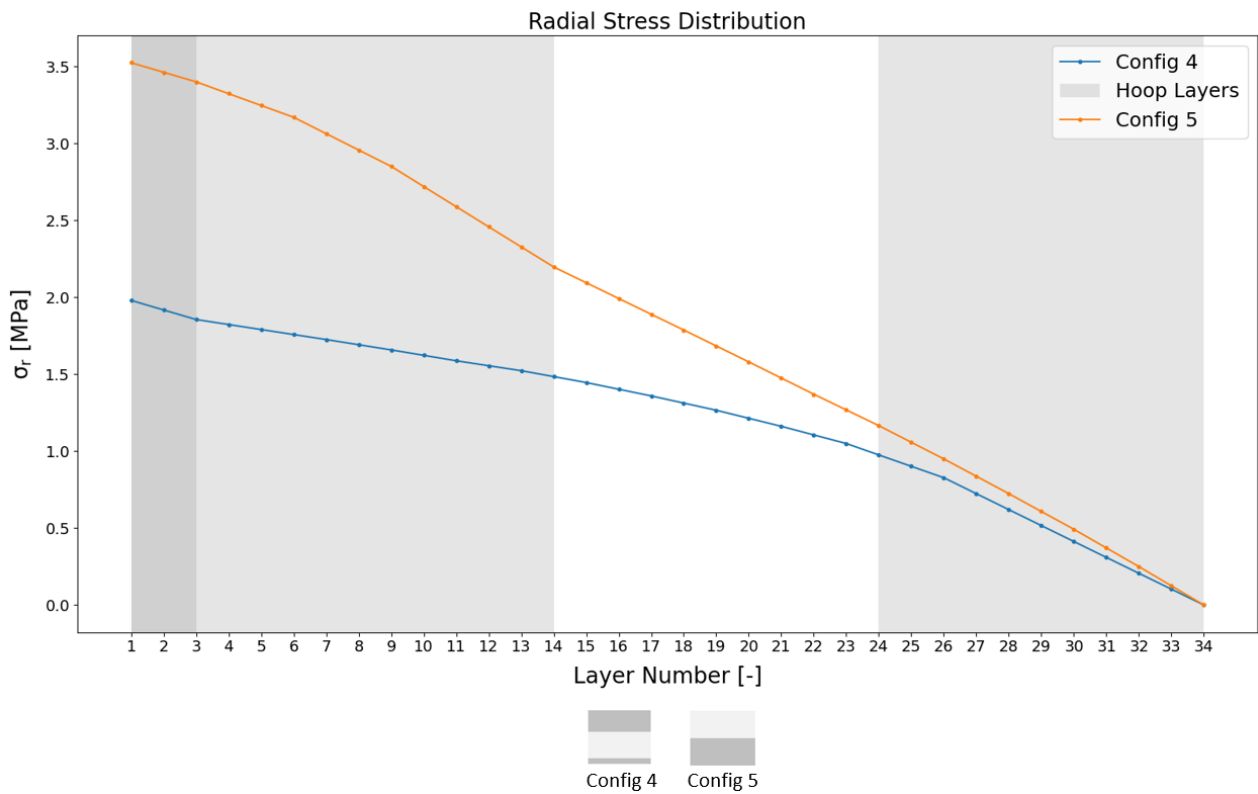


Figure 3.14: Radial stresses generated during winding two different configurations with different stacking sequences, Config 4 and Config 5.

By only considering a cylinder in the analytical model, the hoop layers are the critical layers. As a result, increasing the compaction of the hoop layers and increasing the FVF in these layers, is expected to increase the vessel's burst performance, rather than increasing the compaction in the helical layers. As a result, based on the difference in compaction, it is expected that Config 5 would have a higher burst performance than Config 4.

To anticipate the changes in length, the low-angle helical layers could be considered separately. As the helical layers are more compacted in Config 4, then a higher squeezing force is exerted by these layers on the liner, causing a decrease in the vessel's length. Additionally, the pressure increments were applied in Config 4 whenever hoop layers were wound, thus, the helical layers were wound at lower internal pressure. As a result, the low-angle helical layers exert more force and have lower counteracting pressure. Consequently, it is expected that Config 4 would have a shorter vessel length, in comparison with Config 5.

### 3.3.6. Influence of Changing Vessel's Diameter

The last aspect to investigate is changing the vessel's diameter. This was previously discussed in [subsection 2.3.4](#), where it was concluded that purely increasing the diameter without increasing the stacking sequence and process parameters would lead to lower compaction and burst performance. The geometry of the vessel is directly related to the resultant radial force experienced during winding, where the applied external pressure is dependent on the radius of the vessel. As seen in [Equation 3.8](#), the radius is inversely proportional to the external pressure, thus, at a larger diameter, less compaction would take place due to a lower pressure gradient being created. When comparing the radial compaction of Config 1 and 6 presented in [Figure 3.15](#), it could be observed that lower compaction is indeed experienced when the vessel diameter is increased as expected. As a result, a lower FVF and higher porosity content are expected in Config 6.

The pressure difference could be seen in [Figure 3.16](#) where a more positive pressure difference exists, which would indicate an increase in length. The burst performance was not assessed in this investigation. As mentioned in [subsection 2.3.4](#), there are different parameters that come into play when increasing the vessel diameter that the difference in burst performance, while keeping everything constant, would not be directly attributed to the change in diameter.

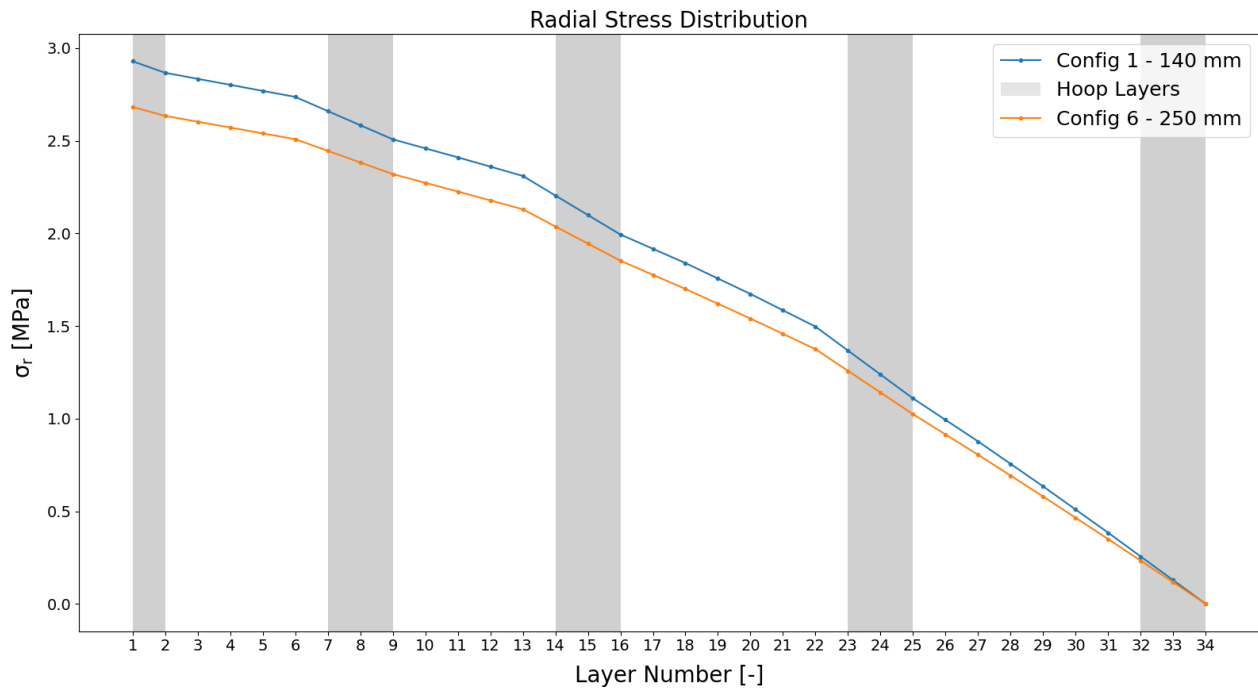


Figure 3.15: Radial stresses generated during winding two different configurations with different liner diameters, Config 1 and Config 6.

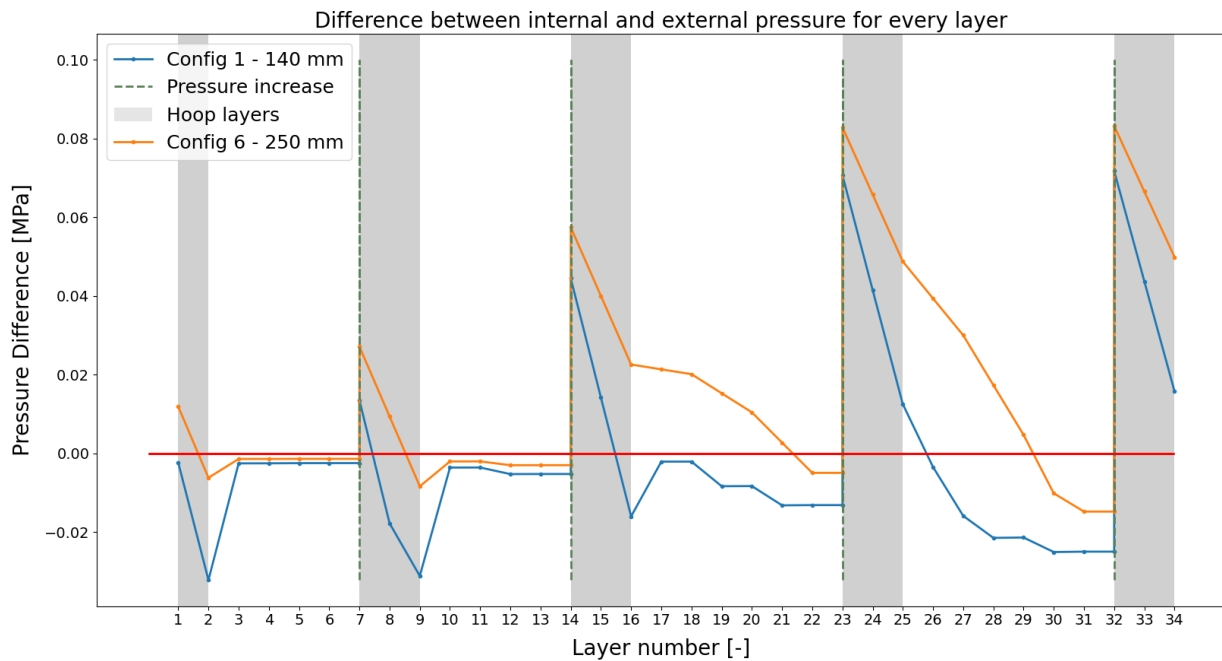


Figure 3.16: Difference in pressure,  $P_{int} - P_{ext}$ , for every layer for the baseline configuration and Config 3, which is at a higher liner diameter.

For practical reasons, manufacturing vessels at different vessel diameters are limited for a few aspects. Mainly, it is limited due to the availability of liners with different vessel diameters as liners are usually produced in large batches. Thus, due to scarcity of resources, the investigation was limited to testing two different vessel diameters, Config 1 at 140 mm and the new vessel configuration, **Config 6**, has the exact same configuration as Config 1, but only the vessel diameter is different at 250 mm.



### 3.4. Analytical Model Hypothesis



In this section, the hypothesis regarding the observed experimental results is summarized. In [Table 3.3](#), the hypothesis regarding changes in length, FVF, porosity content and burst pressure for configurations 2,3,6,7 and 8 with respect to the baseline vessel are listed. Additionally, in [Table 3.4](#), the hypothesis for the two configurations with different stacking sequences, 4 and 5, are grouped together as they are compared relative to each other.

In [section 3.3](#), the hypothesis for configurations 2 till 6 was discussed with supporting graphs and explanations. However, for configurations 7 and 8, no discussions were made as these two vessels were already tested in a previous investigation by Plastic Omnium and as the analytical model is not capable of taking into account changes in FVF. However, the expectations based on the changes in the configurations are listed in [Table 3.3](#).

Table 3.3: Hypothesis regarding experimental results for Config 2,3,6,7 and 8 with comparison to the baseline vessel, Config 1.

Configuration	Attribute wrt Baseline	Change wrt Baseline Vessel			
		Length	FVF	Porosity	Burst Pressure
<b>Config 2</b>	Lower tension force 5N	Longer	Lower	Higher	Lower
<b>Config 3</b>	Higher internal pressure 60% higher	Longer	Higher	Lower	Higher
<b>Config 6</b>	Larger vessel diameter 250 mm	Longer	Lower	Higher	Not tested
<b>Config 7</b>	Lower designed FVF 50%	Longer	Lower	Higher	Lower
<b>Config 8</b>	Higher designed FVF 70%	Shorter	Higher	Lower	Higher

Table 3.4: Hypothesis regarding experimental results for Config 4 and 5 with comparison to each other.

Stacking Sequence	Length	FVF		Porosity		Burst Pressure
		Hoop	Helical	Hoop	Helical	
 Config 4	Longer	Lower	Higher	Higher	Lower	Lower
 Config 5	Shorter	Higher	Lower	Lower	Higher	Higher

## Manufacturing & Experimental Testing

To correlate the previously obtained results and validate the developed analytical model, experimental testing results are required. Current state-of-the-art methods to experimentally characterize CPVs were mentioned in section 1.4. In this chapter, the description of the manufacturing and testing campaign underwent in effort to experimentally assess the quality of the proposed vessel configurations is addressed. The manufacturing and burst testing process held at Plastic Omnium's facility is briefly described. Afterwards, the microscope testing preparation and execution are described in section 4.2.

### 4.1. Manufacturing and Burst Testing of CPVs

#### 4.1.1. Liner Preparation and Assembly

The initial step in the manufacturing process is preparing the liner and its assembly. The plastic liners are produced in batches by the blow moulding process in Plastic Omnium's facilities. The liners are then assembled with boss parts, which are specific to either being headstock or tailstock, to prevent unscrewing of the boss parts while winding or curing. The vessel dimensions and mass are recorded after assembly. A picture displaying the liner assembly for the sub-scale 4L vessels could be visualized in Figure 4.1. The liner material is high-density polyethylene, while for larger vessel sizes (250 mm), the liner material is Polyamide-6.

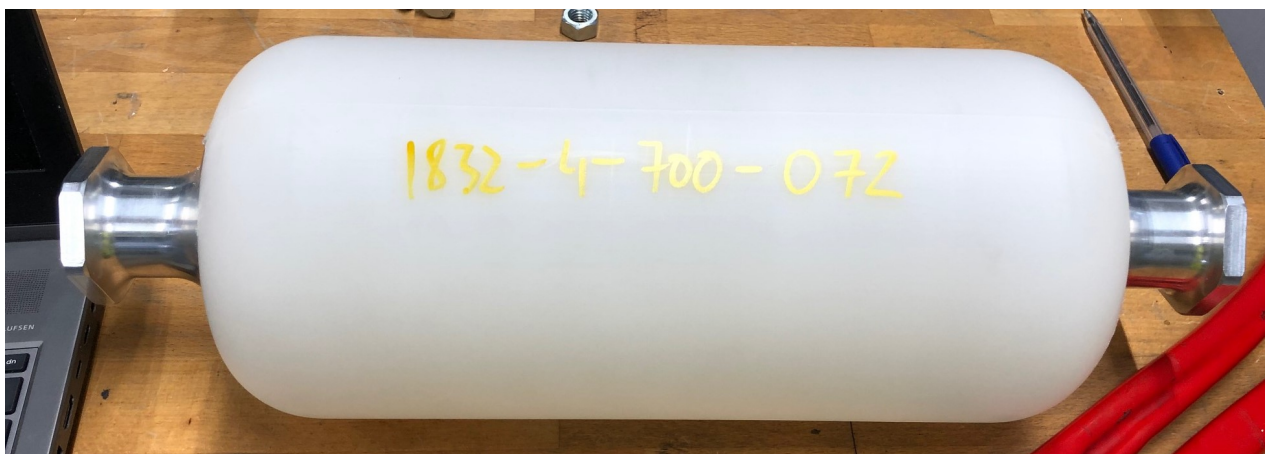


Figure 4.1: Schematic and actual image of liner assembly for sub-scale 4L vessel.

#### 4.1.2. Winding Process

The main centrepiece in the wet winding process is the 6-axis KUKA robot with built-in pressure outlets. The 6-axis include movement of the mandrel in x,y and z directions, rotation of the mandrel around its longitudinal axis, yaw rotation of the mandrel and rotation of the winding eye. The pre-tensioned tows are dipped into the resin bath based on the designed impregnation rate. The tows then reach the winding eyes where they are placed on the mandrel by utilizing the different axis of motion available. A general view of the wet winding setup could be viewed in Figure 4.2.

The robot takes as an input machine motion coordinates which are extracted and generated based on the predefined winding pattern and stacking sequence. These required machine motion coordinates are generated using CompositaD<sup>1</sup>, which is one of the leading winding software in the industry. CompositaD calculates fiber trajectories based on user-defined inputs. These inputs could be the choice of geodesic or non-geodesic fiber path, winding angle, winding pattern and bandwidth. Afterwards, all these results would be translated into a series of machine motions, which is something that is defined based on the robot language, that is then exported into the winding machine.

After manufacturing, the last reached internal pressure is kept constant until after curing to avoid liner deformation and maintain laminate quality. The vessels are placed in the oven, where four vessels could be placed simultaneously, and are rotated while curing. After curing, an additional vessel inspection step takes place where the internal

<sup>1</sup><https://www.compositcad.com/>

pressure is measured to check if pressure was lost during curing and the surface quality is inspected. Lastly, the dimensions and mass of the vessel are recorded and measured.



Figure 4.2: Robot-assisted wet winding machinery available at Plastic Omnium.

### 4.1.3. Burst Testing

If the vessel passes the quality inspection steps, it is either passed for burst pressure testing or microscope testing. Burst testing is done at Plastic Omnium's facility where the vessel is placed inside a concrete bunker to avoid any debris splashing outside. It is then connected to a Maximator high-pressure pump where water is added at a constant rate until a burst occurs. The burst pressure value is then recorded and used for later comparison. There is a possibility of using a high-speed camera to monitor the failure mode and location of the vessel, but for the duration of this research project, it was not possible. The location of failure of every vessel could be concluded by inspecting the vessel after failure.

## 4.2. Microscope Sample Preparation and Testing

The second type of experimental testing that would be performed in this research project is microscope testing, where samples are taken from manufactured vessels at different configurations. For these different configurations, different information is extracted via microscope testing as FVF and porosity content for the overall laminate or specific layers.

### 4.2.1. Microscope Sample Preparation

Sample preparation steps could be concisely summarized in [Figure 4.3](#). The first step is cutting the samples that are manufactured for microscope testing into 3 rings at 3 different positions. As microscope testing is a very localized method of testing, samples from different vessel sections are extracted to minimize the localization effect. The idea is that two rings are taken right after the dome sections from both sides and a ring from the middle of the cylinder. The vessels were cut using UZAY MAKINA® band saw cutting machine available at Plastic Omnium's facility.

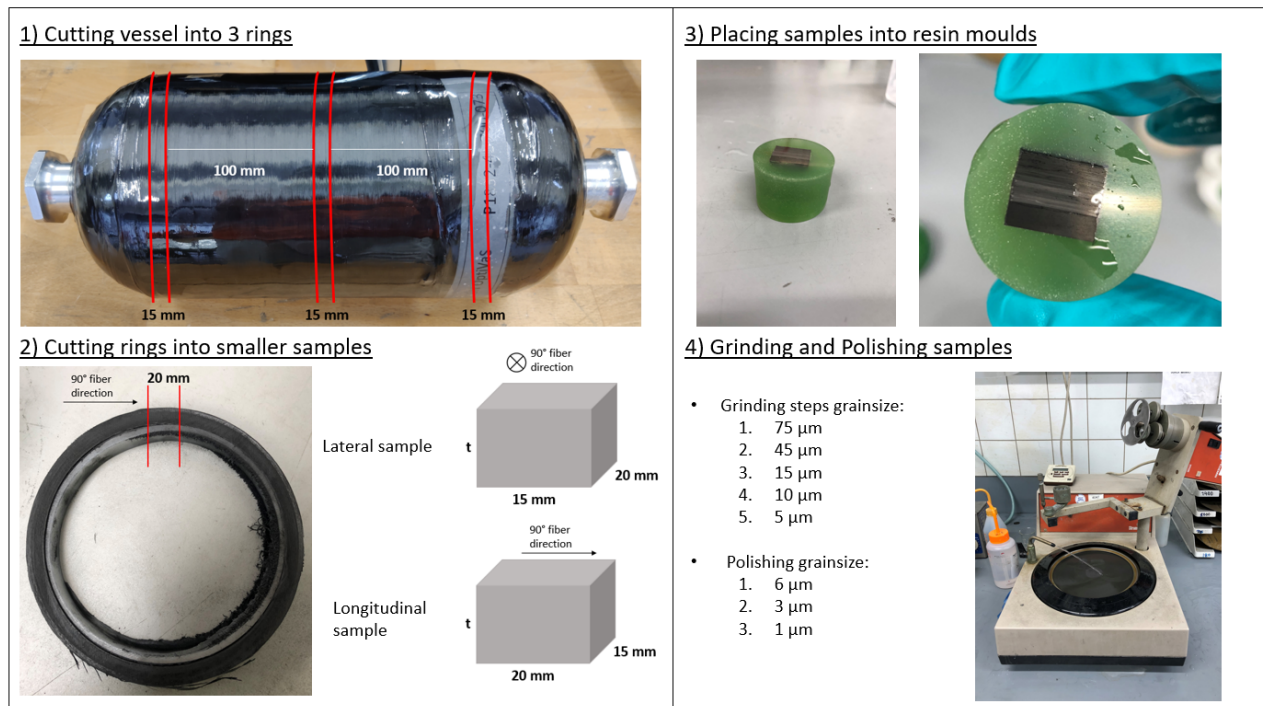


Figure 4.3: Description of the microscope sample preparation steps followed.

Followed by that, the rings are then cut into two different types of samples, either a lateral or longitudinal one as displayed in Figure 4.3. The aim of the lateral sample is to be used for measuring FVF and porosity content, while the longitudinal sample is to view the compaction of layers, especially inner ones. Starting from this step, the preparation takes place at Delft Aerospace Structures & Materials Laboratory (DASML) where the rings were cut using Struers® diamond cutter. The cutting wheel speed was set at 3000 rpm.

Afterwards, the cut samples were cleaned and then placed in an epoxy resin mould using Technovit® 4071 fast curing powder and liquid. The side which would be examined needs to be placed facing the bottom of the mould. The following step is to grind the prepared resin moulds to remove micro-shattering caused by the cutting process and to flatten the surface in preparation for polishing. The grinding method followed is wet grinding, while water is continuously applied as the plate is rotating. Grinding was done in five steps that each sample has to follow at 5 different grain sizes; 75,45,15,10,5  $\mu\text{m}$  in descending order.

The last step in sample preparation is polishing to remove all the scratches created while cutting and grinding and to have a clear view of the sample under the microscope. Polishing is also done in three steps with three different grain sizes; 6,3,1  $\mu\text{m}$  in descending order. Before polishing, the samples need to be cleaned, which is done via an ultrasonic bath full of ethanol. Afterwards, diamond paste corresponding to the polishing plate and grain size is applied on the sample and then polished. This step is repeated three times for the three different grain sizes. Once done, the samples are dried using air pressure and stored in sample containers with the corresponding label.

#### 4.2.2. Microscope Testing

Once the samples are ready, they could then be viewed under the microscope. To ensure the sample is flat from the microscope perspective, it is placed on top of clay on a metal piece, to flatten out the top surface of any bending and avoid light reflection. The used microscope is Keyence® laser microscope VK-X1000. The microscope with one of the samples placed could be seen in Figure 4.4.

There are several magnifications available. To clearly see the fiber diameter, a 20x wide lens was used to capture images. As there are 3 longitudinal samples per vessel, 2 images were taken at different locations at such magnification to measure FVF and porosity content. Lower magnifications were used to capture an image of the entire sample as it is very time-consuming to capture images of a large area with high magnification. This is because the microscope works by stitching, where several images are taken at the predefined magnification to cover the required area, and then combined together to form one final image.

For analysis of the result, IA was opted for as it is the most convenient method. ImageJ® software was used to measure thickness, FVF and porosity content. Thickness is measured by adjusting the number of pixels to the predefined scale added to the image, then any distance could be measured. FVF and porosity are measured using thresholding, a



Figure 4.4: Keyence® laser microscope VK-X1000 used for microscope testing.

segmentation method. The images generated are 8-bit, which then creates  $2^8 = 256$  intensity graduations that could be attributed to every pixel. The two extremes, 255 and 0 are white and black respectively. Anything else is between are different shades of grey. By thresholding, pixels that fall within a desired range of intensity are separated from the others and a percentage is given of the content of these pixels. By specifying the intensity range for fibers and voids, percentages of FVF and porosity content could be determined. The captured images for estimations for the lateral samples are under 20x magnification. The steps of specifying intensity ranges for FVF and porosity content could be displayed in Figure 4.5. The images are first cropped and then rotated to be aligned with the horizontal axis. Afterwards, thresholding is done by adjusting the intensity scale to either select the fibers, resin or voids.

In high-resolution images, it is possible to distinguish certain layer groups depending on the diameter of the fibers. An example could be seen in Figure 4.6 where a clear distinction could be made between high- and low-angle helical layers and hoop layers. This distinction is useful when a comparison of FVF and porosity percentages between different layer grouping is made, which is most relevant for configurations where the stacking sequence was changed. Also, an example of the difference between resin-rich areas and porosity could be displayed as well.

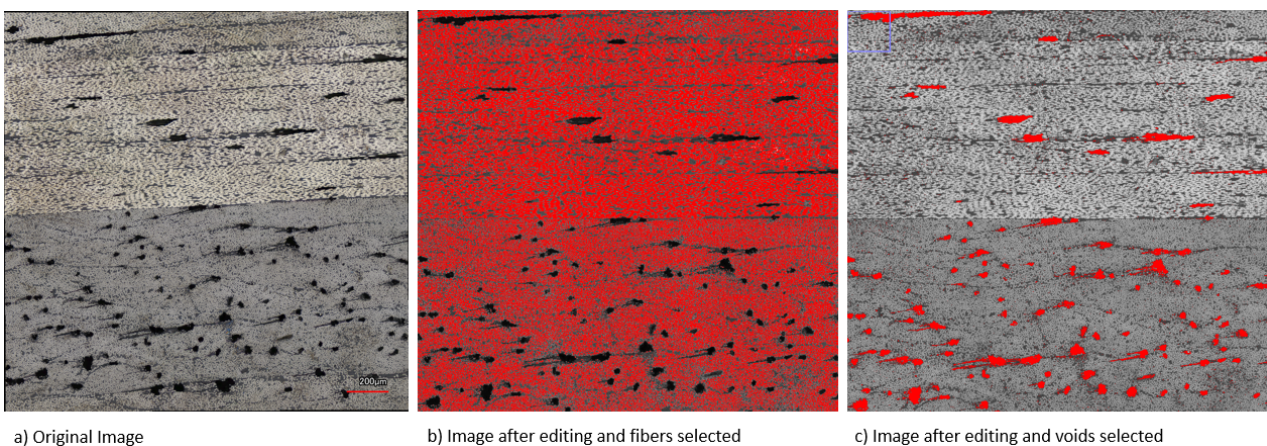


Figure 4.5: Image analysis approach to estimate FVF and porosity content based on colour intensity using ImageJ software.

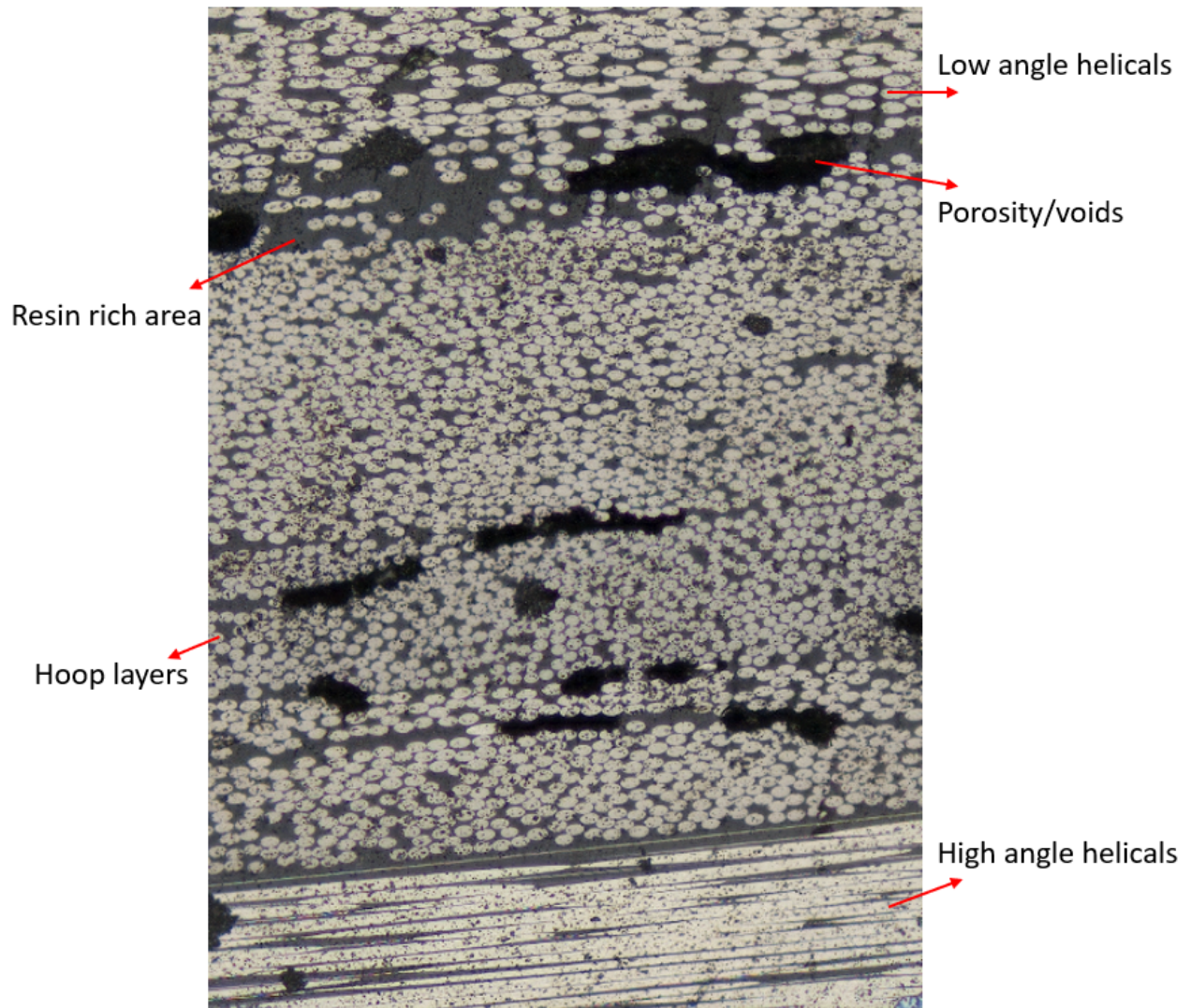


Figure 4.6: Visualization of different layer grouping and difference between resin-rich areas and porosity which could be viewed under 20x magnification.

## Results & Discussion

Due to the extreme operating conditions of CPVs, the experimental characterizations tend to become consequently complex. In this chapter, the obtained experimental results are displayed where the change in length, diameter and mass before and after winding and curing were recorded. It was observed that these parameters change correspondingly with the vessel configuration where the results are displayed in section 5.1. The first set of experimental results is the burst pressure testing results presented in section 5.2. The following results displayed in section 5.3, following the description in section 4.2, are the microscope results containing FVF, porosity content and laminate thickness comparison for different configurations. The set of results is then followed by a discussion in section 5.4 where the previously presented results are discussed and compared to results from the literature and analytical model in an attempt to answer the proposed research questions. Finally, in a concluding way, a framework for determining manufacturing parameters for CPVs is proposed in section 5.5 based on the previous discussion.

It should be noted that in this chapter, two different vessels for Config 5 were tested. One of which, would be referred to as Config 5-no pressure, where due to an error in setting up the winding program during manufacturing, no pressure increments were applied. This vessel was however tested as a support for the investigation of the influence of internal pressure on the end-product quality.

### 5.1. Dimensions Results

The length, vessel diameter and mass were measured before winding and after curing. The change in diameter is essentially twice the laminate thickness. The laminate mass is also the change in mass. The results are presented to check for correlation in changes in length, laminate thickness and mass with changes in vessel configurations. The results could be displayed in Table 5.1.

For every configuration, there were at least three different vessels that were manufactured to increase the level of reliability. There is one exception to this, being Config 6, the vessel with a larger vessel diameter, as due to resource limitations for this thesis project, only one vessel was manufactured and producing more was not feasible. Additionally, it should be noted that for some configurations, the use of additional vessel data that were previously manufactured was made to boost the reliability of the available data.

Table 5.1: Average percentage change in length, laminate thickness and laminate mass for the different tested configurations.

Configuration	Average Percentage change in length [%]	Laminate Thickness [mm]	Laminate Mass [g]
1	-0.32	10.74	2602.96
2	0.05	12.14	2720.98
3	0.79	11.53	2730.65
4	-0.30	11.36	2645.89
5	0.30	11.01	2670.45
5 - no pressure	0.49	11.63	2735.20
6	-0.30	9.30	11582.00
7	-0.17	11.71	2824.00
8	-0.34	10.24	2506.25

#### 5.1.1. Statistical Analysis

To formulate sound conclusions and observations, statistical analysis was done to check if there is a significant difference between the different configurations. This was done using an independent two-tailed t-test. Independent t-test was used to check for significant difference between two sample groups. Two tailed t-test was chosen to check for positive or negative difference between the two compared configurations. The formula for the t-test is as follows:

$$t = \frac{\bar{x}_1 - \bar{x}_2}{\sqrt{\left(s^2 \left(\frac{1}{n_1} + \frac{1}{n_2}\right)\right)}} \quad (5.1)$$

where  $t$  is referred to as the  $t$ -value,  $\bar{x}_1$  and  $\bar{x}_2$  are the mean values for the two compared groups,  $s^2$  is the standard deviation of both groups and  $n_1$  and  $n_2$  are the number of the observations for both sample groups. P-value is then obtained by using the  $t$ -distribution table. The null hypothesis states that both independent samples have no significant difference based on the compared criterion. If the  $p$ -value is lower than 0.05, then the null hypothesis is rejected, which indicates that there is a significant difference. This was done for the values obtained in [Table 5.1](#) by comparing relevant configurations together. *YES* indicates that the null hypothesis is rejected and a significant difference exists, and vice versa for *NO*. The results for the statistical analysis are indicated in [Table 5.2](#).

Table 5.2: Statistical analysis using two-tailed independent T-test to check for significant difference between the tested configurations for the dimension results.

Comparisons	Percentage Change in Length	Laminate Thickness	Laminate Mass
Config 2 vs Baseline	NO	YES	YES
Config 3 vs Baseline	YES	YES	YES
Config 7 vs Baseline	NO	YES	YES
Config 8 vs Baseline	NO	NO	YES
Config 7 vs Config 8	YES	YES	YES
Config 4 vs Config 5	YES	NO	NO
Config 5 vs Config 5 - no pressure	NO	YES	NO

It should be noted that configuration 6 was not involved in the comparisons as there is only one point available. Hence, it creates an error when computing the  $t$ -test. The statistical analysis still does not give conclusive results whether there is actually a direct correlation or significant difference, due to the low number of data points available. Therefore, theory should be prioritized and statistical analysis results are used as a supporting argument.

### 5.1.2. Observations

Based on [Table 5.1](#) and [Table 5.2](#), the following observations could be made:

1. A change in **FVF** could affect the length, mass and thickness as seen by comparing Config 7 and 8 together. This was not the case when comparing Config 7 and 8 to the baseline vessel, but it is believed as the difference in the actual **FVF** was lower than designed. An increase in **FVF**, causes a direct decrease in mass, which correspondingly is also accompanied by a decrease in length and thickness.
2. A decrease in winding tension force does not cause a significant change in length, but does cause an increase instead of a decrease in length. The thickness and mass significantly increased. This could be seen in Config 2 vs Baseline comparison.
3. An increase in the pressure schedule by 60 %, which is the difference between Config 1 and Config 3, caused a significant increase in length, thickness and mass with respect to the baseline vessel configuration.
4. By comparing vessels of different diameters as Config 1 (140 mm) and Config 6 (250 mm), interesting results are observed. There hasn't been a noticeable change in length. However, the percentage change in thickness and mass seems to decrease significantly by increasing the vessel's diameter. It should be noted that as Config 6 had only one data point, conclusions should not be made as the reliability level of such an observation is low, but a confirmation of the trends could be made.
5. Changing the stacking sequence, between Config 4 and 5, had a strong influence on the percentage change in length. By considering changes in thickness and mass, the differences are minimal between both configurations.

## 5.2. Burst Pressure Results

Furthermore, in this section, the burst pressure results from the manufactured vessels are presented. The approach and setup were previously discussed in [chapter 4](#). The configurations to be burst tested are Configs 1,2,3,4,5,7 and 8, which are summarized in [Table 3.2](#). For every configuration to be burst tested, it was ensured that three vessels



were manufactured and burst tested. This is because the burst pressure tests could have a lot of scattering and variability during manufacturing due to several factors such as variation of process parameters (tension force, internal pressure, winding speed, impregnation rate, etc.). To increase the level of reliability and reduce such a scatter, it was determined to use three vessels for each configuration. Preferably, a higher number of vessels would be used, but due to the limitation of resources, it was limited to three.

Few exceptions existed, as for Config 7 and 8, where the data for these vessel configurations were already available from previous investigations at Plastic Omnium. For these two configurations, only two data points were available, however, they seem to follow the same trend, thus, the need for manufacturing and testing an additional vessel for each configuration was not prioritized. Additionally, the data for Config 1 were mostly from previous investigations available at Plastic Omnium, as it is the baseline vessel configuration. Moreover, for Config 4, three vessels were manufactured to be burst tested, however, only one data point was obtained as the other two vessels experienced difficulty in assembly to the testing chamber, where leaks were continuously observed. A summary of all the results could be displayed in [Table 5.3](#).

Table 5.3: Burst pressure results for the different configurations, alongside the average and standard deviation for every configuration.

Configuration	Burst Pressure [bars]				Average	STD
<b>1</b>	1617	1608	1655	1575	1613.8	28.49
<b>2</b>	1563	1428			1495.5	67.50
<b>3</b>	1661	1579	1619		1619.7	33.48
<b>4</b>	1653				1653.0	0.00
<b>5</b>	1655	1703	1777		1711.7	50.18
<b>5-no pressure</b>	1656				1656.0	0.00
<b>7</b>	1496	1462			1479.0	17.00
<b>8</b>	1661	1629			1645.0	16.00

Statistical analysis using an independent t-test was not utilized in this set of results due to the non-uniform number of available data, which makes such a comparison irrelevant. Thus, the observations were based on comparing the burst values for every configuration using the average and standard deviation. The observations that could be drawn are the following:

1. Decreasing the winding tension force leads to a decrease in burst pressure performance.
2. Increasing the internal pressure has no significant impact on the burst pressure.
3. Grouping and winding the hoop layers closer to the liner leads to an increase in burst pressure, as could be seen by comparing Config 1 and 5. Also, it leads to higher burst performance than winding than grouping and winding the helical layers closer to the liner, which could be concluded by comparing Config 4 and 5.
4. Increasing the [FVF](#) directly increases the burst pressure performance.

The baseline stacking sequence was designed to achieve failure in the circumferential layers in the cylindrical section of the vessel. This was the case for all vessel configurations with the same stacking sequence. However, for the configurations with different stacking sequences, Config 4 and 5, failure was observed in different locations. For Config 4, failure occurred in the dome region, while for Config 5, failure was observed in the boss thread. Therefore, composite failure for Config 5 is actually higher than the burst pressure value recorded. This is considered to be the reason why for configurations 5 and 5-no pressure, the burst values were similar, as the composite was not the limiting factor.

### 5.3. Microscope Testing Results

Lastly, in this section, the microscope testing results would be presented. It involves estimating the [FVF](#) and porosity content of the samples taken from ring sections of vessels of different configurations. Afterwards, comparing laminate thickness and resin residue from compaction on the top surface for different vessel configurations. The configurations that underwent microscope testing were Config 1,2,3,4,5 and 6.

Two different [FVF](#) data were obtained, as previously explained in [section 4.2](#), from microscope testing and the other is based on the mass difference. The second approach involves taking the recordings of the used fiber length from the winding machine, and transferring this into mass using material properties, then dividing over the difference in mass to obtain Fiber Mass Fraction ([FMF](#)). The [FMF](#) is transferred into [FVF](#) using the following equation:

$$V_f = \frac{\rho_r}{\rho_f \left( \frac{1}{FVF} - 1 \right) + \rho_r} \quad (5.2)$$

where  $\rho_r$  is resin's density and  $\rho_f$  is fiber's density. For configurations 7 and 8, only FVF obtained from mass difference was recorded as there were no vessels manufactured and cut for microscope testing.

The second set of results obtained from the microscope testing campaign was measuring the total laminate thickness and resin residue thickness on the top surface, using ImageJ software. Resin residue is created due to compaction whenever resin squeezes out, it tends to accumulate at the top surface. In some configurations, especially with different stacking sequences, resin residue was observed between layer grouping. However, this was harder to measure and compare, so only residue on the top surface was measured. An example of what the resin layer accumulation looks like is shown in Figure 5.1. It should be noted that the observed resin thickness was not always as uniform as in Figure 5.1, but in certain samples it varied significantly within the same sample, or was difficult to measure due to curvature of the vessel.

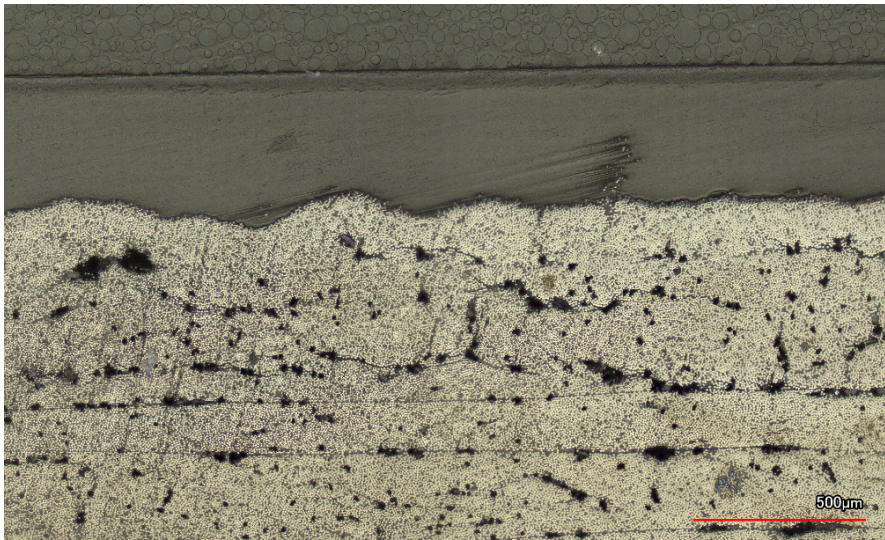


Figure 5.1: An example of an image taken at 20x magnification displaying the resin layer accumulation on the top surface.

The thickness was then measured by calibrating the distance that each pixel would represent using the scale present in the image based on the magnification. Afterwards, based on the specified distance, the number of pixels spanning that length is counted and using the previous calibration, the actual distance is estimated. The final results could be displayed in Table 5.4.

Table 5.4: FVF, laminate and resin thickness results obtained based on mass difference or microscope analysis for all the different configurations.

Configuration	Average FVF - Weight [%]	FVF [%]		Porosity [%]		Laminate Thickness [mm]	Resin Thickness [mm]
		Hoop	Helical	Hoop	Helical		
1	62.71	59.5		4.03		11.58	407.33
2	58.65	50.27		5.89		12.35	219.00
3	58.33	53.47		5.16		11.85	335.00
4	60.93	49.76	62.84	6.79	3.65	11.89	433.33
5	60.23	58.55	53.97	6.28	2.78	12.02	327.67
5-no pressure	58.24	43.75	49.79	14.42	3.75	12.27	135.33
6	68.26	56.53		6.3		10.56	376.33
7	55.21	N/A		N/A		N/A	N/A
8	65.81	N/A		N/A		N/A	N/A

While observing the samples, it was noticed that within the same sample, there is a significant difference in FVF and porosity content between the hoop and helical layers for configurations 4 and 5. An example of such a difference could be displayed in Figure 5.2. As a result, instead of taking an average for the whole vessel as for the other configurations, the recordings were split into hoop and helical layers as seen in Table 5.4.

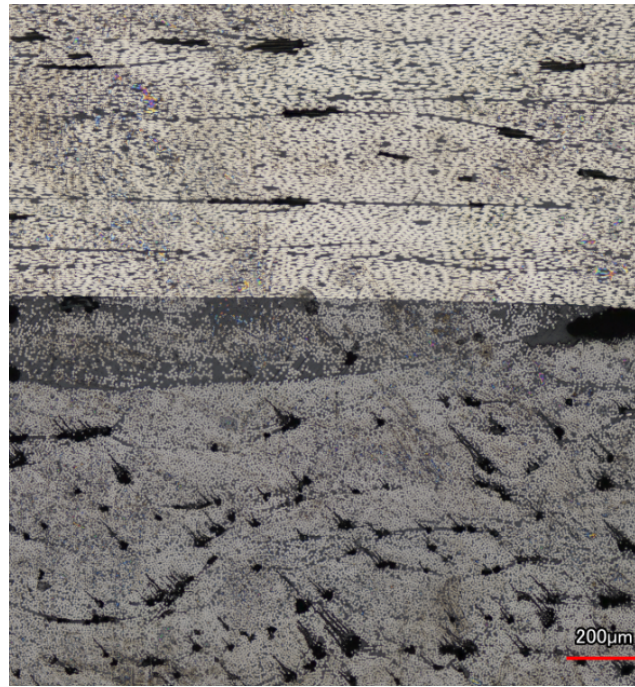


Figure 5.2: Image at 20x magnification for vessel 87 (Config 5) at the interface where the stacking sequence transitions from hoop to helical layers.

### 5.3.1. Comparing FVF Methods

As observed in Table 5.4, the FVF obtained from weight difference and the other from microscope testing have different values. However, the trends seem to be the same. This could be better visualized when considering Figure 5.3.

The difference in magnitudes could be accredited to a few differences. First off, in the FVF computation from FMF, voids are not taken into account in the volume calculation. This is as the entire laminate is assumed to consist of fibers and resin. However, voids occupy a significant area, which would cause this inaccuracy between both calculations. To confirm such a trend, the difference in FVF should then be the porosity content. Such a porosity content calculation is compared with the porosity content obtained from the microscope results and is displayed in Table 5.5.

Table 5.5: Porosity content comparison from the microscope testing results and by using the difference in FVF from laminate weight and microscope testing.

Configuration	Porosity - Micro [%]	Porosity - Weight [%]
1	4.03	3.21
2	5.89	8.38
3	5.16	4.86
4	5.22	4.63
5	4.53	3.97
5 - no pressure	9.09	11.47
6	6.30	11.73

The values do not quite match up, which indicates that it could be part of the reason, but not solely the entire reasoning for such a difference. Additional reasoning could also be that in the microscope testing, only the cylindrical part of the vessel was taken into account. For the same vessel, the dome region could be experiencing higher compaction than the cylindrical region. Thus, the FVF averages out to be higher when compared to FVF from microscope testing. FVF from weight calculation has an additional advantage, that more data is available as at least three data points were available per configuration, whilst from the microscope testing, only three relatively small samples were taken out of one vessel.

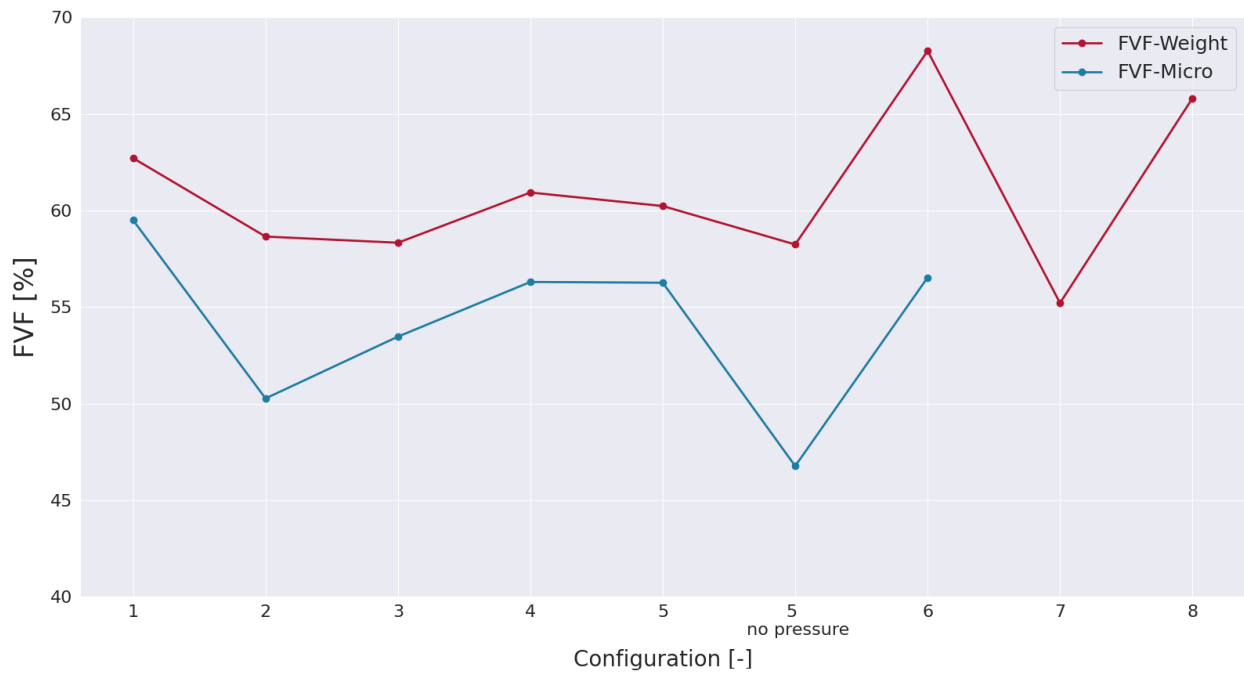


Figure 5.3: Comparison of the two obtained FVF results, from weight difference and microscope testing.

### 5.3.2. Comparing Laminate Thickness

Two different laminate thickness values were computed, first based on the change in diameter in [Table 5.1](#) and other from microscope testing in [Table 5.4](#). Both values could be compared against listed and compared against each other in [Figure 5.4](#). It could be seen that thickness from microscope testing is generally higher than from the one obtained based on the change in diameter. The thickness measured from using the change in diameter was made using pi tape, which is bound to errors if the tape is wrapped around the vessel at an angle. However, both results do follow the same overall trend, where they have similar sensitivity to changes in configurations.

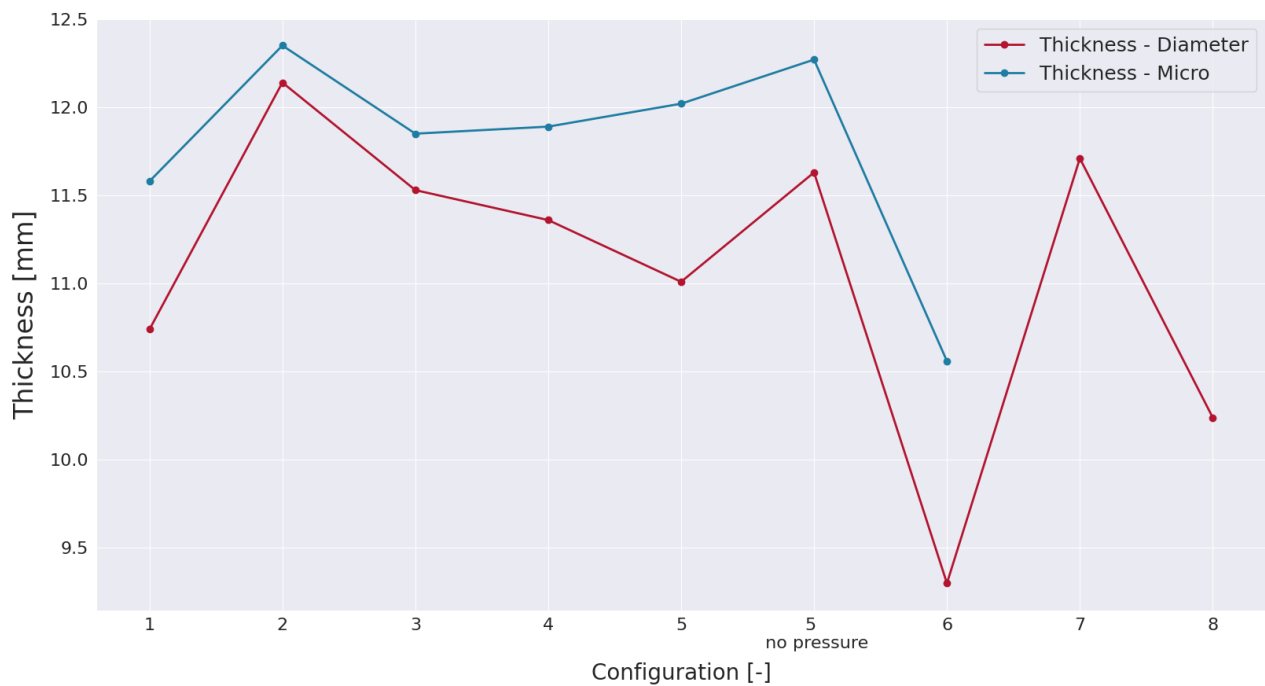


Figure 5.4: Comparison of the two obtained thickness values, from the change in diameter and microscope testing.

### 5.3.3. Statistical Analysis

Following the same approach as in [subsection 5.1.1](#), the significant difference for a predefined comparisons are computed and summarized in [Table 5.6](#). The entries that have *N/A* are added in the case where only one data value or none is available, and hence, a significant difference evaluation could not be established.

Table 5.6: Statistical analysis using two-tailed independent T-test to check for significant differences between the tested configurations for the microscope results

Comparison	FVF-Weight	FVF-Micro		Porosity-Micro		Laminate Thickness	Resin Thickness
		Hoop	Helical	Hoop	Helical		
<b>Config 2 vs Baseline</b>	YES	YES		YES		YES	YES
<b>Config 3 vs Baseline</b>	YES	YES		NO		NO	NO
<b>Config 6 vs Baseline</b>	NO	NO		YES		YES	NO
<b>Config 7 vs Baseline</b>	YES	N/A		N/A		N/A	N/A
<b>Config 8 vs Baseline</b>	NO	N/A		N/A		N/A	N/A
<b>Config 7 vs Config 8</b>	YES	N/A		N/A		N/A	N/A
<b>Config 4 vs Config 5</b>	NO	NO	YES	NO	NO	NO	YES
<b>Config 5 vs Config 5 - no pressure</b>	NO	YES	NO	YES	NO	NO	YES

### 5.3.4. Observations

From [Table 5.4](#) and [Table 5.6](#), observations could be made. First off, general observations regarding relations between values:

1. **FVF** from weight calculation is higher than from microscope calculation but tends to follow the same trend.
2. **FVF** and porosity are inversely proportional, whenever **FVF** increases, porosity decreases and vice versa.
3. Increasing the laminate thickness leads to a decrease in resin residue thickness on the top surface.
4. Laminate thickness calculation from microscope testing is higher than laminate thickness based on the change in diameter.

Additional observations could be made regarding the changes in configurations:

1. By lowering the winding tension force, the **FVF** tend to decrease and the porosity content increases. Correspondingly, the thickness increases and resin thickness decreases, which indicates lower compaction. This could be seen whilst comparing Config 1 and 2.
2. Increasing the internal pressure schedule created a decrease in **FVF** and an increase in porosity. Both laminate and resin thickness are affected slightly, which indicates lower compaction by increasing internal pressure.
3. A counteracting conclusion could be made when comparing configurations 5 and 5 - no pressure. With no internal pressure, **FVF** decreases and porosity increases significantly, especially for hoop layers. The resin thickness increases significantly, which indicates higher compaction by increasing internal pressure.
4. At a larger vessel diameter, slightly lower **FVF** and significantly higher porosity content are observed when comparing Config 1 and 6. A decrease in laminate thickness and resin residue thickness is also observed.
5. For configurations 4 and 5, a significant difference exists in **FVF** and porosity between the hoop and helical layers, where hoop layers are more compacted in configuration 5 and helical layers are more compacted in configuration 4.

## 5.4. Discussion

### 5.4.1. Influence of FVF

The influence of **FVF** on quality in literature has previously been discussed in [subsection 2.3.2](#). **FVF** has always been accredited to be the direct link between varying process parameters in **CPVs** production and the end-product quality. Cohen [35] linked the influence of increasing the winding tension force to the burst pressure by using **FVF** as a segue where when the winding tension force increases, **FVF** increases, and thus, the burst pressure would increase. However, such a trend is only achieved when such an increase in compaction would occur in the critical layers, which are the layers that are designed to fail first. The purpose of this subsection is to establish a direct link between **FVF** and quality for further use in upcoming discussions, where proving that a process parameter affects the **FVF**, would also prove that it affects the quality.

The configurations with different *FVF*, which are Config 1,7 and 8, have presented different changes in length, diameter and mass as seen in Table 5.1. Starting off with changes in mass, it is believed that across all configurations, the difference in mass is correlated with variation in winding settings, whether a more dry or wet winding was experienced. To be able to prove this, the *FVF* calculated from the weight difference is plotted against the laminate mass correlating data from Table 5.1 and Table 5.4. The result could be displayed in Figure 5.5, where the results for Config 6 were excluded as the laminate mass is much higher.

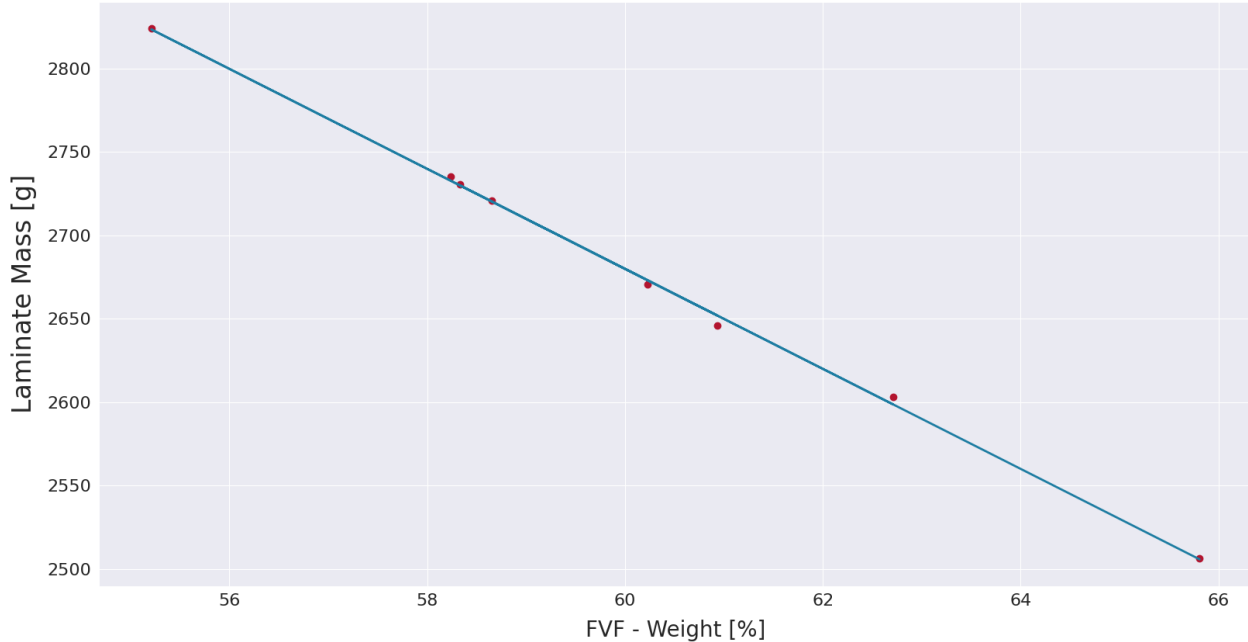


Figure 5.5: Best-fit line correlating *FVF* calculated from mass difference against laminate mass.

What could be concluded from Figure 5.5 is that there is an inverse relationship between laminate mass and *FVF*, which is the reason due to the laminate mass changes to different configurations observed in Table 5.1. During winding, the *FVF* is controlled by controlling the impregnation rate of the fibers in the resin by controlling the gap setting between the drum that dips in the resin bath and the dosing blade. This is usually defined before the winding process starts. The more wet the winding is, the more the fibers are dipped in the resin and thus, the lower the *FVF*. The higher the resin content, the higher the laminate mass as concluded from Figure 5.5.

The changes in length and thickness for configurations 1,7 and 8 could be observed in Figure 5.6. The decrease in length by increasing the *FVF* could be attributed to the compaction of the helical layers, in specific, low-angle helical layers. Low-angle helical layers create the highest axial force relative to other layers, and thus, the higher the experienced compaction, the larger the decrease in length would be as the liner would be highly loaded in the axial direction. At a high impregnation rate or low *FVF*, the composite band tends to spread out around the dome and cylinder-dome transition region, which would lead to a larger spread of the force being exerted by these layers on the liner, leading to less compaction. This is a theoretical justification, as it is hard to quantify that this is in fact the reason. An additional factor could be the presence of high resin content in the previous layers creates a similar effect where it would lead to a spread of the force being applied into a larger surface area, causing less compaction of the liner as the force experienced is less severe.

The increase in resin content, by lowering the *FVF*, causes an increase in the thickness of the laminate. This trend was also found in literature, where Wu et al. [84] measured the thickness of several different prepreg tapes under different *FVF* and concluded an inversely proportional relationship, where whenever *FVF* increases, the thickness decreases. Although this study was performed with prepreg tapes, however, the same trend would be expected in wet winding.

A relation between *FVF* and burst pressure was displayed in Figure 2.4, where it was predicted that fiber volume content controls the strength and stiffness of the vessel. Analytically, Tsai [78] proposed a relation between the average strength of a fiber bundle and relating it to *FVF* using Equation 2.6. On a simpler level as well, the rule of mixture does provide the same conclusion, whereby observing Equation 5.3, it could be seen that increasing *FVF*,  $V_f$ , would cause an increase in the composite strength  $\sigma_c$ .  $\bar{\sigma}_f$  is the average fiber strength and  $\bar{\sigma}_m$  is the average matrix strength.

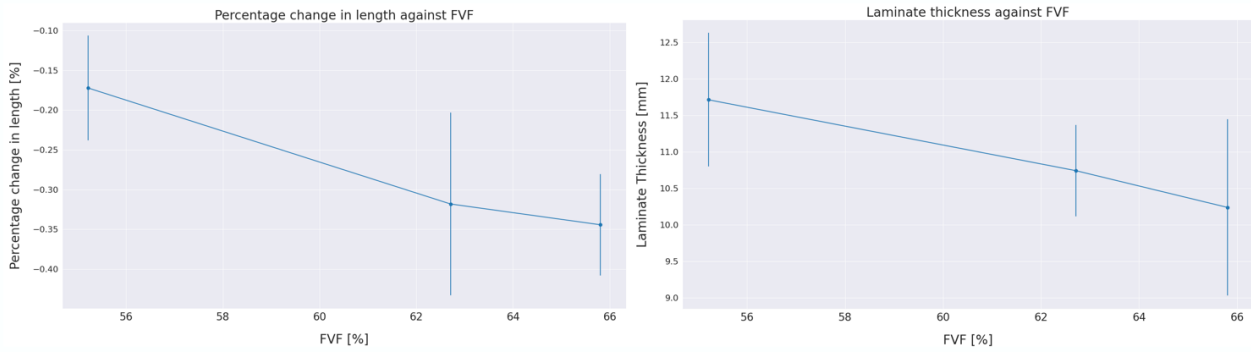


Figure 5.6: Average percentage change in length and laminate thickness against FVF

$$\sigma_c = V_f \bar{\sigma}_f + (1 - V_f) \bar{\sigma}_m \quad (5.3)$$

Comparing these analytical relations and theoretical knowledge with actual experiments obtained from burst pressure testing of configurations with different FVF, which were listed in section 5.2, Figure 5.7 could be obtained. It should be noted that the FVF numbers displayed in Figure 5.7 are FVF calculated based on laminate weight, as they give a more realistic trend than using the designed value.

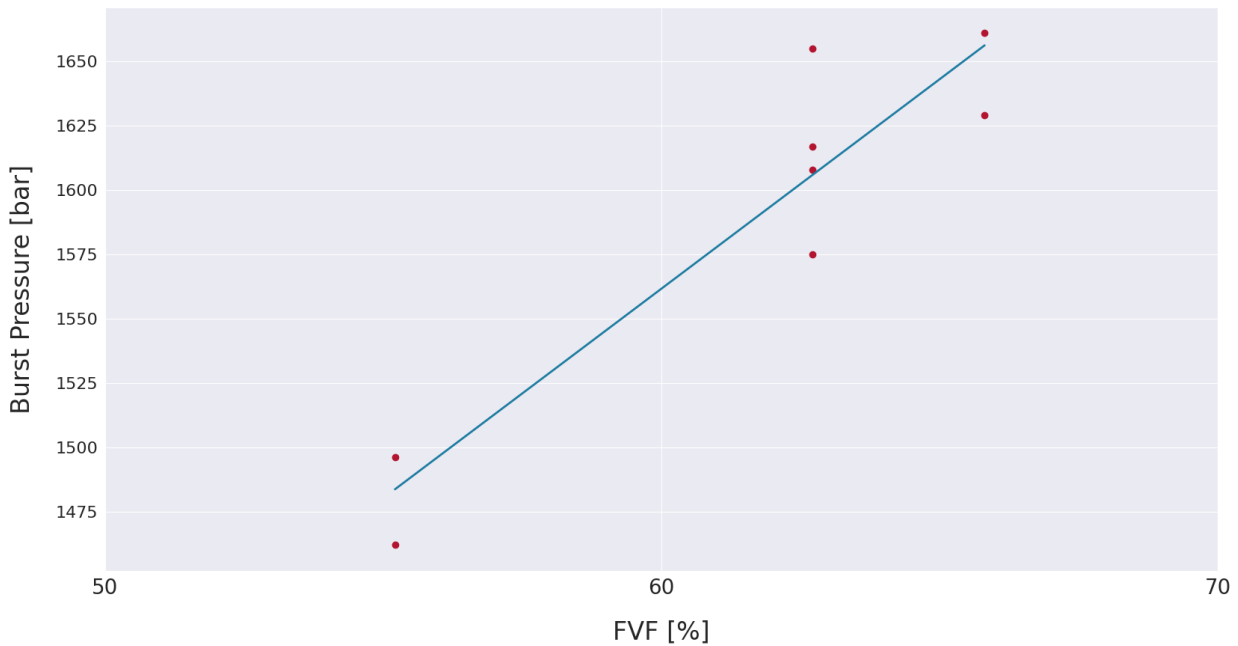


Figure 5.7: Best fit line correlating experimental burst results and FVF.

Comparing Figure 5.7 with Figure 2.4, the same trend is observed where there is a directly proportional link between both parameters. This would then validate Cohen's [35, 56] investigations linking the composite strength with FVF discussed in subsection 2.3.2. Therefore, in the upcoming discussions, whenever a link between a process parameter and FVF is established, it could then be correlated to burst pressure and composite strength.

Comparison of the hypothesis generated using the analytical model in Table 3.3 for configurations 7 and 8 and the experimental results could be displayed in Table 5.7. As could be seen, the experimental results are in agreement with the hypothesis previously set based on the literature and analytical model.

Table 5.7: Comparison of the proposed hypothesis by the analytical model and experimental results for changes in FVF.

Parameter	Change with respect to baseline vessel			
	Config 7		Config 8	
	Analytical Model	Experimental Results	Analytical Model	Experimental Results
Length	Longer	Longer	Shorter	Shorter
FVF	Lower	Lower	Higher	Higher
Porosity	Higher	N/A	Lower	N/A
Burst Pressure	Lower	Lower	Higher	Higher

### 5.4.2. Influence of Winding Tension Force

Understanding the influence of the winding tension force on the end-product quality is one of the main pillars of this thesis and one of the research questions to be answered. This was addressed in multiple stages of this report, starting off with literature in [chapter 2](#) then using the analytical model in [chapter 3](#), which was followed by results of the experimental campaign in the previous sections. In this subsection, all these previous stages are discussed and concluded to give an understanding of how the winding tension force could affect the end-product quality.

Cohen [35] found that winding tension force is one of the process parameters with the highest influence on the vessel's strength. Alongside Mertiny and Ellyin [36], both attributed the reasoning for an increased vessel strength by increasing the winding tension force to an increase in FVF and decrease in porosity content, which as discussed in the previous subsection, leads to a direct increase in strength. It is reasoned that an increase in winding tension force, produced a higher fiber motion where the fiber bed was being compacted due to a higher external pressure being applied. This causes the resin to flow down a pressure gradient out of the fiber bed and accumulate on the top surface. As a result, resin content decreases gradually through the thickness, and subsequently, the FVF increases and porosity decreases. As while bursting the vessel, it experiences fiber-dominated loading as the vessel is expanding in the hoop direction, an increase in fiber volume fraction would then lead to an increase in strength, as long as there is enough resin content to distribute the applied forces across the fiber bundles.

From the results of the analytical model, the same trend was observed whereby increasing the winding tension force, higher compaction was observed. This was due to an increase in the external pressure being applied to the liner, thus, higher compaction is being experienced, squeezing more resin out of the fiber bed and leading to an increase in FVF. Comparing the overall radial stress distribution through the thickness for different tension forces from the analytical model, the results could be seen in [Figure 5.8](#).

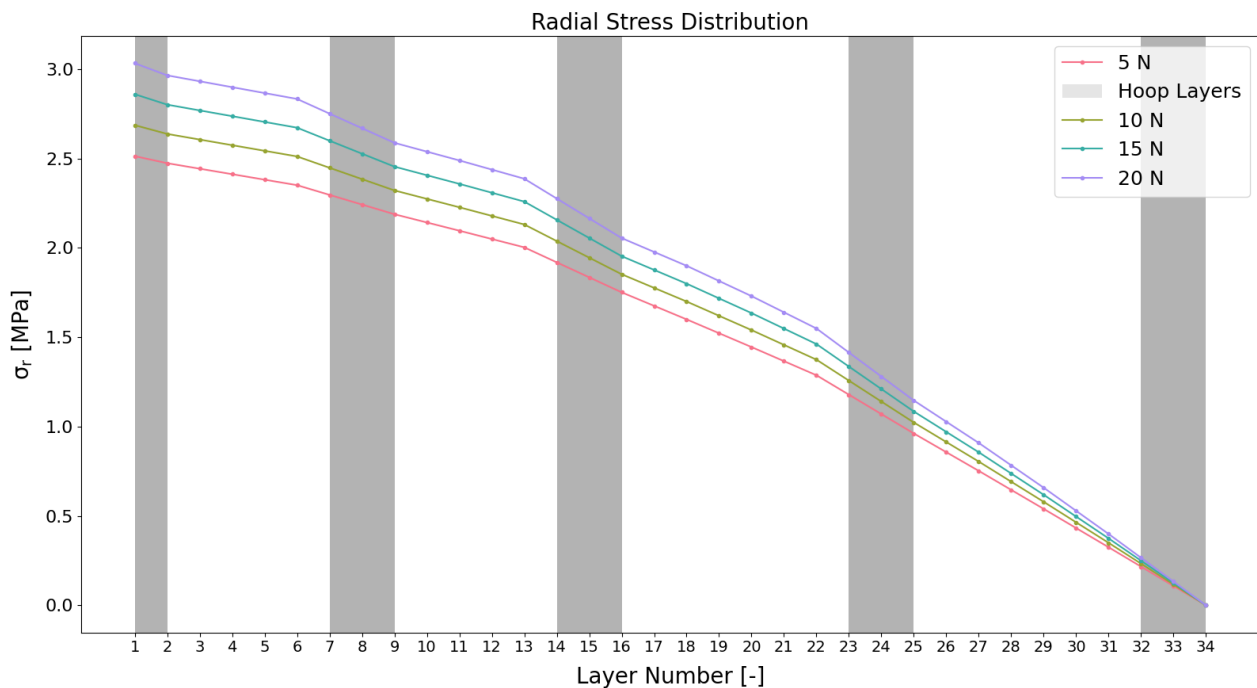


Figure 5.8: Radial stresses experienced by every layer during winding which gives an indication of the radial compaction, at different winding tension forces.



The same trend is observed in the experimental results, whereby decreasing the tension, the FVF decreased and porosity increased as seen in Table 5.4 and confirmed that there is a significant difference by the statistical analysis. This result could be summarized in the left image of Figure 5.9. An increase in winding tension force causes a direct increase in FVF and a decrease in porosity as the layers become more compacted together. Observing the compaction and the difference in FVF and porosity could be seen as well in the microscope images in Figure 5.10. By looking at the overall laminate, it could be observed that there are more voids in Config 2, indicating a larger porosity content, which is more evident in the higher magnification image. Therefore, the experimental results validate the relation that increasing winding tension force causes an increase in FVF and a decrease in void content.

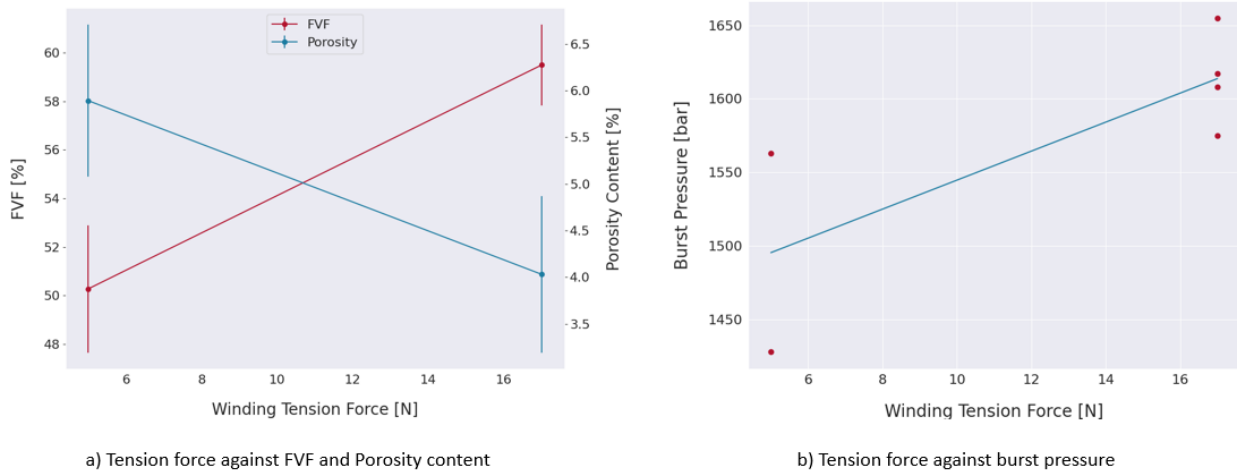


Figure 5.9: Tension force against FVF and porosity content based on microscope testing results (left) and tension force against burst pressure (right).

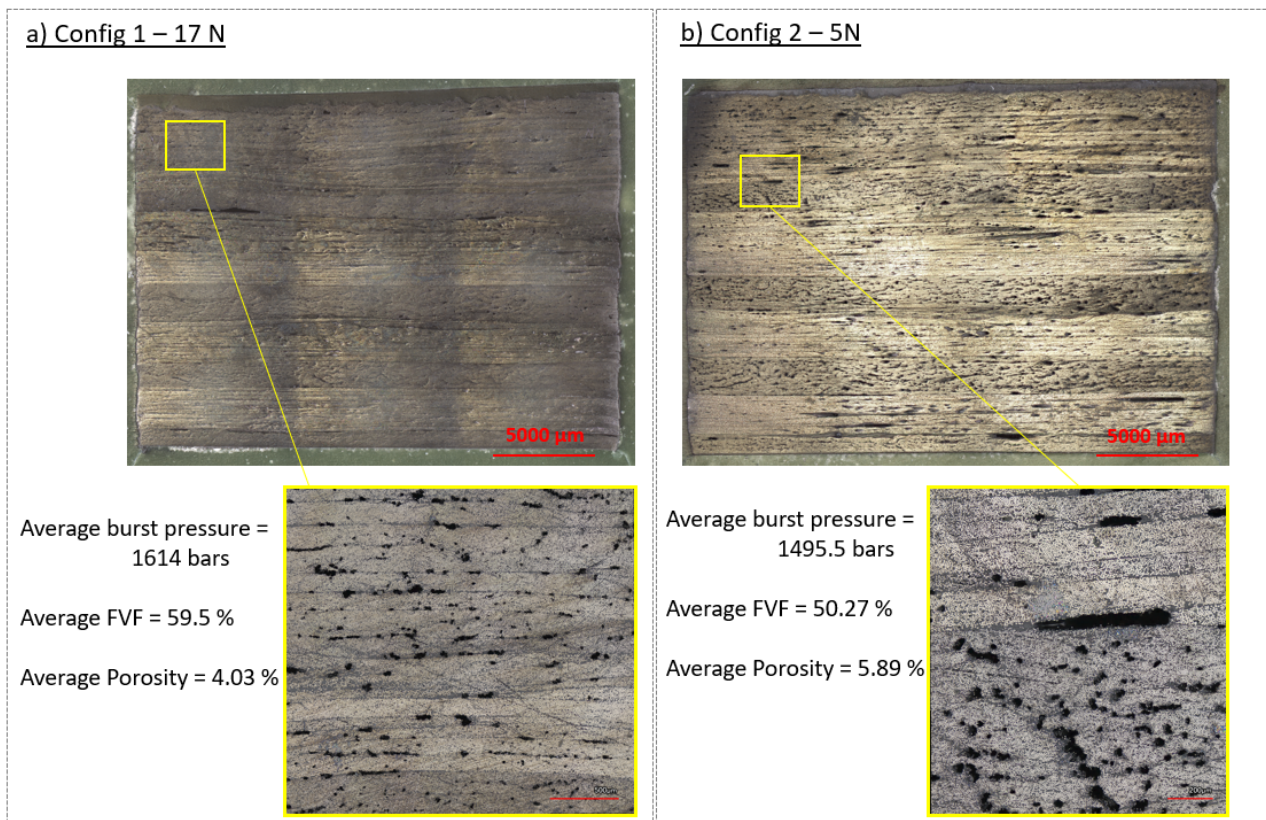


Figure 5.10: Microscope image results of two configurations at different winding tension forces. The top images were taken at 2.5x magnification while the lower images are at 20x.

An increase in FVF and a decrease in porosity content by increasing the tension force, due to higher compaction, leads to a direct increase in burst performance as established in subsection 5.4.1. Comparison of burst pressure

results at different tension forces was seen in Table 5.3 and summarized in the right figure of Figure 5.9 where a direct relationship exists as expected.

In Config 1, the resin residue is thicker than in Config 2, which is visible in Figure 5.10. It was also previously concluded that there is a significant difference in the measured resin residue thickness between both configurations in section 5.3. The same effect was discussed in literature by Mertiny and Ellyin [36] where it was observed that by increasing the winding tension, more resin is squeezed out from the fiber bed, down a potential gradient into the surface creating more resin accumulation. Therefore, the higher the tension, the higher the compaction, and the higher the resin accumulation as supported by literature and experimental results.

Another effect caused by the higher compaction experienced by increasing the winding tension is the decrease in wall thickness. This was discussed by Nebe [34] in Figure 2.5 as at a higher winding tension force, the thickness around the cylinder-dome transition region decreased. This could be compared with experimental results, although the diameter and thickness were measured around the cylindrical section, the same trend was observed. In Table 5.1 and Table 5.4, it could be observed that increasing the winding tension, caused a decrease in thickness and diameter. The trend caused by increasing the tension force on length and diameter could be displayed in Figure 5.11.

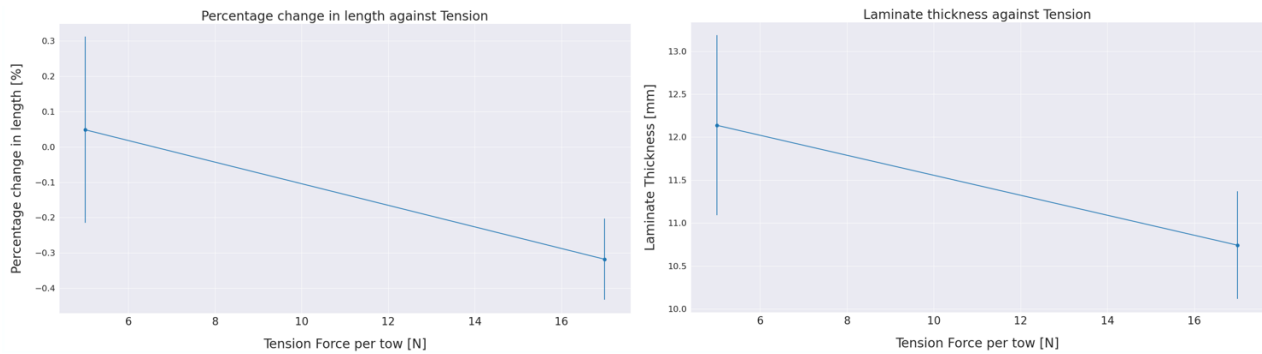


Figure 5.11: Average percentage change in length and laminate thickness against winding tension force.

The decrease in diameter is caused by the higher compaction caused by the higher tension force caused by the higher radial compaction experienced. The change in length shifts from positive to negative in this case at the two tested winding tension forces. This is because the low-angle helical layers, which are the most critical layers affecting the change in length, are more compacted at a higher tension force, exerting a larger compaction force on the liner, especially when winding around the dome region. This would then cause the liner to deform more, causing a larger decrease in length. However, based on this set of experimental results and the statistical analysis, it was observed there is no significant difference exists between changing tension force and change in length. However, this is assumed to be due to the low number of available data points.

Comparing the hypothesis from the analytical model and experimental results, an agreement seems to exist as seen in Table 5.8. However, the change in length would need additional data points to check for a significant difference.

Table 5.8: Comparison of analytical model hypothesis and experimental results for configuration 2, at a lower winding tension force.

Parameter	Change with respect to the baseline vessel	
	Analytical Model	Experimental Results
Length	Longer	Longer
FVF	Lower	Lower
Porosity	Higher	Higher
Burst Pressure	Lower	Lower

### 5.4.3. Influence of Internal Liner Pressure

The second critical process parameter, which is heavily linked with the winding tension force, is the internal liner pressure. In essence, the liners are pressurized during manufacturing to prevent liner deformation as plastic could easily deform during winding. The internal pressure prevents and/or decreases liner deformation by counteracting the external pressure being applied by the winding tension force while winding every layer. Subsequently, this interaction is what defines the consolidation of every layer as based on the magnitude of the internal and external

pressure, the compaction and pressure gradient is defined, which in turn then controls the amount of resin being squeezed out of the fiber bed and the *FVF* gradient through the thickness. As a result, the winding tension force and internal liner pressure are parameters that should be defined together as their interaction is critical.

It is then expected that by increasing the internal pressure inside the liner, the compaction would increase, decreasing liner deformation, increasing the *FVF* and decreasing the void content through the thickness. Based on the results from the analytical model, this is indeed the case as could be displayed in Figure 5.12. The radial stresses increase by increasing the internal pressure, which indicates that more compaction is being experienced.

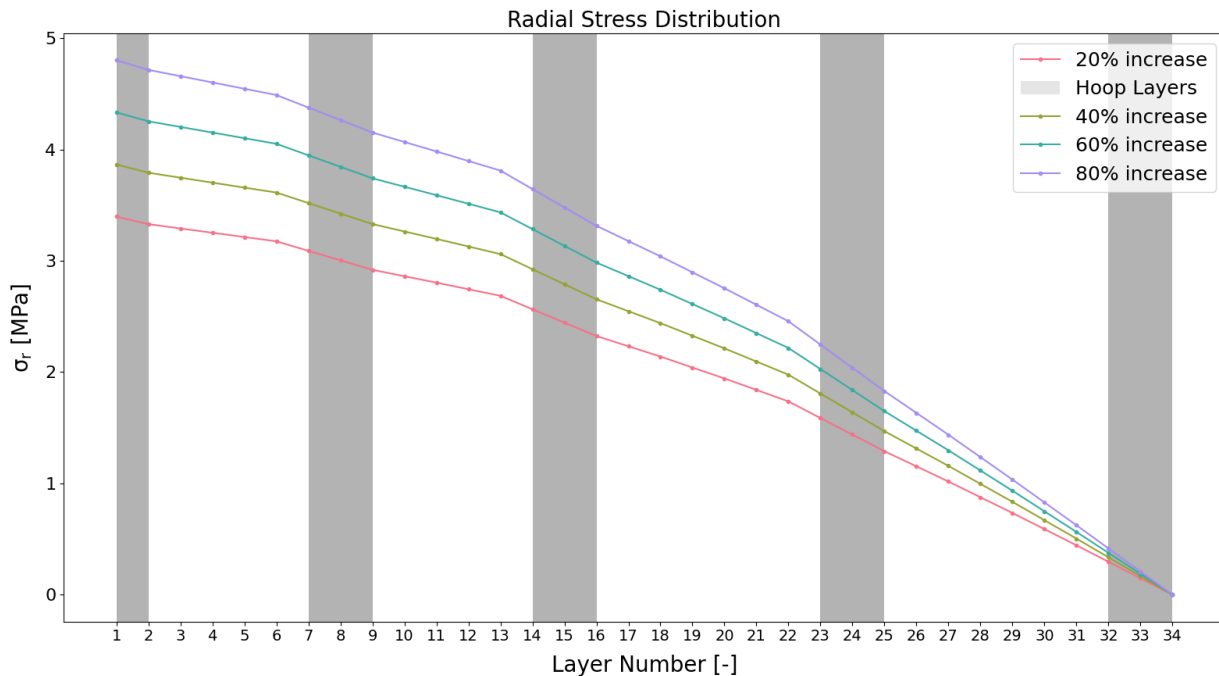


Figure 5.12: Radial stresses experienced by every layer during winding which gives an indication of the radial compaction, at different internal pressurization schedules.

Comparing these expected results with experimental ones, starting with *FVF* and porosity analysis via microscope testing, Config 1 and 3 were compared where Config 3 had 60 % higher internal pressure than Config 1. In this comparison, Config 3 had a significant decrease in *FVF* with respect to baseline vessel as seen in Table 5.6. A comparison of the microscope images could be seen in Figure 5.13. This is an unexpected result, as it indicates that increasing the internal pressure, decreases the *FVF*, which hints toward lower compaction. However, this could still not be concluded as porosity and resin residue thickness are not significantly different, which are indications of compaction as well. This unexpected result could be explained using *FVF* from laminate weight calculation. Ideally, all the vessels should have the same value, if the set impregnation rate is the same. For Config 3, the *FVF* from laminate weight was significantly different than Config 1, which indicates a more wet winding, as-in more resin was used. As a result, this could be attributed to this difference in *FVF* under microscope testing.

Config 5 and 5-no pressure could be then used to correlate the relation between *FVF* and porosity experimentally, as *FVF* from laminate weight calculation is not significantly different. In Table 5.4, there is a significant decrease in *FVF*, increase in porosity content and decrease in resin thickness by losing the internal pressure. This could also be visualized in more detail in Figure 5.14. This then indicates that increasing the internal pressure, leads to higher compaction, as expected from the analytical model.

The results in Table 5.2 indicate that by comparing Config 3 with baseline, a significant difference exists between length, diameter and mass. The change in mass as discussed earlier was proved to be related to the difference in winding settings and thus affecting the *FVF* and does not relate to the change in configuration. The change in length and laminate thickness against internal pressure could be summarized and visualized in Figure 5.15. An increase in length is observed when increasing the internal pressure, which is as expected. This is as the internal pressure hence counteracts the external pressure, mainly caused by low-angle helical layers, creating axial compaction on the liner. In this case, the internal pressure was more than sufficient, it lead to the resultant force creating an increase in length. Additionally, the laminate thickness also increases for the same reason, where instead of axial forces, tangential ones are to be considered and instead of low-angle helical layers, it would be high-angle helical and circumferential layers.

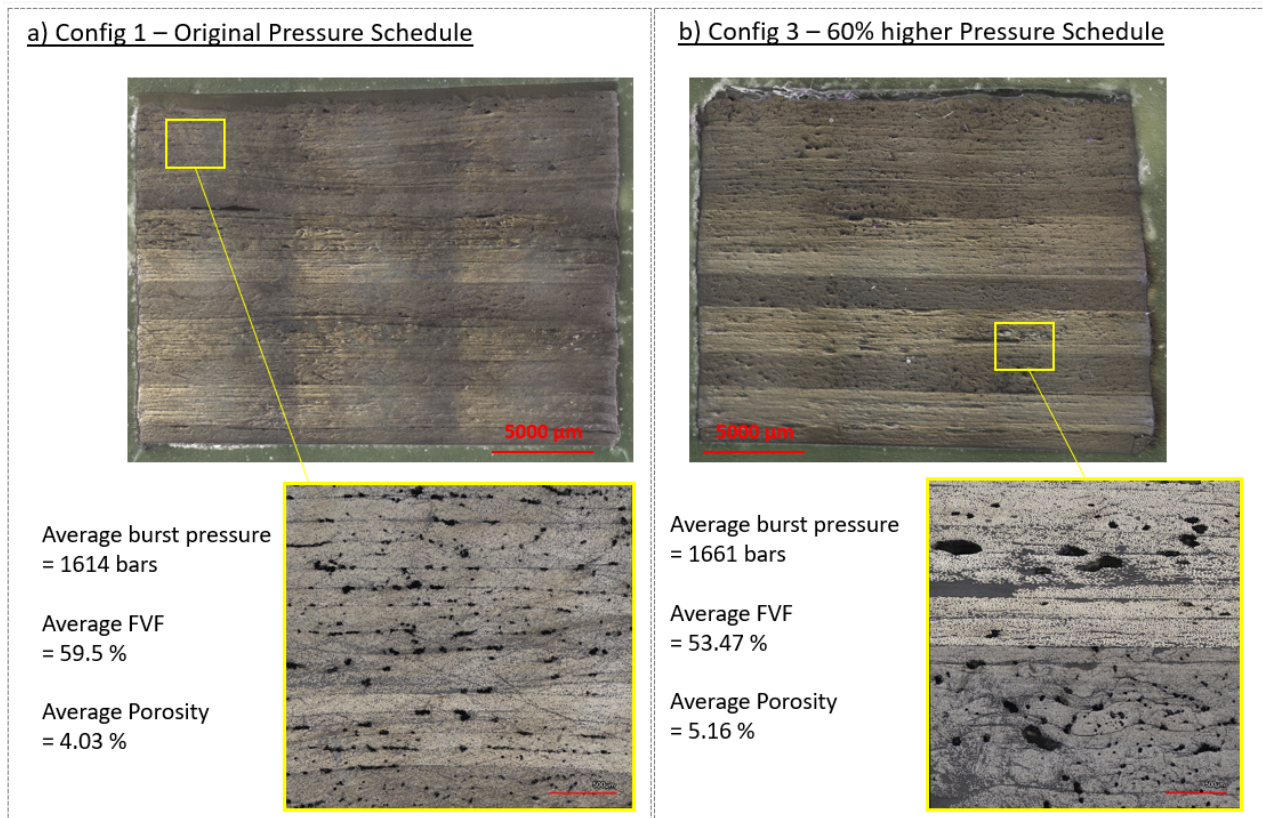


Figure 5.13: Microscope image results of two configurations, Config 1 and 3, at different internal pressure. The top images were taken at 2.5x magnification while the lower images are at 20x.

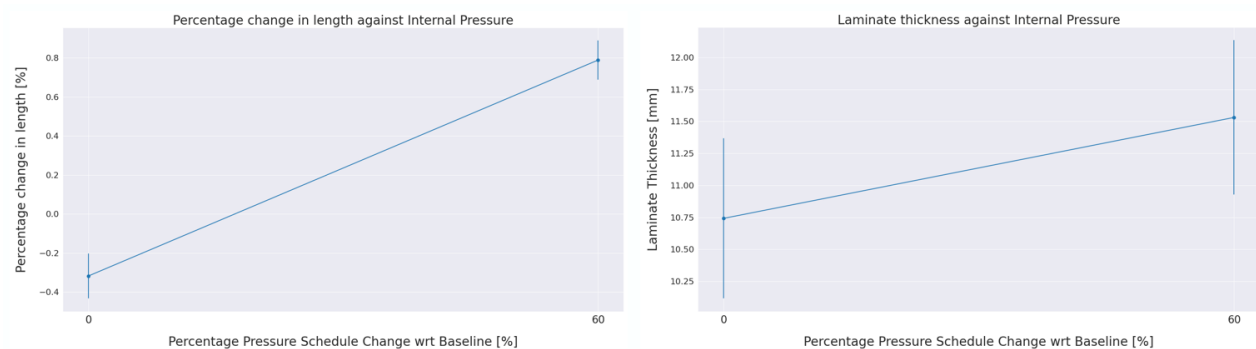


Figure 5.15: Average percentage change in length and laminate thickness against internal pressure.

As higher compaction is experienced by increasing the internal pressure, a higher burst performance is expected as well. This is as higher compaction is linked with a higher FVF, and as established earlier, would lead to a higher burst performance. However, when comparing burst results with both configurations, it appears that there is not much of a significant change as listed in Table 5.3. The reasonable explanation is that due to the scatter of the data of both configurations, there has not been a trend that could be concluded. Using the results from Config 5 and 5-no pressure is not conclusive as they also show no significant difference, although only one data point is available for Config 5-no pressure. Therefore, based on the current results, a direct relationship between the changing internal pressure and burst pressure could not be formulated, but a relation between other aspects of end-product quality has been established and validated as discussed earlier. To establish such a relation, additional data points might be required.

To summarize this discussion, a comparison between the analytical model hypothesis and experimental results are indicated in Table 5.9. All the results are in agreement, except for the burst pressure prediction.

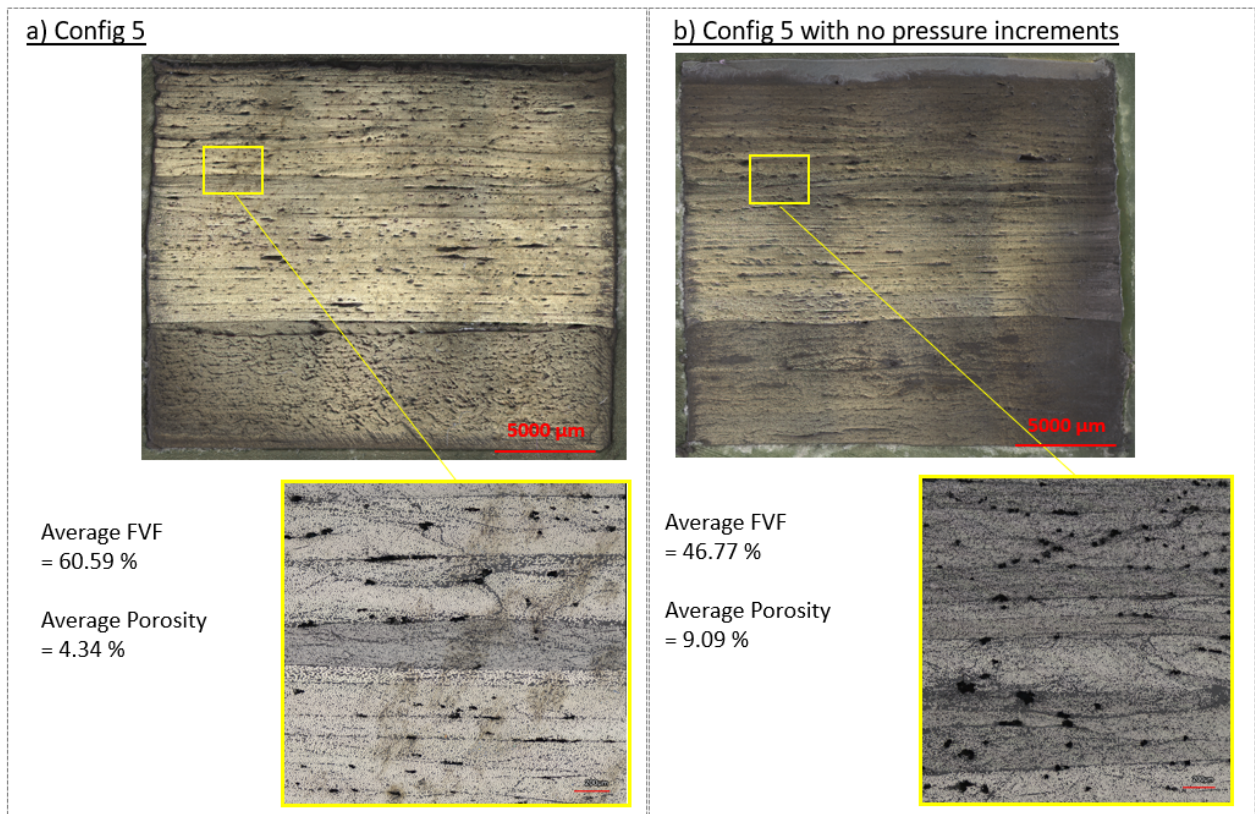


Figure 5.14: Microscope image results of two configurations, Config 5 with and without pressure increments, at different internal pressure. The top images were taken at 2.5x magnification while the lower images are at 20x.

Table 5.9: Comparison of analytical model hypothesis and experimental results for configuration 3, at a higher internal liner pressure.

Parameter	Change with respect to baseline vessel	
	Analytical Model	Experiment Results
Length	Longer	Longer
FVF	Higher	Higher
Porosity	Lower	Lower
Burst Pressure	Higher	No change

#### 5.4.4. Influence of Diameter

Nebe [34] profoundly discussed the design attributions that are necessary to transform a certain layup design from a sub-scale vessel design to a full-scale one, inherently increasing the diameter of the liner. To investigate the effect of changing the diameter on the end-product quality by merely changing the vessel diameter would give a much lower burst pressure value. This is as the diameter of the liner increases, the required tangential reinforcement needed increases so more hoop layers are required, which could be concluded from the classical mechanics of cylinders. The whole stacking sequence would need to be changed as just increasing hoop layers would create a large stiffness gap between the cylindrical section and dome region, thus, additional high-angle helical layers are to be added to bridge such a gap. Therefore, additional variables then come into account when comparing the burst value of two vessels with different diameters, making an unfair comparison and the difference could not be attributed back to the original change in diameter. Therefore, based on the aforementioned theoretical knowledge, it was decided to not perform burst pressure testing for investigating the influence of vessel diameter to validate the theoretical knowledge.

Based on the applied external pressure, it is inversely proportional to the radius as seen in Equation 3.8. Thus, by increasing the diameter, the exerted external pressure would decrease, lowering the pressure gradient through the thickness and the compaction of the layers. This would in turn also squeeze less resin out of the fiber bed,

leading to less resin accumulation on the top surface, lower FVF and higher porosity content when compared to having a smaller diameter. To compare the experienced compaction, the radial stress distribution for four different liner diameters is shown in Figure 5.16. The trend is by increasing the liner diameter, lower radial compaction is experienced, and thus, lower FVF and higher porosity content are expected.

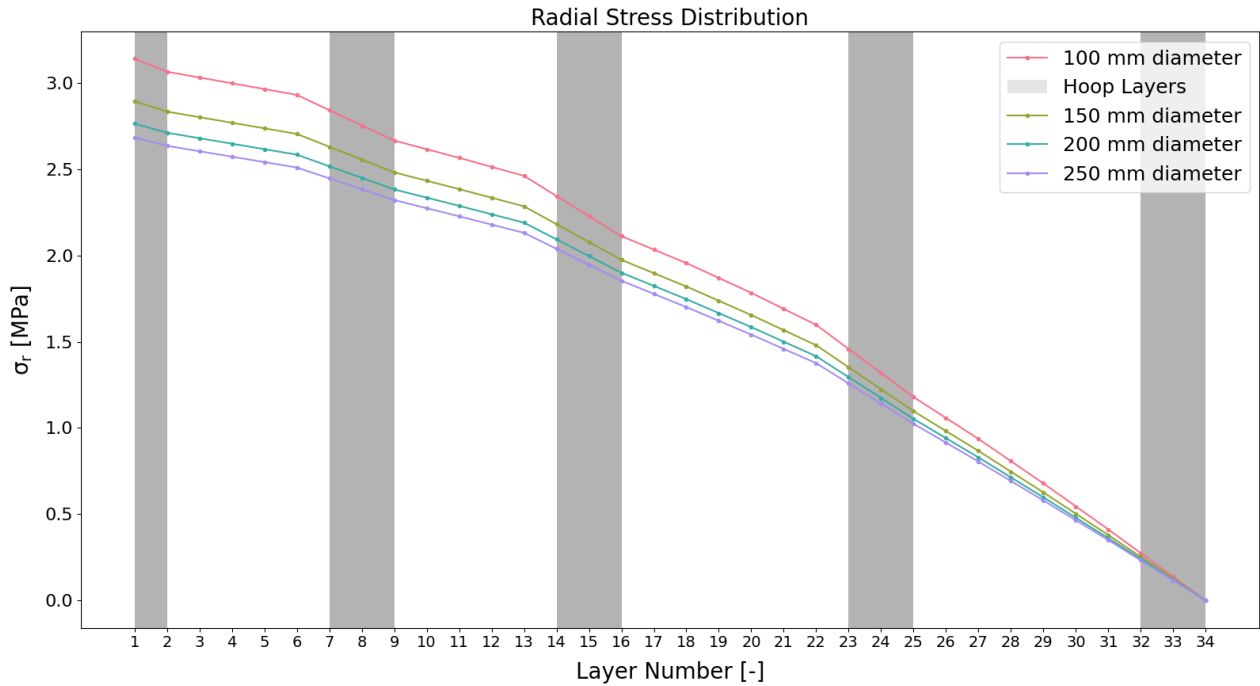


Figure 5.16: Radial stresses experienced by every layer during winding which gives an indication of the radial compaction, at different liner diameters.

Comparing these results with experimental results that were obtained from microscope testing, the FVF, from microscope testing, and porosity content for two different configurations with exactly everything the same except the liner diameter, Config 1 and 6. The results of FVF and porosity across the different diameters are displayed in Figure 5.17. As could be seen, the results validate the literature hypothesis and analytical model results, whereby increasing the liner diameter, the FVF decreases and porosity content decreases due to less compaction present. However, from statistical point of view, there is a significant difference in porosity, but not in FVF.

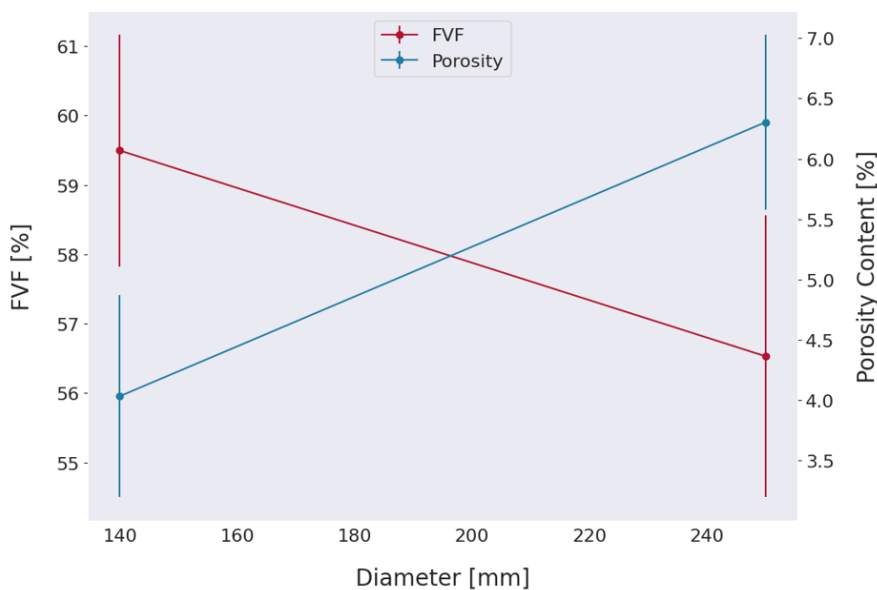


Figure 5.17: Microscope testing results for Config 1 and 6 with different liner diameter displaying the FVF and porosity content

This could also be supported by investigating an example of two images of different magnifications for the two configurations at Figure 5.18. A higher FVF and void volume could be observed when comparing the images, especially at 20x magnification. Additionally, the resin residue thickness is lower but not significantly. This again supports the argument that at a larger vessel diameter, less compaction takes place which leads to lower FVF, higher porosity content and lower resin residue thickness.

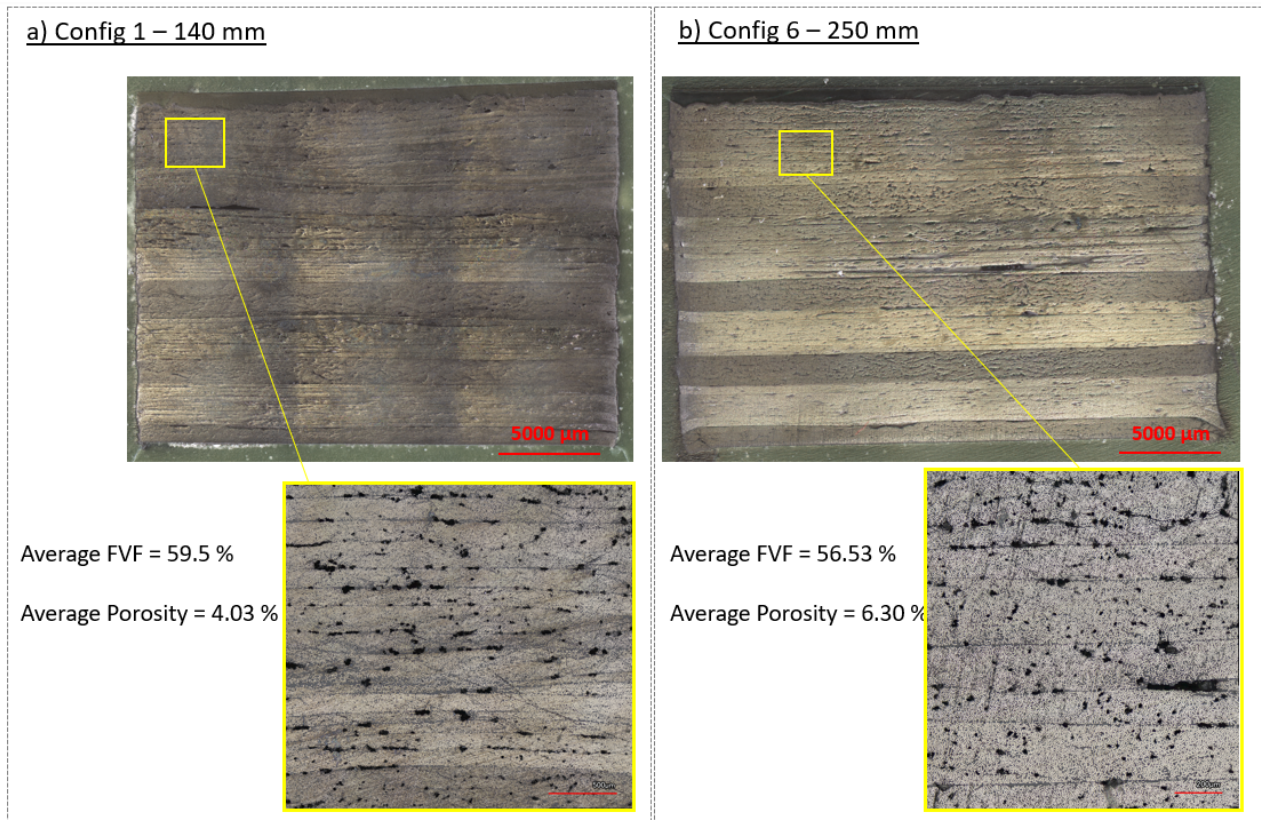


Figure 5.18: Microscope image results of two configurations at different liner diameters. The top images were taken at 2.5x magnification while the lower images are at 20x

An unexpected result was the correlation of the change in length and laminate thickness with the change in liner diameter. As there is lower compaction, it was expected that an increase in length would be present, due to lower external pressure by the winding force. This was not the case, however, where the change in length was almost the same. Additionally, following the same line of logic, the change in diameter should be higher, however, it was significantly lower. The difference, in this case, was accredited to the difference in liner materials used, where for the 140 mm vessels, high-density polyethylene was used and for the 250 [mm] vessel, polyamide-6 was used. Polyamide-6 is much stiffer and stronger than high-density polyethylene where the stiffness is almost 2.5 times and strength is 3 times higher, therefore, it resists the deformation along the axial direction caused by the helical layers and along the hoop direction by the hoop and high-angle helical layers. The difference in stiffness between liner materials outweighs the difference in compaction due to changing vessel diameters.

Again, a summary of the comparison of the analytical model hypothesis and experimental results are shown in Table 5.10.

Table 5.10: Comparison of analytical model hypothesis and experimental results for configuration 6, at a higher liner diameter.

Parameter	Change with respect to baseline vessel	
	Analytical Model	Experimental Results
Length	Longer	Unchanged
FVF	Lower	Lower
Porosity	Higher	Higher
Burst Pressure	Not tested	Not tested

### 5.4.5. Influence of Stacking Sequence

Stacking sequence investigations are one of the most researched areas in the field of CPVs and composite materials in general. Having the same stacking sequence, and changing the order of winding or grouping, could significantly affect the end-product quality of the vessel. The compaction of individual layers could differ depending on the preceding and following layer, which would then need adjustment of winding parameters. Consequently, this would also affect the stiffness and load distribution in the laminate and hence, also affect the burst pressure performance.

Based on the area of the vessel, the layers that optimize compaction differ. In the cylindrical area, circumferential layers provide the optimal compaction as they are aligned with the hoop direction of the vessel, whereas in the dome or cylinder-dome transition region, (high-angle) helical layers provide the optimal compaction. On the other hand, low-angle helical layers would provide the least possible compaction in the cylindrical section. Therefore, layers wound that is followed by hoop layers, would experience higher compaction than the ones followed by helical layers.

This was investigated by Nebe [34] where three different stacking sequences were manufactured and the FVF and porosity content were measured. The results were previously presented in Figure 2.6. The interesting observation is when the helical layers were wound before the hoop layers, higher FVF and lower porosity content were experienced in comparison to when hoop layers were wound first. This is for the reason above, that the hoop layers provide the highest tangential compaction, leading to compacting the helical layers below even more than if they were placed on the outside. As discussed a few times, higher compaction leads to higher FVF and lower porosity content. Thus, this proved that layer compaction is directly affected based on the positioning within the layer.

From the analytical model perspective, the same trend is expected and was observed in Figure 3.14. Logically, when the helical layers are grouped and wound first, the hoop layers tend to be compacted less. This is because the high-angle helical layers are still capable of compacting layers in the tangential direction in an almost efficient manner. Following the same line of logic, and using the radial stress distribution in Figure 3.14, the hoop layers in Config 5 are more compacted than Config 4, while the helical layers in Config 4 are more compacted. The expected results are summarized in Table 3.4.

Comparing these different results with the experimental ones, Figure 5.19 is used to visualize the experimental results for FVF and porosity content evaluation. Figure 5.19 is structured similarly to Figure 2.6 to allow for easier comparison between literature and own results where the hoop, helical layers and overall laminate FVF and porosity are compared for the three configurations with different stacking sequence. For Config 1, no helical or hoop FVF and porosity content data is obtained as it is an alternating stacking sequence where it is difficult to measure each individual layer. The hoop layers in Config 5 are more compacted than Config 4 and helical layers in Config 4 are more compacted than Config 5, which is in agreement with the analytical model hypothesis. A closer look into the difference in FVF and porosity content could be observed in Figure 5.20. A significant difference was only in difference in FVF in helical layers, but not in hoop layers, nor in porosity content.

The FVF and porosity content are used as an indication of the level of compaction experienced by every layer group at different configurations. It could be used to also explain the percentage changes in length and laminate thickness observed as presented in Table 5.1. Config 5 had a significantly more positive percentage change in length than Config 4. As mentioned a few times, the layers that are most responsible for the change in length are the low-angle helical layers. In Config 4, the helical layers are more compacted than in Config 5 as they are followed by hoop layers. As low-angle layers in Config 4 are more compacted, then the low-angle helical layers exert higher forces on the liner, causing a larger deformation than Config 5. In Config 5, the hoop layers are the ones that are more compact, creating larger hoop stress, which in turn generates positive axial stresses that create a positive increase in length. Following this same line of logic, this is why Config 5 had a slightly lower diameter than Config 4. Additionally, in Config 4, the low-angle helical layers are wound at a lower internal pressure, thus, there is less counteracting pressure, leading to an even higher axial force being applied.

Regarding burst performance analysis, as displayed earlier and lately in Figure 5.20, Config 5 appears to have a slightly higher average burst pressure value. This could be linked back to the FVF results mentioned earlier. As the circumferential layers are the ones that provide the highest stiffness in the cylindrical region, and as it is designed that these layers to be the critical ones, increasing the FVF and decreasing the porosity content of these layers, prolongs the burst performance of such a configuration. Therefore, this was the reasoning for the higher burst pressure prediction by the analytical model. However, as Config 4 had one value, which seems to lie inside the scatter of Config 5, no conclusion regarding burst performance could be made. The reasoning for having such close values could be explained based on the failure location, where in Config 5, the circumferential layers became too stiff, making the composite stronger than the boss thread, which is where the failure occurred. Therefore, in Config 5, composite failure should be much higher than the observed value, but it is not quantified in this investigation.

An additional interest while varying the stacking sequence, was to check whether any of the different stacking se-



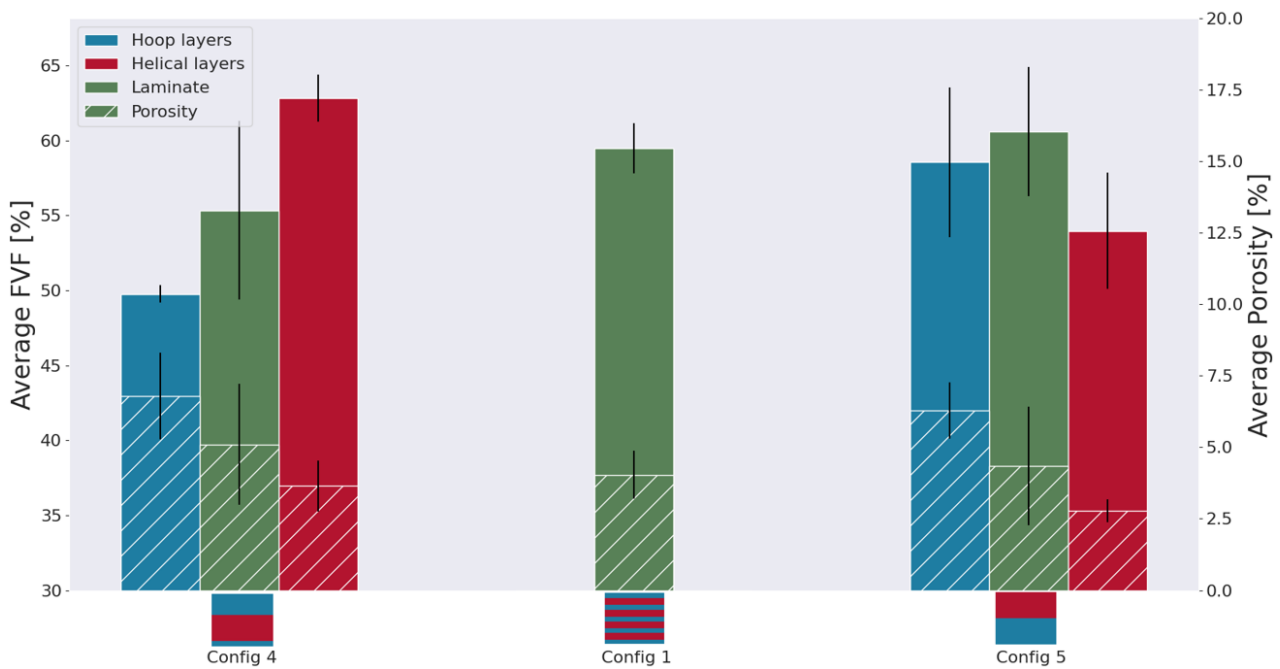


Figure 5.19: Average FVF and porosity content comparison for three different vessel configurations with different stacking sequences.

quences would cause any wrinkling effect to the inner layers due to high compression forces while winding. As the main forces being experienced by the layers while winding are hoop stresses, which could be either compressive or tensile. Compressive stresses would tend to cause wrinkling, where the threshold is unknown but expected to be nonexistent for uncured carbon fiber strands. To investigate this, samples along the longitudinal direction of the sample were taken and investigated at 5x, where the comparison between Config 4 and 5 could be seen in Figure 5.21. There was not any wrinkling that could be observed. Abnormality in the middle of Config 4 could be observed, however, this is because of the fiber tow disconnecting during winding where the winding had to be stopped and a tie-on had to be made again, and it appeared that a cut was made in that region.

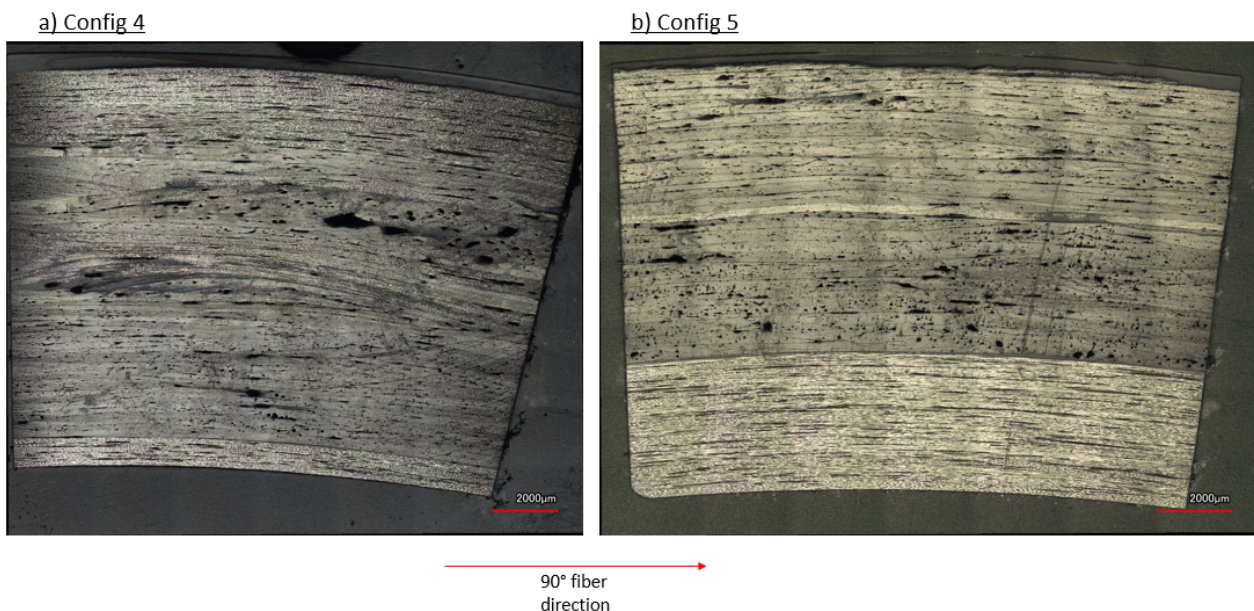


Figure 5.21: Longitudinal samples displaying a cross-section of the laminate at 5x magnification.

Summarizing the experimental results from the aforementioned discussion and comparing them with the analytical model hypothesis previously stated in section 3.4, Table 5.11 could be concluded.

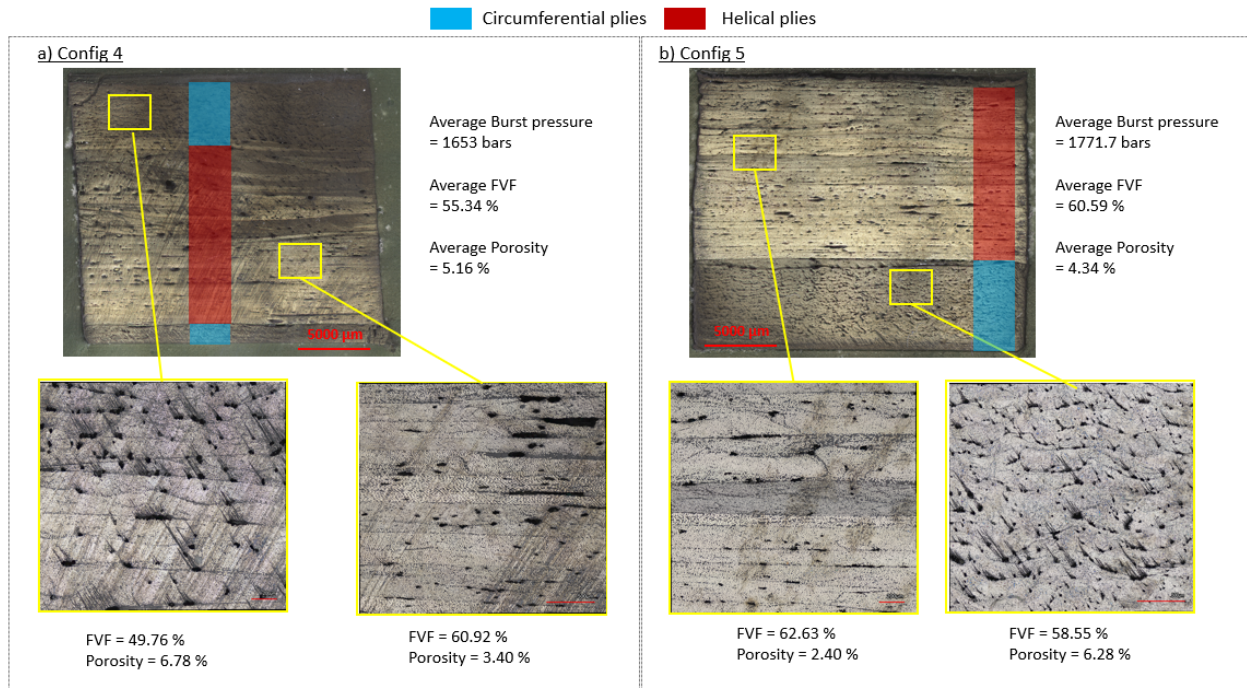


Figure 5.20: Microscope image results of two configurations at different stacking sequences. The top images were taken at 2.5x magnification while the lower images are at 20x

Table 5.11: Comparison of analytical model hypothesis and experimental results for configurations 4 and 5, at different stacking sequences.

			<b>Config 4</b>	<b>Config 5</b>
<b>Length</b>		<b>Analytical</b>	Longer	Shorter
		<b>Experimental</b>	Longer	Shorter
<b>FVF</b>	<b>Hoop</b>	<b>Analytical</b>	Lower	Higher
		<b>Experimental</b>	Lower	Higher
	<b>Helical</b>	<b>Analytical</b>	Higher	Lower
		<b>Experimental</b>	Higher	Lower
<b>Porosity</b>	<b>Hoop</b>	<b>Analytical</b>	Higher	Lower
		<b>Experimental</b>	No difference	No difference
	<b>Helical</b>	<b>Analytical</b>	Lower	Higher
		<b>Experimental</b>	No difference	No difference
<b>Burst performance</b>		<b>Analytical</b>	Lower	Higher
		<b>Experimental</b>	Lower	Higher

## 5.5. Framework for Determining Optimum Process Parameters

Changing certain manufacturing or geometrical parameters of the vessel could have a significant effect on the end-product quality of the vessel, as defined in [section 2.1](#). For a vessel configuration, the optimum process parameters are the combination of parameters that maximize the end-product quality. In the context of this project, this is by achieving the lowest possible change in dimensions and the maximum mechanical performance. In this section, a framework recommendation is proposed to determine the optimum winding parameters for a given vessel configuration. The guidelines given in these chapters for choosing manufacturing parameters are in place to have a positive influence on the burst pressure for a frozen laminate design.

### 5.5.1. Limitations and Defects Induced by Tension and Internal Pressure

Following the discussion in [subsection 5.4.2](#) and [subsection 5.4.3](#), it is noticed that the tension force and internal liner pressure have significant control over the compaction of the vessel. Subsequently, it could then control the **FVF** and porosity content distribution through the thickness. Higher compaction might always seem preferred. However, it is preferable for the vessel to have a **FVF** as close as possible to the designed value. Higher **FVF** is not always the best solution quality-wise, as in matrix-dominated loading, where during pressurization the matrix is significantly

loaded and results in cracks all over the microstructure, the vessel would fail earlier than expected. Or even, the layers could become too dry that there is not enough resin to ensure proper load transfer between the fibers. An additional consideration is a change in dimensions, where an optimal combination of process parameters should lead to a 0 % change in length. As size restrictions often limit a vessel design due to customer requirements, deviation from the intended value, even if it ensures higher quality, is not desirable.

The internal liner pressure is added to counteract the external pressure caused by the filament winding tension. This is to prevent or reduce the liner deformation created by winding that could affect the final geometry of the vessel. As mentioned, these two pressure forces should be equal for the internal pressure to sufficiently counteract the applied force due to tension force. However, if the external pressure is significantly higher, different kinds of defects could be introduced if such an equilibrium does not exist. Excessive compression stresses could be experienced by the layers, especially the innermost layers, which could cause fiber wrinkling. If the applied tension force is too high, fiber breakage might occur. On the other hand, if the applied internal pressure is significantly high, then minimal compaction could take place, which could lead to gaps between the liner and composite material. Such defects should be taken into account as well when choosing the optimal process parameters.

To find the upper limit for tension force to prevent fiber breakage, it is derived from the ultimate tensile stresses of the fibers, with a reasonable safety factor. Keeping into account that during winding, there are peaks and valleys in the experienced tension force, especially while winding helical layers depending on the acceleration/deceleration applied. An upper limit also exists for the internal pressure, which is derived from the liner material, based on its maximum yield stress. This is to prevent the liner from deforming or exploding and not being capable of withstanding the applied internal pressure.

### 5.5.2. Relating Tension and Pressure with Compaction and Deformation

To maintain the intended FVF and avoid changes in dimension, ideally, the applied external pressure due to winding as given by Equation 3.8, should be equal to the internal pressure within the liner. This however is not as simple as it sounds as the effect of the internal pressure for every layer decreases as the laminate gets thicker. Thus, additional pressure increments are necessary. It is advised to add these pressure increments before winding the layers that create the highest external pressure, which are the circumferential layers. An example could be if there is an alternating stacking sequence, to add a pressure increment at every group of hoop layers, as done in the baseline vessel configuration.

The interaction between the applied tension and force and internal liner pressure is what defines the change in dimensions and the compaction. A matrix displaying possible combinations and their effect is presented in Table 5.12. This idea is that no matter the magnitude, as long as the applied tension and pressure forces are equal, then no change in dimensions is expected. If the tension is higher, then a decrease in length and diameter would be expected. This was seen in Table 5.1 by comparing Config 2 with the baseline vessel. On the other hand, if the pressure is higher then an increase in length is expected, whereas seen in Table 5.1, in Config 3, where pressure is higher, a significant increase in length and diameter was observed. Visualization as trend graphs could be done by observing Figure 5.11 and Figure 5.15.

Table 5.12: Matrix displaying the effects of tension and pressure on the compaction and change in dimensions.

	High Pressure	Low Pressure
High Tension	- High compaction - No change in dimensions	- Medium compaction - Decrease in dimensions
Low Tension	- Medium compaction - Increase in dimensions	- Low compaction - No change in dimensions

Regarding compaction, it is defined based on the independent magnitudes of tension force and internal pressure. An increase in tension force, whilst keeping the pressure constant, leads to a direct increase in compaction as visualized in Figure 5.9. The same also applies to internal pressure following the discussion in subsection 5.4.3. This is as the force experienced by the laminate, from either side, increases proportionally.

### 5.5.3. Steps to Derive the Optimum Process Parameters

The developed analytical model could be used as a rapid iteration tool to iterate between possible combinations of process parameters for any vessel configuration to maximize product quality. In general, below are the listed outputs of the analytical model and how they could be utilized:

- Pressure difference graph: to predict changes in dimensions based on positive or negative difference.

- Radial stress distribution: to predict compaction of individual layers.
- Hoop stress distribution: checking for high compressive or residual stresses.

The steps to follow to derive the optimum combination of process parameters are displayed in the flowchart in [Figure 5.22](#). When a redefinition of tension and/or pressure is needed, as when compaction is not high enough or there are high compressive or tensile tangential stresses, the trends presented in the previous subsection are used.

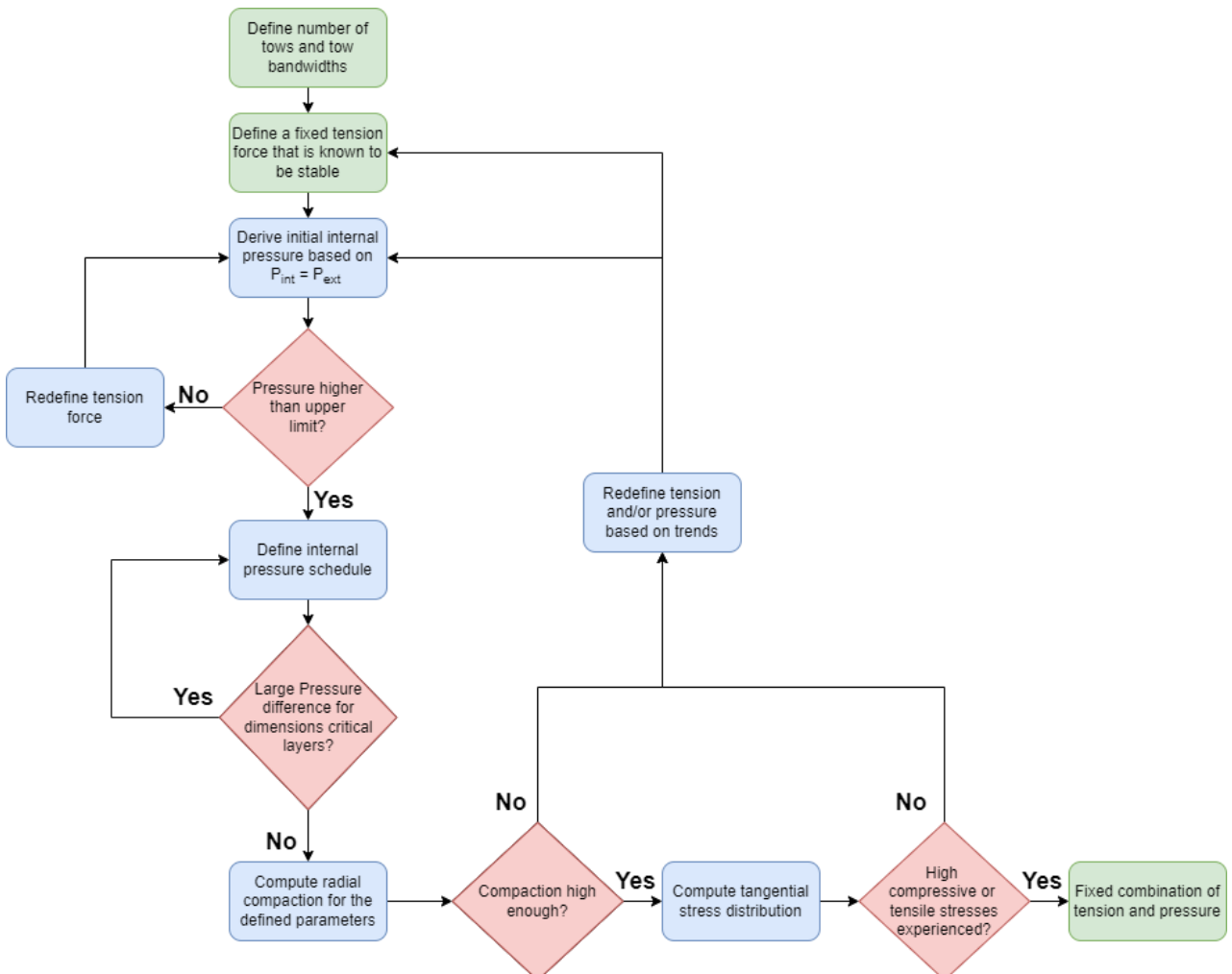


Figure 5.22: Flowchart displaying the proposed framework steps to determine the optimum process parameters.

#### 5.5.4. Influence of Stacking Sequence and Diameter

From the discussion in [subsection 5.4.5](#) and [subsection 5.4.4](#), the following trends were observed:

- Stacking sequence grouping affects the quality, where the grouping that is innermost would have a higher *FVF* and lower porosity compared to if wound outside.
- Grouping hoop layers closer to the liner and compacting it more causes an increase in burst and mechanical performance.
- Increasing the liner diameter decreases the compaction as the applied external pressure decreases. Thus, it leads to lower *FVF* and higher porosity.

As seen, changes in diameter and stacking sequence lead to changes in compaction. To counteract these changes, variations in the manufacturing parameters are necessary. As a result, the process parameters are directly dependent on the vessel configuration in question. Fixing changes in compaction and dimensions would follow the same line of logic as in the previous discussion, in specific in [Table 5.12](#).

## Conclusions & Outlook

### 6.1. Summary

The increasing demand for sustainable transportation has led to the introduction of Fuel-Cell Electric Vehicles (FCEVs) as an alternative to Internal Combustion Engines (ICEs). A critical component of FCEVs is Composite Pressure Vessels (CPVs), which are used for hydrogen storage at high-pressure levels. CPVs have received much attention and have reached a high technological readiness level, however, cost reductions are necessary to present FCEVs as a feasible option. Cost reductions are achieved by a decrease in the materials used, which is attainable by an increase in the reliability and robustness levels. CPVs' reliability could be boosted with an increased level of understanding of the manufacturing process and the influence it has on mechanical performance.

This report presents the development of an analytical modelling tool capable of representing the manufacturing process to relate changes in manufacturing parameters to the final product quality. The objective of this tool is to perform a quantitative comparison of different combinations of manufacturing parameters to a fixed vessel configuration to maximize the attainable mechanical performance. The applicability of this tool was compared to eight different vessel configurations, where experimental data were obtained. This is in an effort to lower the observed scatter in mechanical performance for CPVs and fully exploit the materials used.

#### 6.1.1. Analytical Model

The developed analytical model described in this study is founded on the basis of recreating the winding process and estimating the stresses experienced. The main challenge of this model was dealing with uncured composite laminate. As the resin is still in liquid form, no load transfer exists between layers and thus, the analysis required a unique modelling approach. For simplification of the analytical model, the vessel geometry was limited to the cylindrical section and thus, the dome regions were not considered. This introduces inaccuracy in the model, however, in the context of generating quantitative comparison, results are unaffected.

Consequently, the model adopted Classical Laminate Theory (CLT) as the main analysis approach utilized for this analytical model where every individual layer being wound was considered separately. The only interaction between layers was through the transfer of radial loads. The model is structured to account for different vessel diameters and stacking sequences, and additionally, as inputs, it takes in the defined internal pressure schedule and winding tension force. By defining these values, information regarding changes in length and thickness, compaction and burst pressure could be extracted. This is done by utilizing model outputs such as pressure differences for every wound layer, and overall radial and tangential stresses experienced by every layer after winding is finalized. Using this previous information, a comparison between different pressure and tension settings could be made to establish which combination would have a more positive effect on quality.

Hypotheses for eight different configurations were established and later compared with experimentally obtained results. A baseline configuration was set, which was used as a reference for comparison where either a manufacturing parameter or a vessel configuration value was changed with respect to the baseline configuration. The majority of the analytical model hypotheses were in harmony with the experimental results. However, it shed light on a limitation of the current model, which is the inability to account for different fiber volume fractions (FVF).

#### 6.1.2. Experimental Campaign

An extensive experimental campaign has been presented in this thesis report that consists of two different testing campaigns; burst pressure testing and microscope inspection. The total number of manufactured vessels was 22, where 15 were burst tested and 7 were inspected under the microscope. Additional data was utilized from previous investigations already available at Plastic Omnium making the total number of vessels considered 33. For all the vessels manufactured, recordings were made of changes in length, laminate thickness and mass and were correlated to the vessel configurations.

Burst pressure testing took place at Plastic Omnium's facilities, where it was ensured that at least three data points were available for every configuration with a few exceptions due to unforeseen circumstances. The extracted information from burst testing was the burst pressure value and the failure location. Microscope inspection entailed cutting vessels into rings and then into smaller samples. A larger set of information was extracted as FVF, porosity content, laminate thickness and resin residue thickness.

The tested configurations entailed differences in manufacturing parameters whereas decreasing the tension force led to a 4 % decrease in FVF, 2 % increase in porosity and 8 % decrease in burst performance. Increasing internal pressure led to a 2 % increase in FVF, a 4.5 % decrease in porosity but no noticeable change in burst performance. By varying the stacking sequence positioning and grouping, differences up to 13 % in FVF, 4 % in porosity and 6.5 % in burst performance were observed. Increasing the liner diameter led to differences of 3 % in FVF and 2.5 % in porosity, as no burst tests were performed for this configuration.

## 6.2. Conclusions

To provide a concise answer to the formulated research questions, a brief discussion is presented for each question below:

### *1. How do tension and pressure affect each other and affect the composite material microstructure during the filament winding process of CPVs?*

In literature, extensive research existed into investigating the winding tension force, where the internal pressure is often neglected. Although the internal pressure is inherently added to prevent liner deformation, adequate control could lead to mechanical performance improvements. To prevent deformation, the pressure forces exerted by the tension should be equally counteracted by the internal pressure, where a mismatch would cause a change in the vessel's dimensions. As a result, the manufacturing parameters' magnitude is derived from each other and heavily interlinked.

It was shown that these two parameters have a significant influence on the composite microstructure. The interaction between both parameters is what defines the consolidation process and compaction. It was observed that the higher the magnitude of each, the higher the pressure gradient, leading to higher compaction through the thickness. This in turn causes an increase in FVF and decreases porosity gradually. This was proven in the analytical model where higher radial compaction was observed when there is an increase in either parameter and was validated with experimental testing.

It was shown that these two parameters are incredibly influential in the winding process and have a significant influence on the composite microstructure and final product's dimensions and mechanical performance. The results and conclusions of this study provide a basis for future improvements that could be attained during manufacturing by proper definition of both parameters, for a fixed vessel configuration.

### *2. How does changing the stacking sequence affect the required liner pressure and winding tension force during the filament winding process?*

Accounting for stacking sequence changes was an important aspect in the development of the analytical model as with changing customer requirements such as vessel dimensions and nominal working pressure, different stacking sequences are required. Thus, the tool needs to adapt to such changes. It was also varied to check whether the observed correlations only existed for one particular stacking sequence or if it was a general trend.

The developed analytical modelling tool is capable of accounting for compaction changes by varying the grouping and positioning of layers, which was done for configurations 4 and 5. Whilst having the same number of layers, significant changes in length, FVF, porosity content and burst performance were observed. Changes in dimensions were observed by changing layer positioning, each layer hence experiences a different combination of tension and internal pressure as the internal pressure varies by winding more layers. It was also shown that layers experience different compaction levels depending on the preceding layers. In general, differences up to 13 % in FVF, 4 % in porosity and 6.5 % in burst performance were observed by varying the stacking sequence.

Circumferential layers compaction and positioning proved to be critical aspects. When the circumferential layers were wound closer to the liner, and thus more compacted as they were followed by high-angle helical layers, led to a significantly improved burst performance than if they were wound furthest from the liner.

Changing the stacking sequence also creates a change in failure mode and location. When large numbers of layers of the same winding angle are grouped together, cracks could easily propagate through. It was noted that heavily compacting the hoop layers, led to failure in the boss parts. As the composite became too stiff, a more critical area was observed.

It was shown that adjustments in manufacturing parameters are required by changing the stacking sequence, which could lead to improved vessel quality. The results of this study could be used as a solid baseline for further investigations in this area where the manufacturing parameters could be varied for individual layers or layer grouping depending on their positioning and winding angle.

### *3. How does the required liner pressure and winding tension force vary by changing the liner's diameter?*

As customer requirements often lead to changes in stacking sequences, it also often implies a change in vessel diameter to confine to space restrictions in the vehicle. In this thesis, the vessels manufactured were sub-scale vessels for their ease in manufacturing and testing. For investigation of the influence of increasing the vessel diameter, a full-scale vessel was manufactured and examined under a microscope.

It was shown in the analytical model and validated with experimental results that by increasing the vessel diameter and keeping everything else constant, a direct decrease in compaction was observed. The decrease in compaction was characterized by a decrease of 3 % in FVF and an increase of 2.5 % in porosity by increasing the diameter from 140 mm to 250 mm. This was attributed to a decrease in the external pressure exerted by the winding tension force. As established from the literature, the external pressure equation is inversely proportional to the liner diameter. Thus, it was observed that to compensate for this decrease in compaction, an increase in winding tension force is required to attain the same level of external pressure.

Burst pressure testing was not investigated due to resource limitation and as it does not provide much-added value in this investigation as comparing vessels with different diameters but the same stacking sequence is not a fair comparison. Future investigations could entail comparing burst performance of different vessel diameters but with a stacking sequence that is theoretically capable of achieving the same burst performance.

#### *4. How could the obtained relations relating winding tension and internal pressure be validated using experimental results?*

The obtained relations from the developed analytical model and literature were compared via the experimental campaign previously described. Important information was extracted from the experimental campaign that was inter-related and correlated back to the vessel configurations. Additional information was also obtained as changes in length, laminate thickness and laminate mass by measuring the dimensions and mass of the vessel before and after winding.

The configurations tested included changes in winding tension, internal liner pressure, stacking sequence and vessel diameter, where eight configurations were tested in total. In general, the results were in agreement with the predictions of the analytical model. The model managed to predict changes in compaction excellently. However, the few exceptions were predictions of burst pressure. Due to the scatter of data and the limited number of data points, trends relating to burst pressure were not observed for configuration 4 where the stacking sequence was changed and configuration 3 where the internal pressure was increased.

#### *5. How could the validated relations be generalized to form a method to determine the needed internal pressure and winding tension?*

Based on the observed trends relating changes in tension, pressure, stacking sequence and diameter to quality, recommendations could be made in terms of defining the optimal process parameters for a given vessel configuration. The term optimum process parameters is a general term, but in the context of this investigation is defined as the parameters that maximize mechanical performance for a fixed vessel configuration whilst keeping changes in vessel dimensions to a minimum.

The observed trend in this investigation is that increasing the tension force leads to a direct increase in compaction, which then increases FVF and lowers porosity, which leads to higher burst performance. However, an upper limit was set to prevent having a too-dry laminate or leading to fiber breakage. This upper limit was set based on the fiber's ultimate strength and applying a reasonable safety factor. This value however may be too high and not attainable by the winding machine and would instantly damage the liner. Thus, a reasonable judgment and comparison with nominal values are also required. Similarly, an upper limit is also set for the internal liner pressure, as the plastic liner has an upper limit based on its ultimate yield stress, where a higher value would burst the liner during winding.

It was shown that the internal liner pressure and tension need to be determined simultaneously in an iterative process. Judging based on the limited experience manufacturing the vessels in this thesis project, it is much easier to set the value for tension force to ensure tow stability first, then derive the required internal pressure accordingly. Different settings could be obtained and then compared using the analytical model to find the optimal combination. It should be noted that the analytical model does not have an incorporated upper limit for manufacturing parameters.

It was also concluded that changes in stacking sequences and liner diameter would directly need a change in process parameters to maintain a uniform compaction level. In general, positioning of hoop layer grouping is significantly critical for burst performance and changes in dimensions. Hoop layers provide the highest tangential compaction, thus, for these layers, a decrease in manufacturing parameters might be needed to prevent high levels of compaction. An option is having two different winding settings, a high for helical layers and a low for hoop layers. Moreover, as discussed, varying the diameter would need direct intervention to either increase or decrease compaction based on the variation.

### 6.3. Recommendations for Future Work

Although this thesis project yielded interesting results, there are still outstanding issues and limitations that are to be addressed. Areas of improvement still remain and are identified in this section that could be followed up on in future work at Plastic Omnium using the work of this thesis as a basis.

#### Modelling the Entire Vessel

The current analytical model restricted the geometry of the vessel by only considering the cylindrical section of the vessel. This imposes a level of inaccuracy on the obtained results and limits the obtained results. It is believed that by considering the entire vessel geometry, not only would information regarding the axial stress be available, but also more accurate predictions of tangential stresses would be performed due to coupling effects. By considering the axial stress and the axial forces imposed by winding helical layers, accurate predictions of changes in length could be made. This could then be correlated back to changes in manufacturing parameters. As a result, the analytical model could then give a value estimate, instead of a quantitative comparison regarding dimensions change.

#### Prediction of FVF Distribution through-the-thickness

A possible addition to the analytical model is to quantify the FVF distribution through the thickness. This could be related to the experienced radial compaction using a flow simulation model, as per Darcy's law, the resin flow rate through every layer could be determined. With an estimate of the winding time, that could be extracted from the winding software or from in-line data recordings, the volume of resin flowing out of every layer could be determined. With correlation to the impregnation rate through winding, the FVF distribution of every layer could be estimated and quantified.

This helps in addressing one of the limitations of the analytical model is not quantifying the compaction but rather as a qualitative comparison. The FVF values could be correlated with the chosen process parameters This would also aid in avoiding choosing a combination of process parameters that would lead to a too-dry vessel.

#### Prediction of Burst Pressure Performance

Another recommendation to convert all the hypotheses from quantitative predictions to qualitative predictions is to estimate the failure burst pressure. For this to be accurately estimated with a relatively high accuracy level, the curing stresses would need to be also superimposed on the obtained winding stresses. The curing stresses are generated due to chemical shrinkage and thermal stresses. Once superimposed with the winding stresses, a final estimation of the residual stresses within the final product is available, similar to the approach followed by Kang et al. [74].

The next step is to apply a suitable failure criterion and damage mechanisms for the prediction of burst pressure by gradually increasing the internal pressure. An extensive amount of work in the literature has been done on burst pressure prediction with different levels of accuracy. Depending on the required level of accuracy, computational costs increase simultaneously. The current intention is to keep the tool as time-efficient as possible to allow engineers to perform rapid iterations on-site during the development phase. However, a shift could be made into a more detailed analysis by trading-off computational cost. In this case, numerical approaches could be a viable option where the residual stresses could be directly inputted there and accurate burst pressure predictions are to be made.

#### Differentiating Process Parameters Based on Winding Angle

An interesting investigation would be to investigate the influence of varying the process parameters based on the winding angle. An example would be having different tension settings for hoop and helical layers. This is as in the current investigation, the process parameter setting was kept constant, irrespective of the winding angle. It is believed that investigating such a variation could be beneficial for the final product quality. Especially for controlling the changes in dimensions, by actively decreasing/increasing the compaction of certain layers, their force may be lower/higher. The same also applies to controlling the FVF and porosity distribution through the thickness.

#### Experimentally Validating the Winding Stresses and Strains

The obtained tangential winding stress distribution through the thickness from the analytical model has not been validated in this investigation. This mainly stems from the difficulty in assessing the strain of uncured composite laminate during manufacturing. An option that could be adapted is the use of Fiber Bragg Grating (FBG) that could be joined to the fiber strands while winding, and hence, have an estimate of the experienced strain by certain layers and then correlate back to the analytical model. This would be rather interesting to investigate whether any compression is experienced by the inner layers. However, this comes with direct difficulty as installing FBG is a complicated process that often requires experts.



# References

- [1] G. Jennings et al. “Share the Road Global outlook on walking and cycling”. In: United Nations Environment (2016).
- [2] R. van den Hoed. “Sources of radical technological innovation: the emergence of fuel cell technology in the automotive industry”. In: *Journal of Cleaner Production* 15.11 (2007), pp. 1014–1021. ISSN: 0959-6526.
- [3] C.C. Chan. “The state of the art of electric, hybrid, and fuel cell vehicles”. In: *Proceedings of the IEEE* 95.4 (2007), pp. 704–718.
- [4] Environmental Protection Agency. “US transportation sector greenhouse gas emissions: 1990–2011”. In: Office of Transportation and Air Quality EPA-420-F-13-033a (2013).
- [5] M. Ehsani et al. *Modern electric, hybrid electric, and fuel cell vehicles*. CRC press, 2018.
- [6] X. Li. *Principles of fuel cells*. CRC press, 2005.
- [7] Regulation No 134 of the Economic Commission for Europe of the United Nations (UN/ECE) — Uniform provisions concerning the approval of motor vehicles and their components with regard to the safety-related performance of hydrogen-fuelled vehicles (HFCV) [2019/795]. May 2019.
- [8] Toyota UK. *ToyotaMirai: the safety facts*. 2015. URL: <https://blog.toyota.co.uk/toyota-mirai-safety-facts/toyotablog-h2-safety-pict-n2>.
- [9] T. Beer et al. “Fuel-cycle greenhouse gas emissions from alternative fuels in Australian heavy vehicles”. In: *Atmospheric environment* 36.4 (2002), pp. 753–763.
- [10] European Parliament. “Regulation (EC) No 79/2009 of the European Parliament and of the Council on Type-approval of Hydrogen-powered Motor Vehicles, and amending Directive 2007/46/EC”. In: (2009).
- [11] ISO 11439. *Gas cylinders — High pressure cylinders for the on-board storage of natural gas as a fuel for automotive vehicles*. Standard. Geneva, Switzerland: International Organization for Standardization, 2013.
- [12] D. Wang et al. “Development of regulations, codes and standards on composite tanks for on-board gaseous hydrogen storage”. In: *International Journal of Hydrogen Energy* 44.40 (2019), pp. 22643–22653.
- [13] A. Ibrahim, Y. Ryu, and M. Saidpour. “Stress analysis of thin-walled pressure vessels”. In: *Modern Mechanical Engineering* 5.01 (2015), p. 1.
- [14] J. Hashemi et al. “New method in design and manufacturing of fluid-filled multi-layered spherical pressure vessels”. In: *International journal of pressure vessels and piping* 58.3 (1994), pp. 355–360.
- [15] S. Li and J. Cook. “An analysis of filament overwound toroidal pressure vessels and optimum design of such structures”. In: *J. Pressure Vessel Technol.* 124.2 (2002), pp. 215–222.
- [16] L. Zu et al. “Design of filament-wound spherical pressure vessels based on non-geodesic trajectories”. In: *Composite Structures* 218 (2019), pp. 71–78.
- [17] C. P. Fowler, A. C. Orifici, and C. H. Wang. “A review of toroidal composite pressure vessel optimisation and damage tolerant design for high pressure gaseous fuel storage”. In: *International Journal of Hydrogen Energy* 41.47 (2016), pp. 22067–22089.
- [18] A. Hokine et al. “Analysis of failure pressures of composite cylinders with a polymer liner of type IV CNG vessels”. In: *International Journal of Mechanical, Aerospace, Industrial and Mechatronics Engineering* 7 (2013), pp. 148–152.
- [19] M. Legault. *The first commercial Type V composite pressure vessel*. 2012. URL: <https://www.compositesworld.com/articles/next-generation-pressure-vessels> (visited on 02/10/2022).
- [20] V.V. Vasiliev, A.A. Krikanov, and A.F. Razin. “New generation of filament-wound composite pressure vessels for commercial applications”. In: *Composite structures* 62.3-4 (2003), pp. 449–459.
- [21] M. Munro. “Review of manufacturing of fiber composite components by filament winding”. In: *polymer Composites* 9.5 (1988), pp. 352–359.
- [22] M.G. Bader. “Selection of composite materials and manufacturing routes for cost-effective performance”. In: *Composites Part A: Applied science and manufacturing* 33.7 (2002), pp. 913–934.
- [23] F.C. Shen. “A filament-wound structure technology overview”. In: *Materials Chemistry and Physics* 42.2 (1995), pp. 96–100.
- [24] N. Minsch et al. “Analysis of filament winding processes and potential equipment technologies”. In: *Procedia CIRP* 66 (2017), pp. 125–130.
- [25] S.R. White and Z. Zhang. “The effect of mandrel material on the processing-induced residual stresses in thick filament wound composite cylinders”. In: *Journal of reinforced plastics and composites* 12.6 (1993), pp. 698–711.

- [26] T. Sofi, S. Neunkirchen, and R. Schledjewski. "Path calculation, technology and opportunities in dry fiber winding: a review". In: *Advanced Manufacturing: Polymer & Composites Science* 4.3 (2018), pp. 57–72.
- [27] M. Quanjin et al. "Design and optimize of 3-axis filament winding machine". In: *IOP conference series: materials science and engineering*. Vol. 257. 1. IOP Publishing, 2017, p. 012039.
- [28] S. Koussios. "Filament winding: A unified approach." PhD dissertation. Delft University of Technology, 2002, pp. 1–300.
- [29] M. Hojjati, V.S. Ardebili, and S.V. Hoa. "Design of domes for polymeric composite pressure vessels". In: *Composites Engineering* 5.1 (1995), pp. 51–59.
- [30] B.S. Johansen, A. Lystrup, and M.T. Jensen. "CADPATH: a complete program for the CAD-, CAE-and CAM-winding of advanced fibre composites". In: *Journal of materials processing technology* 77.1-3 (1998), pp. 194–200.
- [31] L. Zu, S. Koussios, and A. Beukers. "Design of filament-wound domes based on continuum theory and non-geodesic roving trajectories". In: *Composites Part A: Applied Science and Manufacturing* 41.9 (2010), pp. 1312–1320.
- [32] W.F. Trench. "Elementary differential equations with boundary value problems". In: (2013).
- [33] W.D. Callister and D.G. Rethwisch. *Materials science and engineering: an introduction*. Vol. 9. Wiley New York, 2018.
- [34] M. Nebe. "In Situ Characterization Methodology for the Design and Analysis of Composite Pressure Vessels". PhD dissertation. TU Dortmund University, 2021.
- [35] D. Cohen. "Influence of filament winding parameters on composite vessel quality and strength". In: *Composites Part A: Applied Science and Manufacturing* 28.12 (1997), pp. 1035–1047.
- [36] P. Mertiny and F. Ellyin. "Influence of the filament winding tension on physical and mechanical properties of reinforced composites". In: *Composites Part A: Applied Science and Manufacturing* 33.12 (2002), pp. 1615–1622.
- [37] C.C. Liang, H.W. Chen, and C.H. Wang. "Optimum design of dome contour for filament-wound composite pressure vessels based on a shape factor". In: *Composite structures* 58.4 (2002), pp. 469–482.
- [38] V. Alcantar et al. "Optimization of Type 4 composite pressure vessels using genetic algorithms and simulated annealing". In: *International Journal of Hydrogen Energy* 42.24 (2017), pp. 15770–15781.
- [39] M. Madhavi, K. Rao, and K.N. Rao. "Design and Analysis of Filament Wound Composite Pressure Vessel with Integrated-end Domes." In: *Defence science journal* 59.1 (2009).
- [40] M. Musthak et al. "Prediction of Structural Behavior of FRP Pressure Vessel by Using Shear Deformation Theories". In: *Materials Today: Proceedings* 4.2 (2017), pp. 872–882.
- [41] P. Balicevic, D. Kozak, and T. Mrcela. "Strength of pressure vessels with ellipsoidal heads". In: *Strojniški vestnik* 54.10 (2008), pp. 685–692.
- [42] S. Koussios, O.K. Bergsma, and A. Beukers. "Isotensoid related composite structures". In: *American Society for Composites, 21st annual Conference*. DEStech publications, Inc. 2006, pp. 1–15.
- [43] H. Fukunaga and M. Uemura. "Optimum design of helically wound composite pressure vessels". In: *Composite structures* 1.1 (1983), pp. 31–49.
- [44] D. Leh et al. "Multi-sequence dome lay-up simulations for hydrogen hyper-bar composite pressure vessels". In: *Composites Part A: Applied Science and Manufacturing* 52 (2013), pp. 106–117.
- [45] D. Leh et al. "A progressive failure analysis of a 700-bar type IV hydrogen composite pressure vessel". In: *international journal of hydrogen energy* 40.38 (2015), pp. 13206–13214.
- [46] D. Leh et al. "Optimisation of 700 bar type IV hydrogen pressure vessel considering composite damage and dome multi-sequencing". In: *international journal of hydrogen energy* 40.38 (2015), pp. 13215–13230.
- [47] Z. Hashin. "Fatigue failure criteria for unidirectional fiber composites". In: (1981).
- [48] L. Wang et al. "Continuum damage modeling and progressive failure analysis of carbon fiber/epoxy composite pressure vessel". In: *Composite Structures* 134 (2015), pp. 475–482.
- [49] J. P. B. Ramirez et al. "700 bar type IV high pressure hydrogen storage vessel burst-Simulation and experimental validation". In: *International Journal of Hydrogen Energy* 40.38 (2015), pp. 13183–13192.
- [50] B. Ellul and D. Camilleri. "The influence of manufacturing variances on the progressive failure of filament wound cylindrical pressure vessels". In: *Composite Structures* 133 (2015), pp. 853–862.
- [51] M. Nebe et al. "Analysis on the internal pressure loading of composite pressure vessels: FE modeling and experimental correlation". In: *Composites Part B: Engineering* 212 (2021), pp. 108–550.
- [52] ASTM International. *ASTM D2734-16 Standard Test Methods for Void Content of Reinforced Plastics*. 2016.
- [53] ASTM International. *ASTM D792-13 Standard Test Methods for Density and Specific Gravity (Relative Density) of Plastics by Displacement*. 2013.
- [54] ASTM International. *ASTM D3171-15-Standard Test Methods for Constituent Content of Composite Materials*. 2015.

- [55] K.K. Kumar. "Approaches to determine the constituent elements of discontinuous fibre-reinforced polymer composites". In: Research Student Conference 2018 Faculty of Technology, Design and Environment Oxford Brookes University Ox, p. 54.
- [56] D. Cohen, S.C. Mantell, and L. Zhao. "The effect of fiber volume fraction on filament wound composite pressure vessel strength". In: *Composites Part B: Engineering* 32.5 (2001), pp. 413–429.
- [57] S. Harada et al. "A simplified method for predicting burst pressure of type III filament-wound CFRP composite vessels considering the inhomogeneity of fiber packing". In: *Composite Structures* 190 (2018), pp. 79–90.
- [58] A. Onder et al. "Burst failure load of composite pressure vessels". In: *Composite structures* 89.1 (2009), pp. 159–166.
- [59] H. Sepetcioglu, N. Tarakcioglu, and R. Rafiee. "Experimental investigation of graphene nanoplatelets effect on the fatigue behavior of basalt/epoxy composite pressure vessels". In: *Thin-Walled Structures* 171 (2022), p. 108672.
- [60] T.J. Osse and T.J. Lee. "Composite pressure hulls for autonomous underwater vehicles". In: *OCEANS 2007. IEEE. 2007*, pp. 1–14.
- [61] J. A. Júnior et al. "Engineering properties of carbon/epoxy filament wound unidirectional composites". In: *16th European Conference on Composite Materials. Vol. 16. 2014*, pp. 1–8.
- [62] ASTM International. AASTM D3039-07 -Standard Test Method For Tensile Properties Of Polymer Matrix Composite Materials.
- [63] ISO 527-1. *Plastics — Determination of tensile properties — Part 1: General principles. Standard. Geneva, Switzerland: International Organization for Standardization, 2019.*
- [64] ASTM International. AASTM D3039-07 -Standard Test Method for In-Plane Shear Response of Polymer Matrix Composite Materials by Tensile Test of a 45° Laminate1. 2007.
- [65] KHKS-0121. Technical standard for aluminum liner/carbon fiber composite vessels The High Pressure Gas Safety Institute of Japan 2005 (in Japanese).
- [66] P. Mertiny and F. Ellyin. "Selection of optimal processing parameters in filament winding". In: *International SAMPE Technical Conference. Vol. 33. 2001*, pp. 1084–1095.
- [67] Europe Union. "Regulation (EC) No 78/2009 of the European Parliament and of the Council of 14 January 2009: on the Type-Approval of Motor Vehicles with Regard to the Protection of Pedestrians and Other Vulnerable Road Users, Amending Directive 2007/46/EC and Repealing Directives 2003/102/EC and 2005/66/EC". In: *Europe Official Journal of The European Union* 4.2 (2009), pp. 1–35.
- [68] N. Nguyen and L. R. Gambone. "Hydrogen and Fuel Cell Vehicles UN Global Technical Regulation No. 13: Latest Updates Reflecting Heavy Duty Vehicles". In: (2019).
- [69] R. Saulsberry, C. Nichols, and J. Waller. *Smart Composite Overwrapped Pressure Vessel-Integrated Structural Health Monitoring System to Meet Space Exploration and International Space Station Mission Assurance Needs. Tech. rep. 2012.*
- [70] M.A. Sutton, J.J. Orteu, and H. Schreier. *Image correlation for shape, motion and deformation measurements: basic concepts, theory and applications. Springer Science & Business Media, 2009.*
- [71] A.I. Torres Guijarro. "Experimental and Analytical Determination of Interfiber Fracture Mechanisms and Patterns in Type IV Composite Pressure Vessels". In: (2019).
- [72] ASTM International. AASTM E1067/E1067M-18 -Standard Practice for Acoustic Emission Examination of Fiberglass Reinforced Plastic Resin (FRP) Tanks/Vessels. 2018.
- [73] B. Rahul, D.S. Chand, and J. Dharani. "A comprehensive review on the performance analysis of composite overwrapped pressure vessels". In: *Engineering and Applied Science Research* 49.2 (2022), pp. 272–287.
- [74] C. Kang et al. "Determination of residual stress and design of process parameters for composite cylinder in filament winding". In: *Advances in Materials Science and Engineering 2018* (2018).
- [75] Z. Cai. "Simulation of the manufacture of closed shape composite structures". PhD thesis. Massachusetts Institute of Technology, 1990.
- [76] Z. Cai, T. Gutowski, and S. Allen. "Winding and consolidation analysis for cylindrical composite structures". In: *Journal of composite materials* 26.9 (1992), pp. 1374–1399.
- [77] D.H. Lee et al. "Smart cure of thick composite filament wound structures to minimize the development of residual stresses". In: *Composites Part A: Applied Science and Manufacturing* 37.4 (2006), pp. 530–537.
- [78] S.W. Tsai and H.T. Hahn. *Introduction to composite materials. Routledge, 2018.*
- [79] M. Nebe et al. "Experimental and analytical analysis on the stacking sequence of composite pressure vessels". In: *Composite Structures* 247 (2020), p. 112429.
- [80] H. Lu et al. "Effects of tape tension on residual stress in thermoplastic composite filament winding". In: *Journal of Thermoplastic Composite Materials* 18.6 (2005), pp. 469–487.
- [81] D. Lydzba and J.F. Shao. "Stress equivalence principle for saturated porous media". In: *Comptes Rendus Mecanique* 330.4 (2002), pp. 297–303.

- 
- [82] S. Lee and G.S. Springer. "Filament winding cylinders: I. Process model". In: *Journal of Composite Materials* 24.12 (1990), pp. 1270–1298.
  - [83] T.A. Bogetti and J.W. Gillespie Jr. "Process-induced stress and deformation in thick-section thermoset composite laminates". In: *Journal of composite materials* 26.5 (1992), pp. 626–660.
  - [84] M. Wu, T. Centea, and S.R. Nutt. "Compression molding of reused in-process waste—effects of material and process factors". In: *Advanced Manufacturing: Polymer & Composites Science* 4.1 (2018), pp. 1–12.
  - [85] University of Washington. Lecture notes on Thick-walled Pressure Vessels.

# A

## Cylinder Stress Derivation

In this appendix, the stresses following both the thick- and thin-walled assumptions are derived and stated as they are used repeatedly in this thesis report.

### A.1. Thick-walled Cylinder Stresses

Considering an element on a thick-walled vessel that experiences both internal and external pressure as shown in Figure A.1.

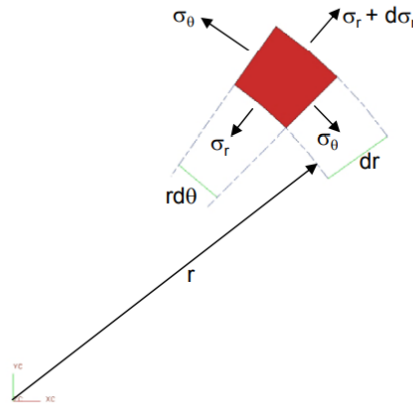


Figure A.1: Element with radius  $r$  and angle  $\theta$  of a thick-walled cylinder - taken from [85]

For this element, assuming no body forces exist, radial force equilibrium would yield the following equation:

$$(\sigma_r + d\sigma_r)(r + dr)d\theta = \sigma_r r d\theta + \sigma_\theta d\theta dr \quad (\text{A.1})$$

whereby ignoring second-order terms, the equilibrium equation becomes:

$$\frac{d\sigma_r}{dr} + \frac{\sigma_r + \sigma_\theta}{r} = 0 \quad (\text{A.2})$$

Considering the strains in this element, due to symmetry there is no tangential displacement, only radial displacement,  $u$ . Therefore, the radial strain  $\varepsilon_r$  and tangential strain  $\varepsilon_\theta$  could be given as:

$$\begin{aligned} \varepsilon_r &= \frac{u + du - u}{dr} = \frac{du}{dr} \\ \varepsilon_\theta &= \frac{(r + u)d\theta - rd\theta}{rd\theta} = \frac{u}{r} \end{aligned} \quad (\text{A.3})$$

Using Hooke's law, the strains are given as:

$$\begin{aligned} \varepsilon_r &= \frac{du}{dr} = \frac{1}{E}(\sigma_r - \nu\sigma_\theta) \\ \varepsilon_\theta &= \frac{u}{r} = \frac{1}{E}(\sigma_\theta - \nu\sigma_r) \end{aligned} \quad (\text{A.4})$$

Using the previous two strain equations and solving for the radial strain  $\sigma_r$  and tangential stress  $\sigma_\theta$ , the following expressions could be found:

$$\begin{aligned}\sigma_r &= \frac{E}{1-\nu^2} \left( \frac{du}{dr} + \nu \frac{u}{r} \right) \\ \sigma_\theta &= \frac{E}{1-\nu^2} \left( \frac{u}{r} + \nu \frac{du}{dr} \right)\end{aligned}\quad (\text{A.5})$$

By substituting into Equation A.2, it yields the following:

$$\frac{d^2u}{dr^2} + \frac{1}{r} \frac{du}{dr} - \frac{u}{r^2} = 0 \quad (\text{A.6})$$

This could be solved using a solution of  $u = C_1 r + \frac{C_2}{r}$  where  $C_1$  and  $C_2$  are constants. As a result, the stresses could be rewritten as:

$$\begin{aligned}\sigma_r &= \frac{E}{1-\nu^2} \left[ C_1(1+\nu) - C_2 \left( \frac{1-\nu}{r^2} \right) \right] \\ \sigma_\theta &= \frac{E}{1-\nu^2} \left[ C_1(1+\nu) + C_2 \left( \frac{1-\nu}{r^2} \right) \right]\end{aligned}\quad (\text{A.7})$$

Using boundary conditions of  $\sigma_r(r_i) = P_i$  and  $\sigma_r(r_o) = -P_o$ , where  $r_i$  is inner radius and  $r_o$  is outer radius. The constants could be found, which lead to the final expressions for the stresses, which are rather known as Lamé's equations:

$$\begin{aligned}\sigma_r &= \frac{r_i^2 P_i - r_o^2 P_o}{(r_o^2 - r_i^2)} - \frac{(P_i - P_o) r_i^2 r_o^2}{(r_o^2 - r_i^2) r^2} \\ \sigma_\theta &= \frac{r_i^2 P_i - r_o^2 P_o}{(r_o^2 - r_i^2)} + \frac{(P_i - P_o) r_i^2 r_o^2}{(r_o^2 - r_i^2) r^2}\end{aligned}\quad (\text{A.8})$$

## A.2. Thin-walled Cylinder Stresses

Deriving the stresses in the thin-walled cylinder is relatively simpler than in thick-walled as the stress is assumed to be constant throughout the thickness, unlike thick-walled where it is a function of the radius. A vessel is considered thin-walled if the ratio  $D/t$  is larger than 10. The hoop stress could be found by considering a cross-section of the vessel subject to internal pressure and setting the following force equilibrium:

$$PLD = 2\sigma_y L t \quad (\text{A.9})$$

where  $L$  is the length,  $D$  is the diameter and  $t$  is the thickness. The hoop stresses could be found as:

$$\sigma_y = \frac{Pr}{t} \quad (\text{A.10})$$

Following the same approach for the axial stresses, the stress could be found as follows:

$$\begin{aligned}P\pi r^2 &= \sigma_x \pi D t \\ \sigma_x &= \frac{Pr}{2t}\end{aligned}\quad (\text{A.11})$$

The radial stresses are assumed to be constant in a thin-walled cylinder across the thickness. It could be found by setting the force equilibrium and then finding the stress equation as the previous stress components, which is displayed as follows:

$$\begin{aligned}\sigma_r \pi r^2 + P_o \pi r^2 &= P_i \pi r^2 \\ \sigma_r &= P_i - P_o\end{aligned}\quad (\text{A.12})$$

It should be kept in mind that the direction of the internal and external pressure are vector components in the opposite direction of each other. Thus, the absolute values should be added to each other.

# B

## Analytical Model Verification

As defined by the American Institute of Aeronautics and Astronautics (AIAA), verification is "The process of determining that a computational model accurately represents the underlying mathematical model and its solution". In other words, verification is inherently checking whether the model represents what it was intended to under the based assumptions and requirements. Verification could be divided into two parts: code verification and calculation verification. Code verification is checking via unit and integrated tests whether there are errors in implementing the model (i.e. while programming). After verifying that the functioning units of the model are error-free, the next step is calculation verification which is concerned with comparing the results of the model and checking if it is producing the correct output. This could be done by comparing two different models and finding and analysing the discrepancies between both models.

Code verification was done via several unit and integrated tests throughout the program. Unit tests are the lowest testing level stage that was performed where every calculation was checked if it is coded properly with intermediate integration tests making sure that the previous code section is error-free. An example could be checking Q matrix components are computed correctly and are assembled with no errors. Then an integrated test would be to check whether the overall ABD matrix for a certain layup is correct or not. Various additional unit and integrated tests were performed.

For calculation verification, the thin-walled cylinder stress equation for hoop stress previously mentioned in [Equation 3.10](#) was compared to an alternative analysis model. The hoop stress, given below, is compared to the one obtained by following a thick-walled assumption, which is often referred to as Lamé's equations as derived in [Appendix A](#).

$$\sigma_y = \frac{P_{int}r_i^2 - P_{ext}r_o^2}{r_o^2 - r_i^2} + \frac{r_i^2r_o^2(P_{int} - P_{ext})}{r^2(r_o^2 - r_i^2)} \quad (\text{B.1})$$

To compare these different models, the hoop stress distribution was compared for the layup given in [Figure 3.5](#). The result could be seen in [Figure B.1](#). Both approaches follow the same trend and are not much off. It could be seen that using thick-walled assumption results gives a more conservative stress value, in comparison with thin-walled hoop stresses. On a closer examination of both equations, [Equation B.1](#) and [Equation 3.10](#), it could be seen that thin-walled tends to give a higher value due to assuming a constant radius value that applies for both internal and external pressure. This creates a slight difference, which is assumed to be the difference for magnitudes in [Figure B.1](#).

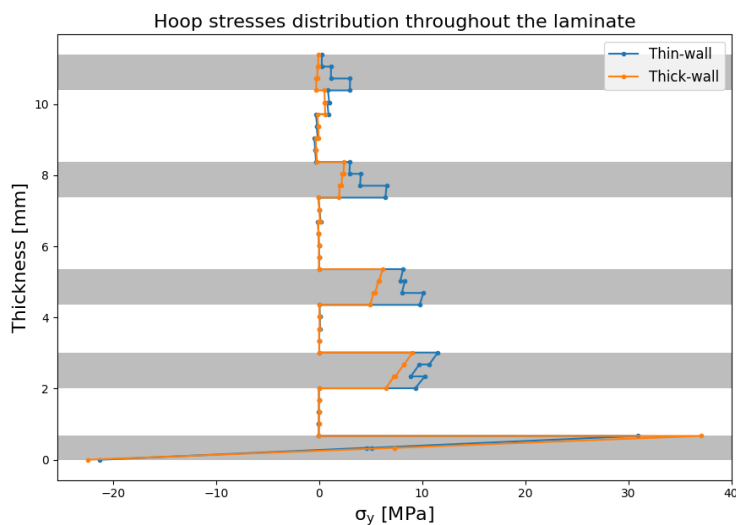


Figure B.1: Calculation verification of the model by comparing thin-walled and thick-walled cylinder hoop stress distribution through the thickness.